Zinc isotopes as a tool to investigate zinc biogeochemical cycling in the SW Pacific Ocean

Moneesha Samanta

May 2017

A thesis submitted for the degree of Doctor of Philosophy of the Australian National University

Declaration

The work presented in this thesis was carried out at the Research School of Earth Sciences at The Australian National University, between 2012 and 2017. I certify that this thesis contains no material that has been accepted for the award of any degree or diploma at any university. All work, including analyses, data and interpretations, is my own original work unless otherwise acknowledged.

Acknowledgements

During this PhD, I got the opportunity to meet some amazing people for which I'll always be grateful. This PhD would not have been possible without the involvement of these people.

First and foremost, I would like to convey my heartfelt gratitude to Michael Ellwood for his continued guidance, support and patience. Thank you, Michael, for being an outstanding supervisor and for helping me in so many ways. I could not have wished for a more understanding supervisor.

I would like to thank Graham Mortimer for all his advice and help in the laboratory. Thank you, Graham, for being such a great friend and guide.

My gratitude to Robert Strzepek for introducing me to the world of algal culturing and providing me with valuable suggestions.

The technical support and advice of Les Kinsley and Steve Eggins is much appreciated.

I would like to thank the RSES student body, academic and administrative staff for being so helpful and making my time here an enjoyable one. Particularly, Sarah, Vikashni, Lucy, Scott, Aimee, Kate, Claire, Sareh, Ali, Graham, John, Ian, Jochen, Ulli, Maree.

I thank the Australian Government for the financial support. The ANU PhD Scholarship and RSES Supplementary Scholarship is gratefully acknowledged.

Finally, I would like to thank my wonderful family for encouraging me and believing in me. Maa, Baba, I can always feel your presence, inspiring me, you made me who I am. Thank you, Rahul, for always being there for me. I thank my grandmother for teaching me resilience. And lastly, thank you Reesha for lighting up my life. This PhD is for you all.

Abstract

Marine phytoplankton account for more than 40% of global primary production and hence play an important role in moderating global climate through ocean-atmosphere CO_2 exchange. Zinc (Zn) is an essential micronutrient and plays an important role in the carbon acquisition system within marine phytoplankton, thus, it has the potential to influence marine primary production. In seawater, Zn bioavailability is dependent on its concentration and its chemical speciation. The free Zn^{2+} ion concentration of the surface ocean is usually in the low picomolar range with the potential to be growth limiting for some phytoplankton species.

The aim of this research is to better understand Zn cycling in the ocean and the relationship between primary production and Zn bioavailability by exploiting variations in the Zn isotope composition of phytoplankton and seawater samples.

To realise this aim, a procedure was developed to measure the Zn isotope composition of marine samples. This procedure utilises the double spike (DS) technique in conjunction with the pre-concentration of Zn from seawater to determine processes that influence the Zn biogeochemical cycling in the ocean. Seawater samples, collected as part of a 2010 GEOTRACES process study, contrasting oligotrophic waters of north Tasman Sea and the mesotrophic waters of south Tasman Sea, were analysed using this technique.

In this study, variability in $\delta^{66}Zn$ of dissolved Zn is observed in the upper ocean (0-200 m) for the mesotrophic waters and is attributed to biological activity of eukaryotic phytoplankton. At stations where eukaryotic phytoplankton dominated, heavier $\delta^{66}Zn$

values coincided with the chlorophyll maxima suggesting preferential uptake of lighter Zn isotopes by phytoplankton.

To complement the field work, a Tasman Sea isolate of the coccolithophore *Emiliania huxleyi* was cultured across a range of free Zn^{2+} ion concentrations to determine the extent of Zn isotope fractionation during Zn uptake. The laboratory results support the field observation that the resident phytoplankton community controls $\delta^{66}Zn$ composition of the upper water column in the south Tasman Sea.

The intermediate and deep waters of the south Tasman Sea have Southern Ocean origin. The Southern Ocean plays a significant role in the global carbon cycle influencing both ocean circulation and biogeochemistry. Much of the surface waters of the Southern Ocean have low iron (Fe) bioavailability. I investigated the role Fe limitation plays in Zn accumulation and Zn isotope fractionation by the Southern Ocean haptophyte *Phaeocystis antarctica*, a major component of the Southern Ocean phytoplankton assemblage. Under Fe-limiting condition an increased cellular quota for Zn (expressed as Zn:P) and heavier $\delta^{66}Zn$ values within the cells is observed; Whereas, cells grown under Fe-replete conditions have a lower Zn quota and a lighter $\delta^{66}Zn$ composition. Thus, Fe bioavailability could regulate the dissolved Zn isotope composition of the Southern Ocean, which in turn would be reflected in other parts of the world ocean.

This study highlights the importance of carefully analysing phytoplankton community structure and the trace metal composition while interpreting $\delta^{66}Zn$ composition of the biologically active upper water column of the ocean.

Table of Contents

Declaration iii

Acknowledgements iv

Abstract vi

List of Figures xv

List of Tables xx

Chapter 1: Introduction to marine zinc biogeochemistry and PhD thesis proposal 1-19

Introduction 1

1.1 Biological importance of Zn in phytoplankton 1

1.2 Zinc biogeochemistry 3

1.3 Zinc isotopes and isotope fractionation 8

1.4 Thesis aims and approach 15

1.5 Thesis structure 17

Chapter 2: A method for determining the isotopic composition of dissolved zinc in seawater by MC-ICP-MS with ^{67}Zn-^{68}Zn double spike 21-56

Abstract 21

2.1 Introduction 23

2.1.1 Choice of double spike 25

2.1.2 Calibration of the double spike 28

2.1.3 Isotope dilution equation 29

2.1.4 The iterative solution method for calculation of $\delta^{66}Zn$ of a sample..... 32

2.1.5 Pre-concentration of trace metals from seawater..... 34

2.1.6 Ion exchange chromatography for Zn separation 35

2.2 Experimental 37

2.2.1 Reagents 37

2.2.2 Preparation of the double spike 37

2.2.3 Pre-concentration of trace metals 38

2.2.3.1 Optimising pH and elution efficiency.....39

2.2.4 Ion exchange chromatography for Zn separation 40

2.2.5 Isotope mass spectrometry 43

2.3 Results and Discussion 46

2.3.1 Solid phase extraction versus the solvent extraction technique 46

2.3.2 Optimising loading pH for extraction and elution efficiency 46

2.3.2.1 Testing the use of HCl over HNO_3 46

2.3.2.2 Recovery versus pH 49

2.3.3 Anion exchange chromatography 50

2.3.4 Method Blanks 51

2.3.5 Reproducibility 51

2.3.6 Inter-calibration samples 52

2.4 Conclusions 54

Acknowledgements 55

Appendix 56

Chapter 3: Dissolved zinc isotope cycling in the Tasman Sea, SW Pacific Ocean 58-101

Abstract 58

3.1 Introduction 60

3.2 Experimental 65

3.2.1 Cleaning 65

3.2.2 Sampling 65

3.2.3 Biological measurements 67

3.2.4 Procedure for dissolved Zn isotope analysis 68

3.3 Results and Discussion 71

3.3.1 Hydrography 71

3.3.2 Biological data 75

3.3.3 Dissolved Zn concentration and isotope results 80

3.3.3.1 Biological control on Zn isotope fractionation and Zn speciation in the upper water column 89

3.3.4 Dissolved Zn and silicic acid 93

3.3.4.1 Zn*and δ^{66}Zn 93

3.3.4.2 δ^{66}Zn and δ^{30}Si 96

3.4 Conclusions 98

Acknowledgements 99

Appendix 100

Chapter 4: Zinc isotope fractionation by *Emiliania huxleyi* cultured across a range of free zinc ion concentrations ……. 103-135

Abstract …….. 103

4.1 Introduction …….. 105

4.2 Methods ……..108

4.2.1 Study organism and experimental design ……..108

4.2.2 Cleaning protocol ……..…109

4.2.3 Medium preparation ……..109

4.2.4 Growth rate measurement …… 111

4.2.5 Measurement of photophysiological parameters …… 111

4.2.6 Cell sizing and cell density ……..112

4.2.7 Scanning Electron Microscope imaging ……..113

4.2.8 Cellular chlorophyll *a* measurement …….. 113

4.2.9 Cell harvesting, Zn:P and Zn isotope determination ……..……114

4.2.10 Statistical analysis …… 117

4.3 Results and Discussion ……118

4.3.1 Specific growth rates and cell morphology ……..118

4.3.2 Photophysiology and cellular chlorophyll *a* concentration ……..121

4.3.3 Zn:P ratio and Zn isotope fractionation …… 125

4.4 Conclusions …….. 133

Acknowledgements …….. 134

Appendix …….. 135

Chapter 5: Variability in zinc isotope fractionation in *Phaeocystis antarctica* under iron replete and iron limiting conditions ……..137-179

Abstract …….. 137

5.1 Introduction ……140

5.2 Methods ……144

5.2.1 Study organism and experimental design ……144

5.2.2 Medium preparation ……..145

5.2.3 Growth rate measurement ……147

5.2.4 Photophysiological parameters ……147

5.2.5 Cell sizing and cell density …….. 152

5.2.6 Cellular chlorophyll *a* measurement …….. 152

5.2.7 Cellular Zn isotope composition and Zn and P concentrations …… 153

5.2.7.1 Cellular Zn and P concentrations …… 154

5.2.7.2 Cellular Zn isotope composition …….. 156

5.3 Results and Discussion ……157

5.3.1 Effect of Fe and Zn limitation on growth rates and cell morphology ……157

5.3.1.1 Growth rates …… 157

5.3.1.2 Cell morphology …….. 159

5.3.2 Effect of Fe and Zn limitation on photophysiological response and chlorophyll *a* concentration of cells ……161

5.3.3 Effect of Fe and Zn limitation on Zn:P ratio and Zn isotope fractionation ……164

5.3.3.1 Zn:P ratio …… 164

5.3.3.1.i Comparison with Zn:P ratio of natural phytoplankton assemblages in the Southern Ocean and implications ……. 166

5.3.3.2 Zn isotope fractionation …… 167

5.4 Conclusions ……..177

Acknowledgements …….. 179

Chapter 6: Thesis Conclusions ……181-191

6.1 Summary ……..181

6.1.1 Chapter 2 …… 181

6.1.2 Chapter 3 ……..182

6.1.3 Chapter 4 ……..183

6.1.4 Chapter 5 ……..185

6.2 General conclusions …….. 187

6.3 Future research directions ……..188

List of References ……. 192-200

Appendices: List of published papers ……..202

List of Figures

Figure 1.1: (a) The possible role of carbonic anhydrase in carbon concentration mechanism within a diatom cell. (b) The role of Pyrenoid in increasing the efficiency of CCM (Hopkinson et al. 2011) ……3

Figure 1.2: Concentration profiles versus depth of dissolved (A.) Nitrate, (B.) Phosphate, (C.) Silicic acid and (D.) Zn in the central North Pacific and North Atlantic Oceans. Figure adapted from (Sunda 2012) ……4

Figure 1.3: Schematic diagrams showing the Zn isotope mass balance in the global ocean with the inputs sources and outputs sinks. Figures adapted from (Little et al. 2014) and (Vance et al. 2016)…… 14

Figure 1.4 and 3.1: Maps of A. Seafloor bathymetry; B. Surface nitrate concentration; C. Particulate inorganic carbonate (PIC) concentration and; D. Chlorophyll *a* concentration of the three process stations (P1, P2 and P3) from which samples were collected for the dissolved Zn isotope work during the 2010 PINTS voyage. East Australian Current, Tasman Front and Subtropical Front are shown in the maps ……16 and 74

Figure 2.1: A 3D diagram showing the DS-sample mixing line, natural fractionation line (inset, magnified) and the instrumental fractionation line (mass bias) in $^{66}Zn/^{64}Zn$, $^{67}Zn/^{64}Zn$ and $^{68}Zn/^{64}Zn$ space (X, Y and Z axes respectively)……26

Figure 2.2: Error magnification in calculating natural fractionation factor associated with varying relative proportion of ^{67}Zn in ^{67}Zn-^{68}Zn DS, and DS in DS-sample mixture (Using MATLAB program by (Rudge et al. 2009)..... 27

Figure 2.3: Calculated $\delta^{66}Zn$ values of a sample with iteration steps……33

Figure 2.4: (a) Relative percentage recovery of Zn from the Toyopearl AF Chelate 650M resin for a deep seawater sample eluted with either 1 mol L^{-1} HCl or 1 mol L^{-1} HNO_3. (b) $\delta^{66}Zn$ values (w.r.t. JMC-Lyon) and percentage yield of dissolved Zn for replicates of a

deep seawater sample eluted from Toyopearl AF Chelate 650M resin using 1 mol L^{-1} HCl and 1 mol L^{-1} HNO_3……47

Figure 2.5: $\delta^{66}Zn$ values and concentration of dissolved Zn for replicates of a deep seawater sample buffered at different pH before solid phase extraction……49

Figure 2.6: Elution curves of different elements for anion exchange chromatography (using AG1X8 resin) loaded and washed with 0.5 mol L^{-1} HCl followed by elution with 0.5 mol L^{-1} HNO_3……50

Figure 3.2. Profiles to 1500 m of: **A.** Temperature, **B.** Salinity, **C.** Dissolved oxygen, **D.** Si*, **E.** raw CTD fluorescence and **F.** a property-property plot of temperature versus salinity for process stations P1, P2 and P3 along with density lines for sigma-t of 26.8, 27.1 and 27.4……75

Figure 3.3. Profiles of dissolved Zn, free Zn^{2+} ion and ligand concentrations for stations **A.** P1, **B.** P2 and **C.** P3 versus depth from 0 to 500 m. Presented in adjacent panel is the $\delta^{66}Zn$ composition of dissolved Zn. Also present are the raw CTD fluorescence and biomarker pigment data for each station. Free Zn^{2+} ion concentration, ligand concentration and pigment data were taken from Sinoir et al. (2016) ……..78

Figure 3.3. (Chapter Appendix): The dissolved Zn, free Zn^{2+} ion and ligand concentrations (from depth 0 to 500 m) of the three Process stations P1, P2 and P3 are shown in separate panels with different scales. Presented in adjacent panel is the $\delta^{66}Zn$ composition of dissolved Zn of stations P1, P2 and P3 along with the deep ocean $\delta^{66}Zn$ composition ……100

Figure 3.4. Seasonal variations in **A.** Picoeukaryotic (Picoeuk.) **B.** Synechococcus (Syn.) and Prochlorococcus (Pro.) cell abundance, **C.** Silicic acid concentration and **D.** Phosphate concentration versus depth for process station P1……..79

Figure 3.5: Profiles of **A.** dissolved Zn concentration, **B.** silicic acid concentration, and **C.** $\delta^{66}Zn$ versus depth. **D.** A property-property plot of Zn versus silicic acid concentration for process stations P1, P2 and P3 ……..83

Figure 3.6: Property-property plots of δ^{66}Zn versus **A.** raw CTD fluorescence and **B**. dissolved Zn concentration for process stations P2 and P3 between 0 and 200 m ……..…84

Figure 3.7: Profiles of **A.** dissolved Zn concentration, **B.** δ^{66}Zn, and **C.** Picoeukaryote and raw CTD fluorescence versus depth **(in log scale)** for process station P1 occupied in the 28-30 January 2010 (summer) and reoccupied on 20 May 2011 (late autumn)……..…92

Figure 3.7 (Chapter Appendix): Seasonal variation in **A.** dissolved Zn concentration, and **B.** δ^{66}Zn, versus depth for process station P1 ……..…101

Figure 3.8: Profiles of Zn* versus depth for A. process stations P1, P2 and P3 and B. process station P1 occupied in the 28-30 January 2010 (summer) and reoccupied on 20 May 2011 (late autumn) ……..94

Figure 3.9: Section of **A.** oxygen and **B.** salinity along the P11S line which extends into the Tasman Sea along 155 ˚E showing the different water masses in the Tasman Sea. **A.** Overlaying the oxygen section are the Zn* profiles for stations P1, P2 and P3. **B.** Overlaying the salinity section are density lines and Zn isotope profiles for stations P1, P2 and P3. ……..95

Figure 3.10: Property-property plots of δ^{66}Zn versus δ^{30}Si for samples collected between 200 and 3500 m for station P3. The δ^{30}Si data is based on δ^{29}Si values obtained by Cardinal et al (2005) for stations CTD17 and CTD24 located at the Subantarctic Zone at 46.9˚S and 48.8˚S, respectively at ~142˚E ……97

Figure 4.1: Variation in specific growth rates and cell size of *E. huxleyi* cultured across a range of free Zn^{2+} concentrations ……..119

Figure 4.2: Scanning electron microscope images of *E. huxleyi* cultured at different free Zn^{2+} concentrations; (a) pZn = 11.9, (b) pZn = 10.0 and (c) pZn = 8.5……..121

Figure 4.3: Variation in (a) the potential photochemical efficiency of PSII reaction centre (F_v/F_m); (b) duration of electron transport from Q_A to Q_B and from Q_B to PQ

Pool; (c) the size of the functional absorption cross section of PSII and the size of the oxidised PQ pool; and (d) Variation in Chlorophyll *a* normalised per cell and per cell volume of *E. huxleyi* with increasing free Zn^{2+} concentrations ……123

Figure 4.4: The cellular Zn normalised to the P content of the cells of *E. huxleyi* (clone CS-1016; diamonds) compared with another clone of *E. huxleyi* (clone BT6; circles) (Sunda and Huntsman 1992) cultured across a range of free Zn^{2+} ion concentrations ……125

Figure 4.5: (a) Zn isotope fractionation by *E. huxleyi* across a range of free Zn^{2+} ion concentrations (unwashed/SOW washed cells and washed/oxalate-EDTA washed cells to remove extracellular Zn) compared to Zn isotope fractionation by the diatom *T. oceanica* (John et al., 2007). (b) Specific Zn uptake rates (mol Zn (mol P)$^{-1}$ day^{-1}) of *E. huxleyi* (clones CS-1016 (this study) and BT6 (Sunda and Huntsman 1992)) and *T. oceanica* (clone CCMP 1005 (John et al., 2007) and clone 13-1 (Sunda and Huntsman 1992)) cultured across a range of free Zn^{2+} ion. ……130

Figure 4.5 (a) (Chapter Appendix): Zn isotope fractionation by *E. huxleyi* (corrected for relative difference between media and standard) across a range of free Zn^{2+} ion concentrations compared to Zn isotope fractionation by the diatom *T. oceanica* (John et al., 2007) ……135

Figure 5.1: a) Excitation of PSII during FRRF and associated photosynthetic pathways b) Calculation of photosynthetic parameters from FRRF (Kolber, http://www.soliense.com/LIFT_Method.php) ……150

Figure 5.2: Schematic representation of with the electron transport chain from PSII to PSI (in focus) within the photosynthetic apparatus (Kolber; http://www.soliense.com/LIFT_Method.php) ……151

Figure 5.3: Variation in specific growth rates of *P. antarctica* grown under high and low Fe and Zn conditions ……158

Figure 5.4: Variation in (a) cell size and (b) surface area/volume of *P. antarctica* grown under high and low Fe and Zn conditions ……160

Figure 5.5: Variation in cellular biomass (obtained by multiplying cell volume with no. of cells per mL) of *P. antarctica* grown under high and low Fe and Zn conditions ……160

Figure 5.6: Variation in (a) F_v/F_m, (b) σ_{PSII}, (c) τ_1 and (d) τ_2 of *P. antarctica* grown under high and low Fe and Zn conditions …… 163

Figure 5.7: Variation in cellular chlorophyll a concentration (normalised to cell volume) of *P. antarctica* grown under high and low Fe and Zn conditions…… 162

Figure 5.8: Variation in cellular Zn normalised to P content in *P. antarctica* grown under high (+) and low (-), Fe and Zn conditions. (a)The Zn:P content of coccolithophore *E. huxleyi* under similar trace metal conditions is shown for comparison; (b) Variation in the Zn:P of natural phytoplankton assemblage (no Fe, no Zn) of the Southern Ocean with added (+) Fe and (+) Zn ; (data from (Cullen et al. 2003)) ……165

Figure 5.9: Zinc isotope fractionation by *P. antarctica* grown under high and low Fe and Zn conditions …… 172

Figure 5.10: (a) Zinc isotope fractionation and (b) Zn:P ratio of *P. antarctica* cultured at a range of Fe' concentrations (data from Grün 2016) ……172

Figure 5.11: Schematic diagrams of alternate hypothesis hypothesis for observed heavy Zn isotopic composition of P. antarctica under Fe limiting (-Fe) conditions. (a) Release of isotopically light Zn in the late-exponential phase of growth in the Fe limited treatments due to cells being less robust than Fe replete (+Fe) treatments. (b) Uptake of isotopically heavy Zn by divalent surface Fe transporters in an attempt to scavenge Fe under Fe limiting conditions. In both senarios (a and b), lighter isotope of Zn is taken up by the cells in the Fe replete treatments…… 173

Figure 5.12: Profile of dissolved δ^{66}Zn versus depth, for process stations P1, P2 and P3 along with corresponding water masses (viz. Sub Antarctic Mode Water, Antarctic Intermediate Water and Circumpolar Deep Water) and the global deep ocean δ^{66}Zn average value…… 176

List of Tables

Table 1.1: Location of the three PINT stations sampled for Zn isotope analysis……16

Table 2.1: Procedural steps involved in (a) extraction and (b) purification of dissolved Zn from seawater……..42

Table 2.2: Isobaric, doubly-charged and polyatomic interferences on Zn isotopes of interest……...45

Table 2.3: The cup configuration of the Thermo Finnigan Neptune Plus for Zn isotope determination……45

Table 2.4: (a) Comparing variations in δ^{66}Zn (‰) for a deep seawater sample preconcentrated by Solvent extraction (using APDC and DDC as chelating agent) and Solid phase extraction (using Toyopearl AF Chelate 650M resin); (b) Comparing variations in δ^{66}Zn (‰) for another deep seawater sample (1500 m) loaded onto Toyopearl AF Chelate 650M resin using different sample loading buffers, MOPS buffer and ammonium acetate plus ammonium hydroxide buffer ……48

Table 2.5: Concentration and isotopic composition of Zn inter-calibration samples…… 53

Table 2.6 (Chapter Appendix): Preparation of ^{67}Zn-^{68}Zn Double Spike……56

Table 3.1: Dissolved Zn isotope composition and concentration data for the process stations P1, P2 and P3 ……..85-88

Table 4.1: Effect of Zn on specific growth rates and cell morphology of *E. huxleyi* cultured across a range of free Zn^{2+} ion concentrations ……119

Table 4.2: Effect of Zn photophysiological parameters (± 1 x S.D.) of E. huxleyi cultured across a range of free Zn^{2+} ion concentrations……124

Table 4.3: Zn uptake and Zn isotope fractionation by *E. huxleyi* cultured accross a range of free Zn^{2+} ion concentrations……..126

Table 4.3 (Chapter Appendix): Zn isotope fractionation by *E. huxleyi* across a range of free Zn^{2+} ion concentrations. $\Delta^{66}Zn$ relates Zn isotope composition of cells relative to the media. The Zn isotope composition of the Zn added to the culture media is 0.06 ± 0.01 relative to the standard reference material (SRM) used to calculate $\delta^{66}Zn_{cells}$. Since the isotopic composition of the Zn added is similar to the SRM, no correction was made and the values for $\Delta^{66}Zn_{(cell\text{-}media)}$ reported in the chapter is essentially $\delta^{66}Zn_{cells}$. The corrected $\Delta^{66}Zn_{(cell\text{-}media)}$ are reported here by subtracting 0.06 from $\delta^{66}Zn_{cells}$ ……135

Table 5.1: Photosynthetic parameters calculated by the LIFT-FRRF……151

Table 5.2: The specific growth rates of *P. antarctica* grown under high and low Fe and Zn conditions…… 158

Table 5.3: Effect of Fe and Zn limitation on cell morphology of *P. antarctica* ……..160

Table 5.4. Effect of Fe and Zn limitation on Chlorophyll *a* concentration and photophysiological parameters of *P. antarctica*…… 163

Table 5.5: Effect of Fe and Zn limitation on cellular Zn and P incorporation of *P. antarctica* …… 165

Chapter 1:

Introduction to marine zinc biogeochemistry and PhD thesis proposal

1.1. Biological importance of zinc in phytoplankton

Marine phytoplankton are primary producers and form the base of the food chain. Of all primary productivity on earth, they account for about more than 40 % of the total (Falkowski 1994; Field et al. 1998). Thus, they play an important role in moderating the climate through the sequestration of carbon dioxide (CO_2) by photosynthesis followed by export of carbon to the deeper ocean. The trace metal micronutrient zinc (Zn) acts as the central metal in many enzymes within marine phytoplankton and so has a significant role in controlling the oceans primary production.

A major use of Zn by phytoplankton is in the enzyme carbonic anhydrase (CA) which catalyses the reversible hydration of carbon dioxide to bicarbonate and H^+ ion. This rapid conversion helps concentrate CO_2 in phytoplankton chloroplasts, necessary for efficient photosynthesis (Badger and Price 1994). Therefore this enzyme is critical to CO_2 transport and fixation by phytoplankton (Christianson and Fierke 1996; Hopkinson et al. 2011; Morel et al. 1994; Sunda and Huntsman 2005).

A probable model of how CA acts as a part of carbon concentrating mechanism (CCM) in diatoms was proposed by Hopkinson et al. (2011), (Figure 1.1). The diatom cell membrane is highly permeable to the non-polar molecules like CO_2 and O_2 but the permeability is reduced for charged species like the HCO_3^- molecule. Since the concentration of CO_2 is low in seawater, the extracellular CA, when present, converts

the abundant HCO_3^- to CO_2 which can then diffuse into the cytoplasm (Milligan and Morel 2002). Within the cytoplasm this CO_2 is then converted back to HCO_3^- to prevent the CO_2 from escaping back to the bulk seawater medium. From the cytoplasm HCO_3^- is actively transported across the chloroplast membrane into the chloroplast. Inside the chloroplast, HCO_3^- is converted back to CO_2 by CA so that it can be fixed by the enzyme ribulose-1, 5-bisphosphate carboxylase-oxygenase (RubisCO). The CO_2 that diffuses back into the cytoplasm from the chloroplast is recovered and converted back to HCO_3^- by the CA in cytoplasm. According to Hopkinson et al. (2011), the presence of the pyrenoid (an organelle within the chloroplast where the CO_2 fixating enzyme is located) increases the efficiency of CCM (Figure 1.1 (b)). Since CA is confined within the pyrenoid there is little if any interconversion of HCO_3^- and CO_2 within the chloroplast, thus HCO_3^- can diffuse passively from the chloroplast into the proteinaceous pyrenoid where it re-equilibrates. In the pyrenoid the CO_2 concentration is raised and is adequate for organic carbon production by RubisCO (Hopkinson et al. 2011). The high CA requirement for CCM highlights the importance of Zn in carbon acquisition by diatoms.

Another important enzyme containing Zn as cofactor is alkaline phosphatase. It is required by phytoplankton to acquire organic forms of phosphorous (Kuenzler and Perras 1965). Other Zn containing enzymes in phytoplankton include RNA polymerase, tRNA synthetase, reverse transcriptase, carboxypeptidase and superoxide dismutase ((Twining and Baines 2013) and references therein).

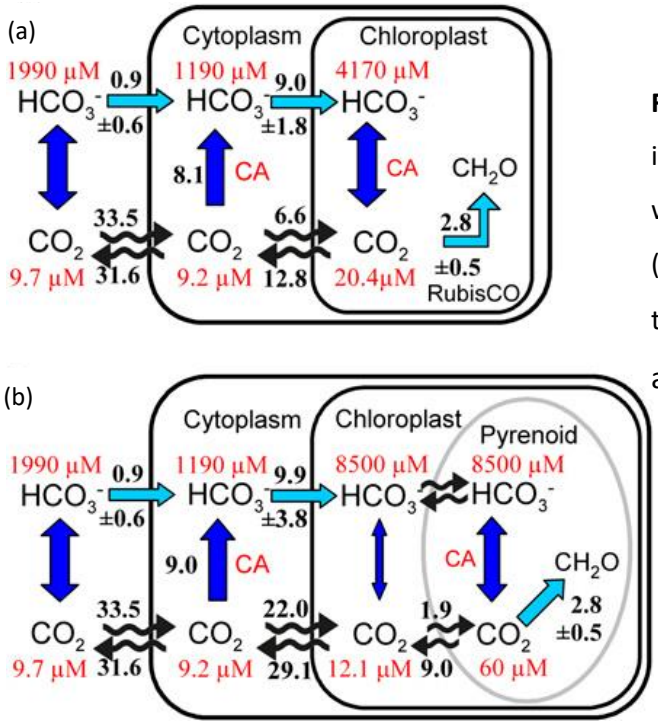

Figure 1.1: (a) The possible role of CA in carbon concentration mechanism within a diatom cell (*P. tricornutum*). (b) The role of Pyrenoid in increasing the efficiency of CCM (Hopkinson et al. 2011).

1.2. Zinc biogeochemistry

In seawater, the distribution of dissolved Zn is nutrient like with depletion in surface waters and higher concentrations at depth. The structure of the dissolved Zn concentration versus depth profile is similar to that of silicate with deeper regeneration relative to that other micro and macro nutrients (nitrate and phosphate; Figure 1.2), suggesting that Zn may be involved in either the uptake or the formation biogenic silica structures (opal) (Bruland et al. 1994; Hunter and Boyd 1999).

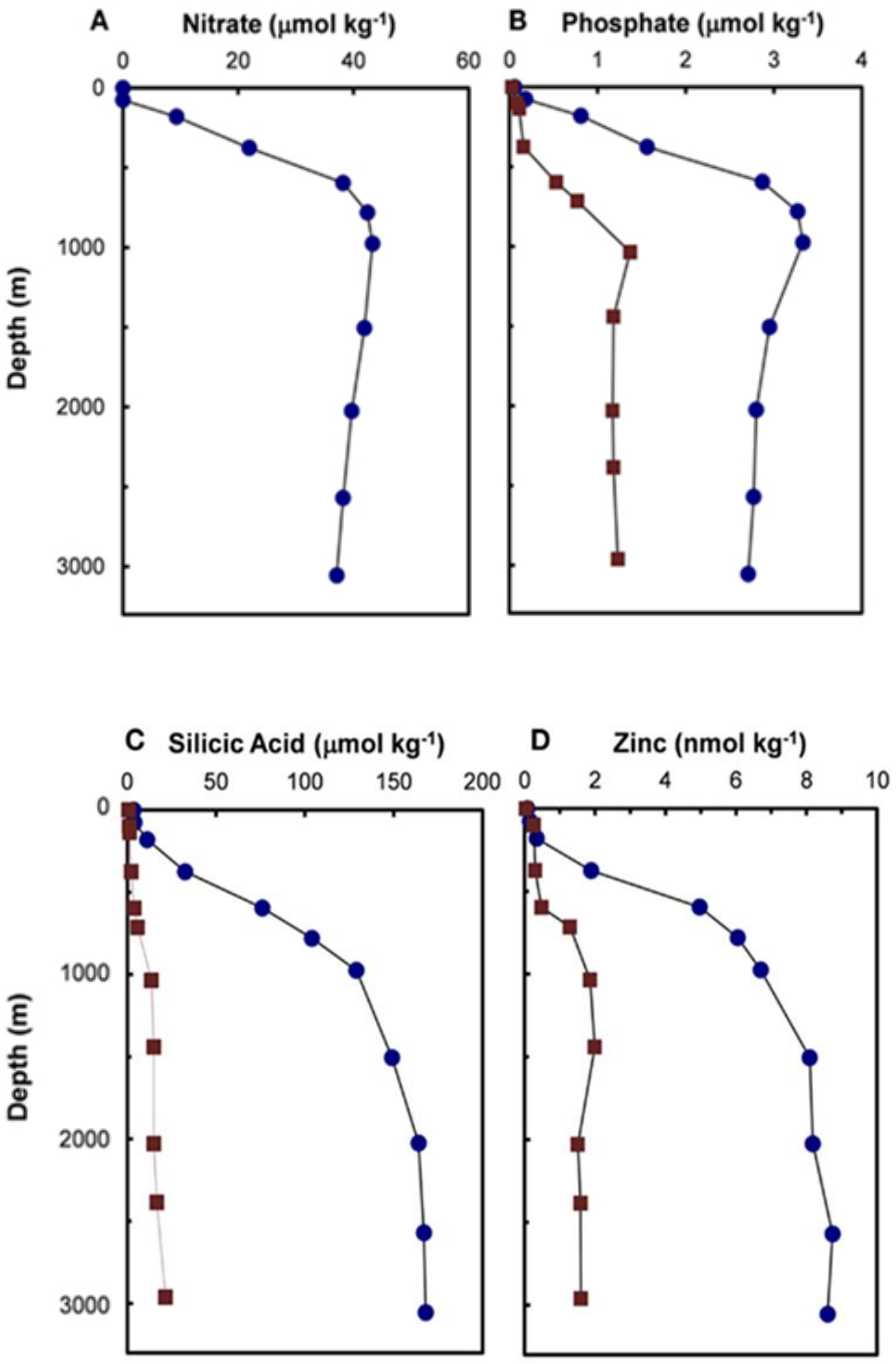

Figure 1.2: Concentration profiles versus depth of dissolved (A.) Nitrate, (B.) Phosphate, (C.) Silicic acid and (D.) Zn in the central North Pacific Ocean (blue circles) and North Atlantic (red squares). Figure adapted from (Sunda 2012).

Rueter and Morel (1981) observed that silicic acid uptake velocities for the marine diatom *T. pseudonana* were higher for cultures grown at higher Zn concentration. The uptake of silicic acid behaved in a similar way to the activity of alkaline phosphatase, a Zn dependent system. Silicic acid uptake rate and alkaline phosphatase activity were reduced when the free Zn^{2+} activity of the culture medium was reduced (Rueter and Morel 1981). This observation suggests that Zn might mediate the uptake of silicon in diatoms through a Zn dependent silicon transporter (Rueter and Morel 1981).

Zinc, present as cofactor of the enzyme carbonic anhydrase, acts as a Lewis acid in the catalytic conversion of carbonic acid to CO_2. An oxygen atom of the carbonic acid donates its electron pair (via co-ordination bond) to the Zn atom thereby facilitating nucleophilic attack on the carbon atom bound to the oxygen atom. Silicic acid being analogous to carbonic acid may undergo similar nucleophilic attack on silicon atom in presence of a Lewis acid such as Zn (Sherbakova et al. 2005). In 2005, Sherbakova et al., proposed a model in which Zn^{2+} ion is chelated by the conserved motif of diatom silicon transporters, SITs CMLD, to form a ternary complex with silicic acid (Grachev et al. 2005; Sherbakova et al. 2005). Thamatrakoln and Hildebrand (2008) tested this idea using a Zn specific membrane permeable chelator TPEN [N, N,N',N-tetrakis(2-pyriddylmethyl)ethylenediamine] at 10 fold molar excess to try and remove Zn from the SITs CMLD motif. However, they did not see any change in silicic acid uptake rates, but did note low free Zn^{2+} concentration inhibits growth of the cultures. These cultures could be revived through the addition of Zn which suggests that Zn limitation did not inhibit silicon uptake by SITs (Thamatrakoln and Hildebrand 2008). Danilovtseva et al., (2009) observed that the synthetic polymer PVA (poly vinyl amine), in the presence of Zn^{2+} ions, could absorb silicic acid from the surrounding media. The polymer was not

active in silicic acid absorption on its own or in presence of Cu^{2+}, Fe^{2+}, Ni^{2+}, Co^{2+}, Cd^{2+} and Mn^{2+} ions. Contrastingly when PVI (poly vinyl imidazole) was substituted for PVA, it did not show any silicic acid absorption. This results from PVI being less basic than PVA and q-PVI (poly 3-methyl-1-vinyl-imidazole-3-ium bromide) having a cationic group are not able to form complexes with Zn^{+2} ions. These results suggested a possibility of complexed Zn^{2+} ions within SITs playing a role in assimilating silicon in SITs (Danilovtseva et al. 2009).

However, it is interesting to note that biogenic silica does not appear to be a significant export vector of Zn from the surface to the deep ocean as the diatom frustule only contain 1-3 % of the total Zn associated with the cell (Ellwood and Hunter 2000). Zhao et al. (2014) argued that Zn, which has a strong affinity for amino and carboxylic group, is associated with the polysaccharide and/or protein coating of the diatom frustule (Gelabert et al. 2006; Zhao et al. 2014). Thus, this organic phase which is intimately associated with the opal phase, is oxidised only after dissolution of the opal phase occurs; which could potentially result in a deeper Zn regeneration profile, like that of silicate. John and Conway (2014), proposed that the deeper regeneration of Zn at a depth similar to silicate might be due to the scavenging of Zn onto the surface of sinking phytoplankton. John and Conway (2014), hypothesised that the Zn released from the disintegrating phytoplankton is scavenged back onto sinking particulate organic matter which is released at depth. It has also been suggested that in the iron limited regions of the world ocean, which includes large parts of the Southern Ocean, subarctic Pacific and northeast Pacific Ocean there is preferential biological uptake (by diatoms) of Zn and silicate compared to nitrate and phosphate which could lead to similar Zn and silicate concentration profiles in these regions (Sunda and Huntsman

2000). Vance et al. (2017) suggested that despite Zn and silicate being in different components of the diatom cell, is transported below the mixed layer in the deep Southern Ocean. As these water masses are laterally transported to the rest of the world oceans the biogeochemical signature of these two elements are also exported. This hypothesis was also supported by model simulations (Vance et al. 2017).

In natural aquatic environments, the interaction between phytoplankton and Zn is complex and depends on the concentration of Zn and its chemical speciation both of which affect Zn availability to phytoplankton. Also different phytoplankton species differ in their requirement for Zn and their response to Zn limitation and toxicity (Anderson et al. 1978).

In seawater the free Zn^{2+} ion concentration is highly dependent on Zn complexation to natural organic ligands which determines Zn bioavailability (Anderson et al. 1978; Ellwood 2004; Ellwood and Van den Berg 2000; Sunda and Huntsman 1992). In the surface waters of the open ocean, approximately 98% of dissolved Zn is bound to strong organic ligands (Bruland 1989; Ellwood 2004; Ellwood and Van den Berg 2000; Jakuba et al. 2012; Sinoir et al. 2016b) with the remaining dissolved Zn available for uptake by phytoplankton. In the Southern Ocean, where there is upwelling of Zn rich waters the dissolved Zn concentration was in excess of the ligand concentrations (Baars and Croot 2011). The chemical species of Zn available for uptake by phytoplankton is the free Zn^{2+} ion (Anderson et al. 1978). However, it has been suggested that Zn bound to weak complexes are bioavailable to the phytoplankton to some extent (Xu et al. 2012). In some parts of the surface ocean, the free Zn^{2+} concentration can be in the low picomolar range. It has been suggested that Zn could limit phytoplankton growth and influence the global carbon cycle by influencing the

air-sea CO_2 exchange (Anderson et al. 1978; Brand et al. 1983; Sunda and Huntsman 1992).

1.3. Zn isotopes and isotope fractionation

Zinc has five naturally occurring stable isotopes: ^{64}Zn, ^{66}Zn, ^{67}Zn, ^{68}Zn and ^{70}Zn with natural abundances of 48.6%, 27.9%, 4.1%, 18.8% and 0.62%, respectively (Rosman 1972). Zinc isotopic fractionation is the process whereby one isotope becomes enriched or depleted relative to a standard. Processes that can lead to isotope fraction can be physical, biological or chemical in nature (Bermin et al. 2006; Johnson et al. 2004; Pichat et al. 2003; Rosman 1972). These isotopic fractionation processes can be under kinetic or equilibrium control (Stewart 1975). It is represented by the following equation

$$\left[\ \delta^{66}Zn‰ = \frac{([^{66}Zn/^{64}Zn]_{Sample} - [^{66}Zn/^{64}Zn]_{Zn\text{-}standard})}{[^{66}Zn/^{64}Zn]_{Zn\text{-}standard}} \times 1000\ \right] \quad \ldots (1.1)$$

Where, $\delta^{66}Zn$ ‰ is the relative deviation of the ^{66}Zn:^{64}Zn ratio of the sample with respect to a Zn standard (normally JMC Lyon Zn standard); expressed in parts per 1000.

Isotopic fractionation of Zn isotopes in the natural waters can occur as a result of variety of process, including complexation with organic ligands (Jouvin et al. 2009), biological uptake (Gelabert et al. 2006; John et al. 2007), and particle scavenging (John and Conway 2014). Therefore, knowing the potential processes that can lead to Zn isotope fractionation may facilitate its use as a biogeochemical tracer for oceanographic research.

An example of biological processes leading to Zn isotopic fractionation has been observed in the marine diatom *Thalassiosira oceanica* and the chlorophyte *Dunaliella tertiolecta* (John and Conway 2014; John et al. 2007) where, during Zn uptake the lighter isotope, ^{64}Zn, was preferentially taken up leading to a lower Zn isotope composition within the cells relative to the media. Adsorption of Zn onto diatom cell surface has shown to lead to heavier isotopic composition (Gelabert et al. 2006; John et al. 2007). Quantum mechanical calculations suggest that more strongly bounded species prefer heavier isotopes (Criss 1999); therefore tetrahedral complexes with shorter bonds would be concentrated in ^{66}Zn as compared to octahedral complexes. The carboxylate species in the external polysaccharide layer of the diatom cell wall or protein side chains which form tetrahedral complexes with Zn^{2+} was shown, using 'FITEQL thermodynamic modelling', to be the dominant group in Zn^{2+} adsorption to the diatom cell surface which explains the preferential adsorption of ^{66}Zn relative to ^{64}Zn from the aqueous solution in which Zn^{2+} forms octahedral complexes with H_2O molecule with longer Zn-O bond (Gelabert et al. 2006). Modelling of Zn isotope fractionation for co-existing Zn inorganic complexes in solution shows that Zn carbonate and bicarbonate complexes are isotopically heavy, whereas, Zn chloride complexes tend to be isotopically light (Fujii et al. 2014). However, Zn isotope fractionations of Zn hydroxide and sulphate complexes are negligible at pH ≥ 8.1. This leads to an estimated negative $\delta^{66}Zn$ value for the free Zn^{2+} relative to the bulk solution, though isotope fractionation is small (Fujii et al. 2014). In the open oceans >98% of dissolved Zn is bound to strong organic ligands so the remaining dissolved Zn available for uptake by diatoms is lighter. The diffusion of the lighter ^{64}Zn is also faster than that of ^{66}Zn, which will result in isotopic fractionation, enrichment of ^{64}Zn within

phytoplankton cells, even at low free Zn^{2+} concentrations (Bruland 1989; John et al. 2007). However, in a recent study looking at the effect of bioavailable Fe in Zn isotope fractionation by diatoms, Köbberich and Vance (2017) reported heavier Zn isotopic composition within the cells of the diatom species *Chaetoceros* at low bioavailable Fe concentration. At this limiting bioavailable Fe concentrations, the diatom grew at less than 60% of its maximum growth rate at ambient Fe concentration (Köbberich and Vance 2017) . The possible explanations put forward by Köberrich and Vance (2017), for the observed heavy Zn isotope composition of *Chaetoceros* species at low bioavailable Fe concentrations are: (a) scavenging of heavy Zn by extracellular polymeric substances, and (b) slow Zn uptake rate leading to pseudo-equilibrium conditions at the transporter site where more stable surface complexes are formed with heavy Zn isotopes. However, for the diatom *T. oceanica* no such effect was observed and the diatom preferentially incorporated the lighter isotope of Zn even at very low bioavailable Fe concentration, although its growth was reduced by 50% of its maximum growth rate (Köbberich and Vance 2017).

Peel et al. (2009) reported that in a eutrophic lake, the Zn isotope composition of the settling particles were the lightest in the productive period and this Zn was chiefly associated with organic matter. This observation suggested that lighter Zn was preferentially taken up by phytoplankton (Peel et al. 2009).

Zinc isotope composition of ferromanganese (Fe-Mn) nodules ($\delta^{66}Zn$ = 0.90 ± 0.28 ‰; (Maréchal et al. 2000)), deep sea carbonates ($\delta^{66}Zn$ = 0.91 ± 0.24 ‰; (Pichat et al. 2003)) diatom opal ($\delta^{66}Zn$ = 1.03 ± 0.19 ‰; (Andersen et al. 2011)) and hexactinellid sponge spicules ($\delta^{66}Zn$ = 0.47 ± 0.27 (Hendry and Andersen 2013) were speculated to

record the Zn isotope signature of the seawater in which they were formed assuming no or little isotopic fractionation relative to the seawater. On the contrary, Zn isotope composition of demosponge spicule showed a wide range (δ^{66}Zn = -0.35 to 1.04 ‰; (Hendry and Andersen 2013)). This variation was theorised to be due to Zn isotope fractionation during internalisation of Zn from the particulate organic matter (POM) they feed on coupled with the wide range of Zn isotope composition of the POM (Hendry and Andersen 2013). It has also been suggested that the heavier Zn isotopic composition of seawater, reflected in the Fe-Mn nodules, biogenic carbonate and opal, could be due to uptake of lighter Zn by phytoplankton making the seawater dissolved Zn heavier (Andersen et al. 2011; Hendry and Andersen 2013; Pichat et al. 2003).

Zn isotope has also been used in geological record to determine resumption of primary production and hypothesise on the important sinks of Zn in the post-Marinoan ocean (John et al. 2017b; Kunzmann et al. 2013). Measurements of Zn isotopes in a Neoproterozoic Nuccaleena cap dolostone, which serves as a proxy for past surface ocean Zn isotope composition, suggest that there was immediate resumption of primary production after snowball earth (Kunzmann et al. 2013). Heavier δ^{66}Zn value (0.8 to 0.98 ‰) in the uppermost dolomite beds is proposed to be a result of removal of light Zn by biological material (John et al. 2017b; Kunzmann et al. 2013).The variations in δ^{66}Zn of the cap dolostone (δ^{66}Zn = 0.1 to 1.0 ‰) is explained by varying significance of biological and sulphidic sink for Zn in the post-Marinoan ocean (John et al. 2017b). However, John et al. (2017b), propose that Zn isotope fractionation is not expressed during removal of Zn as sulphides while removal of Zn with biological material (combination of scavenging and uptake) is suggested in a quantitative model. The lack of obvious Zn isotope fractionation due to Zn sulphide precipitation, even

though there may be an instantaneous isotope effect, could be attributed to closed-system behaviour where all of the Zn is precipitated in the presence of sulphide (John et al. 2017b).

However, until recently, only a few studies have investigated Zn isotope fractionation by phytoplankton and the evidence relating Zn isotope variations in the ocean due to biological activity has been weak. Measuring the dissolved Zn isotope composition is challenging due to contamination issues associated with the collection and handling of samples, the small range of isotope fractionation in natural waters, and the low Zn concentrations in surface waters. Advancements in analytical technique, including development of new generation resins for pre-concentration of trace metals from large volumes of seawater without introducing significant blank, along with the advent of the multi-collector inductively coupled plasma mass spectrometry (MC-ICPMS) have made it possible to measure the isotope composition of dissolved Zn. Recent studies have shown that the Zn isotope composition of the deep water is remarkably homogeneous with a δ^{66}Zn value of ~0.5 ‰ (excluding data near hydrothermal sources and (margin) sediments which has lighter Zn isotopic composition) (Andersen et al. 2011; Bermin et al. 2006; Boyle et al. 2012; Conway and John 2014; Conway and John 2015; Conway et al. 2013; Little et al. 2014; Little et al. 2016; Zhao et al. 2014). Whereas, the δ^{66}Zn of upper water shows large variability; heavier dissolved Zn in the surface ocean is associated with uptake of light Zn by phytoplankton and lighter dissolved Zn is attributed to scavenging of heavy Zn by sinking organic matter and/or release of light Zn from degrading phytoplankton (references as above).

The GEOTRACES programme, which is ‘an international study of the marine biogeochemical cycles of trace elements and their isotopes’, over the last decade also

facilitated access to wide range of seawater samples and enhanced our understanding of Zn isotope system in the ocean.

Despite the recent advancement and measurements of Zn isotopes in the marine realm, our knowledge of Zn isotope biogeochemistry is still limited. Little et al.(2014; 2016) put forward the oceanic mass balance of Zn isotopes compiling the isotopic composition of the different input sources (rivers, dust, hydrothermal fluids, and benthic) and output sinks (sediments including margin sediments, Fe-Mn oxides, biogenic carbonates and silicates (opal)) along with their estimated magnitude for the exchange fluxes between reservoirs (Figure 1.3). Most input sources have a Zn isotopic composition close to the lithogenic value of ≤0.3‰ which is lighter than the deep ocean (~0.5 ‰). This suggests that there are processes in the ocean that fractionates Zn making the isotopic composition of dissolved Zn heavier. The output sinks, except for margin sediments, are isotopically much heavier, suggesting that there is a large isotopically light Zn sink that is missing (Conway and John 2014; Little et al. 2014; Little et al. 2016). In a recent study by (Vance et al. 2016), which analysed Zn isotope composition of seawater and sediments in the Black Sea, it is reported that the Zn isotopic composition of sediments is significantly lighter than the anoxic water above $\Delta^{66}Zn_{\text{(anoxic deep water – euxinic sediment)}}$ = 0.6 ‰. Across the redoxcline in the Black Sea water column, there is a shift in Zn speciation from oxide to sulfide species leading to partitioning of the light Zn isotopes into these sulphide species. The partial removal of Zn sulphides from the dissolved pool results in heavier deep water and lighter sediment Zn isotope signature (Vance et al. 2016). Vance et al. (2016) , hypothesise that a similar process, that is, sequestration of isotopically light Zn to sulphides, in pore waters within organic rich sediments and release back of residual heavy Zn to the

seawater could explain the heavy Zn isotope composition of the deep ocean (Figure 1.3).

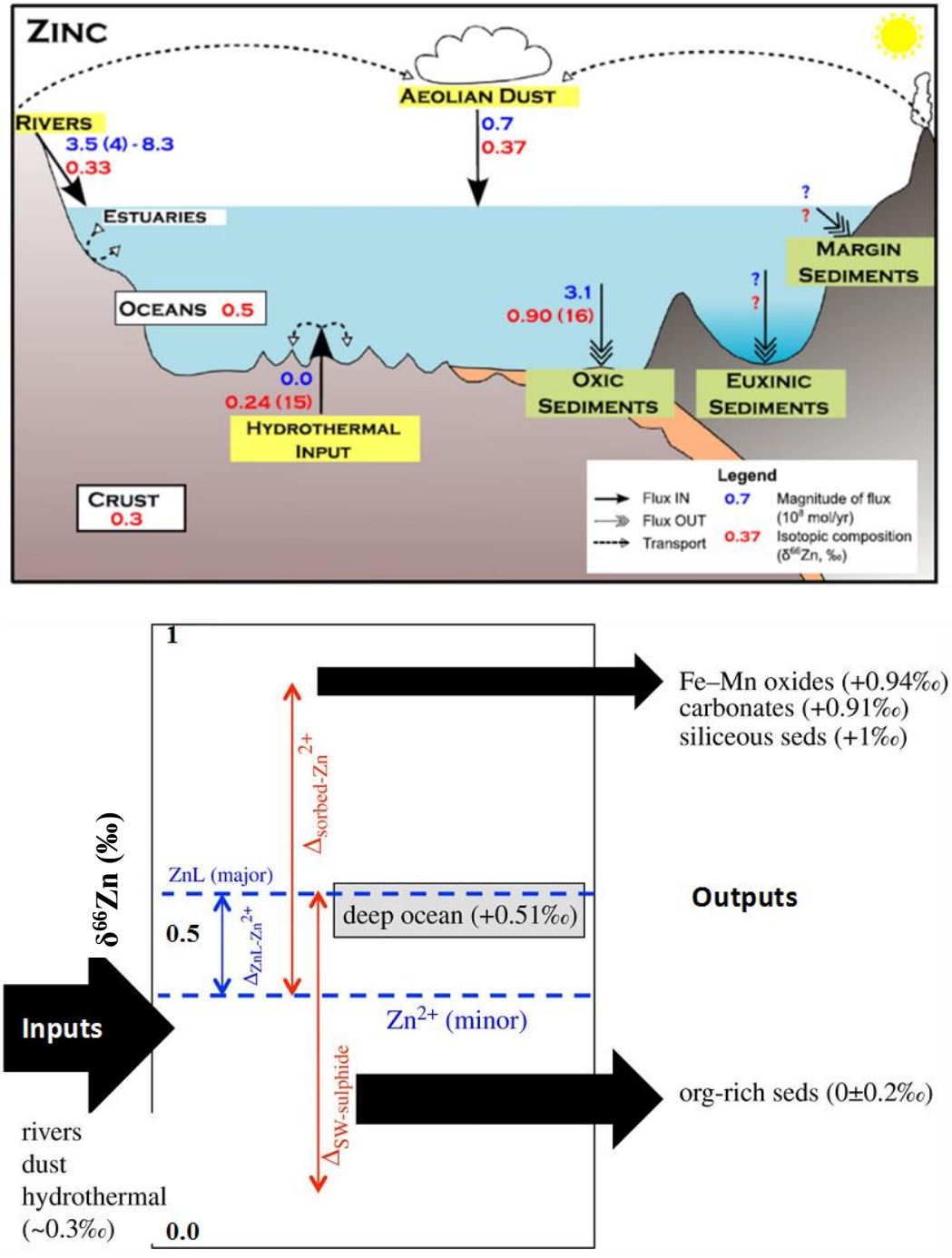

Figure 1.3: Schematic diagrams showing the Zn isotope mass balance in the global ocean with the inputs sources and outputs sinks in the ocean. The Zn isotope compositions of the lithogenic and seawater reservoirs are 0.3 (‰) and 0.5 (‰) respectively. Figures adapted from (Little et al. 2014) and (2016; Vance et al. 2016).

1.4. Thesis aims and approach

The aim of this thesis is to determine the processes that influence the Zn cycling in the ocean and examine the role Zn plays facilitating marine primary production using Zn isotope composition of marine samples.

To understand the processes that lead to isotopic fractionation of Zn in the marine environment, measurement of the Zn isotopes in different oceanographic domains and in different phytoplankton species are necessary. My research focuses in understanding Zn isotopic fractionation in the surface ocean due to Zn uptake by marine phytoplankton. To achieve this goal, I had to first, develop a method to measure the dissolved Zn isotope composition. Once achieved, analysis of dissolved Zn isotope composition was then made on seawater samples collected from chemically distinct oceanographic regions in the Tasman Sea, SW Pacific Ocean (Figure 1.4 and Table 1.1). This was complemented with measurements of Zn isotope fractionation by phytoplankton cultured under environmentally relevant condition.

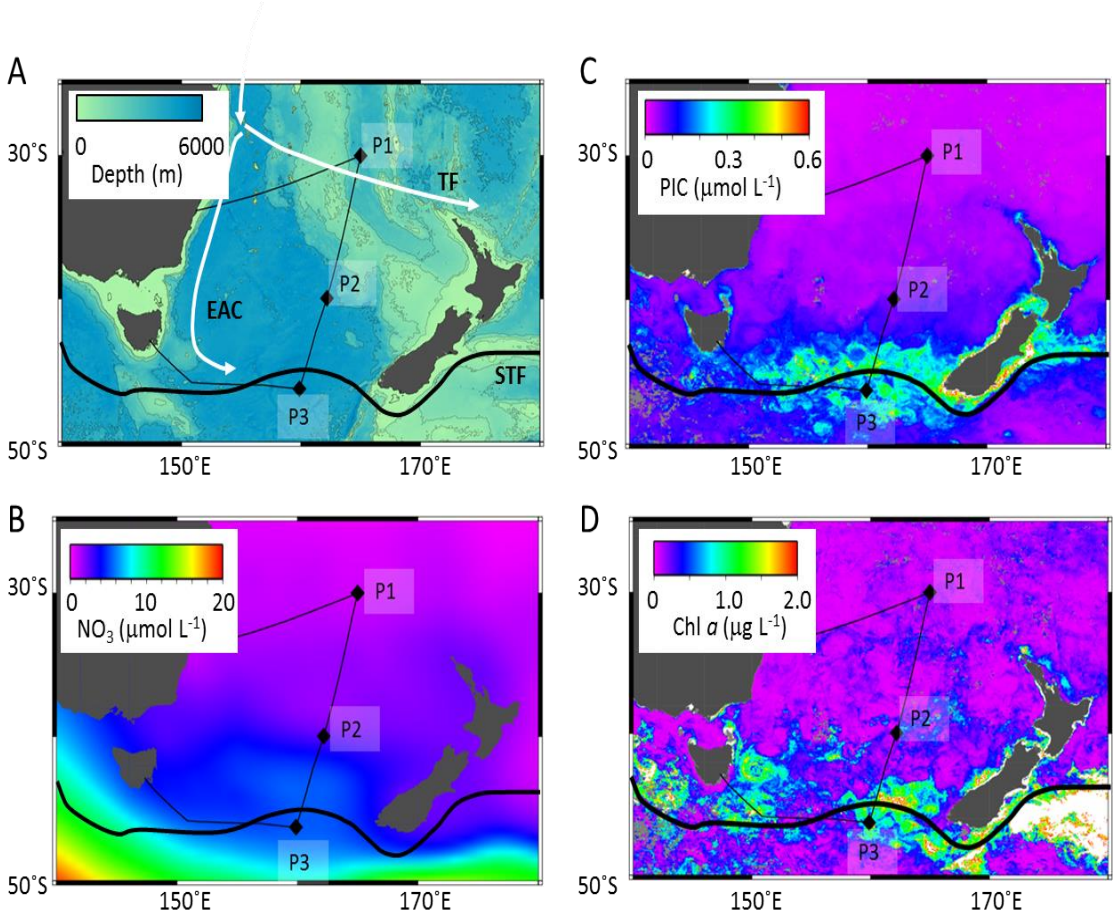

Figure 1.4: Maps of A. Seafloor bathymetry; B. Surface nitrate concentration; C. Particulate inorganic carbonate (PIC) concentration and; D. Chlorophyll *a* concentration. Nitrate concentration data was extracted from the electronic version of the World Ocean Circulation Experiment database compiled by Schlitzer (2006). Surface chlorophyll and PIC data were extracted from the Aqua MODIS dataset via ERDDAP at NOAA (upwell.pfeg.noaa.gov/erddap/). The chlorophyll and PIC datasets cover the January-February sampling period during the 2010 PINTS voyage. P1, P2 and P3 denote the three process stations from which samples were collected for the dissolved Zn isotope work. The abbreviations EAC, TF and STF correspond to East Australian Current, Tasman Front and Subtropical Front, respectively.

Table 1.1: Location of the three PINT stations sampled for Zn isotope analysis.

Station ID	Latitude (S)	Longitude (E)
P1	30.0	165.0
P2	39.6	162.1
P3	46.2	159.5

1.5. Thesis structure

The main chapters in this thesis are as follows:

In Chapter 2, I describe the method developed for determining the isotopic composition of dissolved Zn in seawater by MC-ICP-MS using a ^{67}Zn–^{68}Zn double spike.

In this chapter, I document the mathematical and analytical procedures involved in determining the dissolved Zn isotopic composition of seawater using the double spike technique. The reproducibility and precision of this procedure along with the measurements of GEOTRACES IC1 BATS and SAFe inter-calibration samples is reported.

In Chapter 3, I detail the dissolved Zn isotope profiles measured for the three biogeochemically distinctive sites in the Tasman Sea (Figure 1.4 and Table 1.1).

Seawater samples were collected as part of a 2010 GEOTRACES process study along a transect contrasting the nutrient poor, low productivity waters of north Tasman Sea with the highly productive south Tasman Sea which has intermediate nutrient concentration (Hassler et al. 2014). While the north Tasman Sea site is influenced by the East Australian Current (EAC) which is associated with warm, saline, low oxygen water originating from the Coral Sea region, the south Tasman Sea site is characterised by the cool, fresh, oxygen rich waters which have Southern Ocean origin (Sokolov and Rintoul 2000). During the sampling period, the north Tasman Sea site was dominated by prokaryotic phytoplankton like cyanobacteria: Prochlorococcus, Synechococcus and diazotrophs; which have low Zn requirement (Brand et al. 1983; Saito et al. 2002). Southern waters were dominated by eukaryotic plankton (Hassler et al. 2014). There

was a coccolithophore bloom at the south Tasman Sea site during sampling period which is corroborated by the Aqua MODIS calcite map.

In this chapter, I have explored the relationship between the dissolved Zn isotope composition of the surface waters and the resident phytoplankton community structure. Seasonality in Zn isotope fractionation in surface waters of the north Tasman Sea site is also discussed. Finally, I speculate on the relationship between the dissolved Zn and silicon isotopes in the deep ocean.

In Chapter 4, I examine the Zn isotope fractionation by a Tasman Sea isolate of cosmopolitan coccolithophore *Emiliania huxleyi* (CS-1016); cultured across a range of free Zn^{2+} ion concentrations encompassing the range observed in the world oceans. Coccolithophores are marine phytoplankton species which produce calcium carbonate plates, thus they are important in the transport of both organic and inorganic carbon to the ocean's interior. They are one of the major primary producers and are widespread across the global oceans. Thus, understanding the influence of Zn on *E. huxleyi,* a globally significant species, is important.

This work also complements the dissolved Zn isotope results of the surface waters at the south Tasman Sea site. I have further analysed the influence of Zn on growth of *E. huxleyi* specifically, specific growth rates, cell morphology and photophysiological parameters.

In Chapter 5, I investigate the effect of Fe and Zn limitation on growth (specific growth rates, photophysiology and cell morphology), Zn uptake and Zn isotope fractionation of the Southern Ocean haptophyte P*haeocystis antarctica*.

The south Tasman Sea is characterised by water masses which has Southern Ocean origin (Sokolov and Rintoul 2000). The Southern Ocean connects the Atlantic Ocean, the Indian Ocean and the Pacific Ocean (Talley 2013). It also plays a crucial role in controlling many global oceanic processes which are reflected in other parts of the global ocean (Sarmiento et al. 2004; Sloyan and Rintoul 2001). Thus the Southern Ocean significantly influences both ocean circulation and biogeochemistry and plays an important role in the global carbon cycle (Sarmiento et al. 1998). To understand Zn isotope biogeochemistry in the Southern Ocean, measuring Zn isotope fractionation by Southern Ocean phytoplankton under relevant conditions is important. The haptophyte *Phaeocystis antarctica* form a major component of the Southern Ocean phytoplankton assemblage (Arrigo et al. 1999). Since large parts of the Southern Ocean are iron limited potentially limiting phytoplankton growth (Boyd et al. 2000; Martin 1990), I investigated Zn accumulation and Zn isotope fractionation by *P. antarctica* under Fe limiting conditions.

In the final concluding chapter, I discuss the important conclusions of this thesis and the future directions.

Chapter 2:

A method for determining the isotopic composition of dissolved zinc in seawater by MC-ICP-MS with ^{67}Zn-^{68}Zn double spike.

Moneesha Samanta, Michael J. Ellwood and Graham E. Mortimer[1]

Abstract

The biogeochemical cycling of dissolved zinc (Zn) in seawater is dominated by biological uptake in the surface ocean and its regeneration at depth leading to a large concentration gradient between the surface and deep ocean. The advent of multi-collector inductively coupled mass spectrometry (MC-ICP-MS) provides the marine community with a new way of probing the biogeochemical Zn cycle through changes in its isotope composition. In this chapter, we document the mathematical and analytical procedures involved in determining the dissolved Zn isotopic composition of seawater using the double spike (DS) technique. Seawater samples were spiked with a ^{67}Zn-^{68}Zn DS before processing. Measurement of Zn by the MC-ICPMS requires the sample to be free of the seawater matrix and other interfering elements; for this purpose, Toyopearl AF-Chelate 650M and AG1X8 resins were used to pre-concentrate Zn from seawater and separate it from major cations and anions. The optimum pH range for loading Zn for affinity chromatography was between 5 and 8. After pre-concentration, Zn was purified from other trace element by anion exchange chromatography. The reproducibility of the procedure was excellent for a deep seawater sample [6.55 ± 0.34

[1] Authors' contribution: M.S. developed the method with assistance from G.E.M., and drafted the manuscript with contribution from M.J.E.

nmol L^{-1} and 0.59 ± 0.02 ‰ (n = 9) w.r.t JMC-Lyon] and a shallow seawater sample [0.05 ± 0.01 nmol L^{-1} and 0.08 ± 0.02 ‰ (n = 3). w.r.t JMC- Lyon] analysed over a period of one year. Analysis of GEOTRACES IC1 BATS and SAFe inter-calibration samples produced data in good agreement with data published by other groups.

2.1. Introduction

Zinc acts as cofactors in many important enzymes within marine phytoplankton and hence plays a significant role in controlling the biology of oceans (Morel and Price 2003). Thus, changes in its bioavailability may influence biological production and hence the marine carbon cycle. Isotopic fractionation of Zn isotopes in the natural waters can occur as a result of a variety of process, including complexation with organic ligands (Jouvin et al. 2009), biological uptake (Gelabert et al. 2006; John et al. 2007), and particle scavenging (John and Conway 2014). Therefore, knowing the potential processes that can lead to Zn isotope fractionation may facilitate its use as a biogeochemical tracer for oceanographic research.

The mass dependent fractionation of Zn isotopes in nature is relatively small (Cloquet et al. 2008) and hence requires accurate and precise Zn isotope determination, which can be achieved by using the Multi Collector Inductively Coupled Plasma Mass Spectrometry (MC-ICPMS) (Bermin et al. 2006; Shiel et al. 2009). One disadvantage of MC-ICPMS is that instrumental mass bias occurs, whereby a measured isotope ratio is different to the "true" isotope ratio. These deviations can occur during: (1) ionization within the plasma; (2) mass separation and; (3) ion detection. Mass bias can vary significantly with MC-ICPMS and is dependent on the instrument settings and time (Walczyk 2004).

Mass fractionation (mass bias) of Zn isotopes induced within the mass spectrometer can be corrected by the following methods (Bermin et al. 2006; Mason et al. 2004): a)

conventional standard bracketing; b) doping samples with copper of an known isotope composition and; c) Zn double spike correction.

a) The conventional method of standard bracketing involves running a Zn standard with a known isotopic composition before and after every sample measurement. This requires the samples and the standard to have similar mass bias behaviour and also relatively stable mass bias with time (Archer and Vance 2004).
b) To further account for mass bias samples during Zn isotope analysis samples are usually doped with copper of a known isotopic composition (Archer and Vance 2004; Jouvin et al. 2009; Maréchal et al. 1999; Mason et al. 2004). This approach assumes similar mass bias behaviour of Zn and copper. Also for precise relationships between the mass bias behaviour of Cu and Zn, the mass bias must be sufficiently variable within one analytical session. While this procedure generally works well mass bias can still occur and not be adequately accounted for (Bermin et al. 2006).

c) The double spike (DS) technique can be used to circumvent these issues. The DS technique involves spiking the sample with a mixture of two artificially enriched isotopes of the target element of a known isotope composition (Arnold et al. 2010; Bermin et al. 2006; Siebert et al. 2001). The DS method is only suitable for elements which have four or more naturally occurring stable isotopes. Zn has five stable isotopes ^{64}Zn, ^{66}Zn, ^{67}Zn, ^{68}Zn and ^{70}Zn with natural abundances of 48.6%, 27.9%, 4.1%, 18.8% and 0.62%, respectively, thus it is well suited for the DS methodology. In addition, the DS methodology can also be used to correct for mass dependent isotope fractionation that might occur during sample preparation. Appreciable mass dependent isotope fractionation can occur during ion exchange chromatography as result of Zn interacting

with the ion exchange resin and during the elution process (Maréchal and Albarède 2002). These fractionation processes can be corrected for by adding the DS to the sample before processing. Thus, full recovery of element during sample preparation is not essential, although it is desirable.

2.1.1. Choice of double spike

To minimize error magnification on the natural isotope fractionation factor and for proper working of the DS, the isotope composition of the spike should be as different from the sample or standard as possible (Figure 2.1). Thus, ^{67}Zn and ^{68}Zn with natural isotopic abundances 4.1% and 18.8%, respectively, were chosen for the DS. The minor isotope ^{70}Zn was not chosen for the DS because it was not possible to measure both ^{70}Zn and ^{62}Ni with the available cup settings in the instrument used. ^{62}Ni was measured to monitor isobaric interference of ^{64}Ni on ^{64}Zn. Spectral interference on ^{70}Zn from ^{70}Ge can also be a potential problem. The optimum ^{67}Zn-^{68}Zn DS composition and DS-sample mix for error reduction of α was calculated using the "double spike tool box" of Rudge et al. (2009)(Figure 2.2).

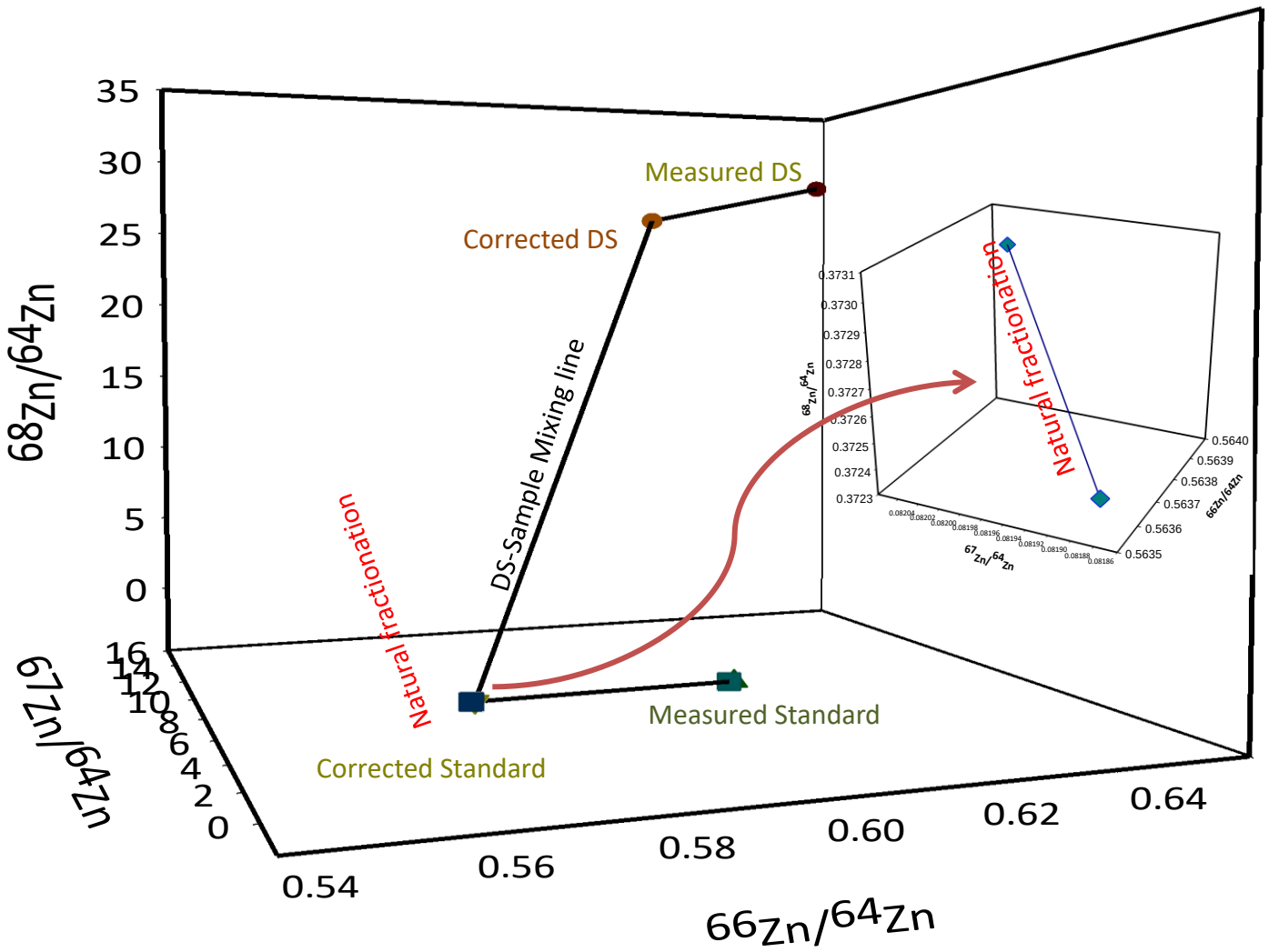

Figure 2.1: A 3D diagram showing the DS-sample mixing line, natural fractionation line (magnified; inset) and the instrumental fractionation line (mass bias) in $^{66}Zn/^{64}Zn$, $^{67}Zn/^{64}Zn$ and $^{68}Zn/^{64}Zn$ space (X, Y and Z axes respectively). To minimize error magnification on the natural isotope fractionation factor (α) and for proper working of the DS, the isotope composition of the spike should differ from the sample or standard as much as possible

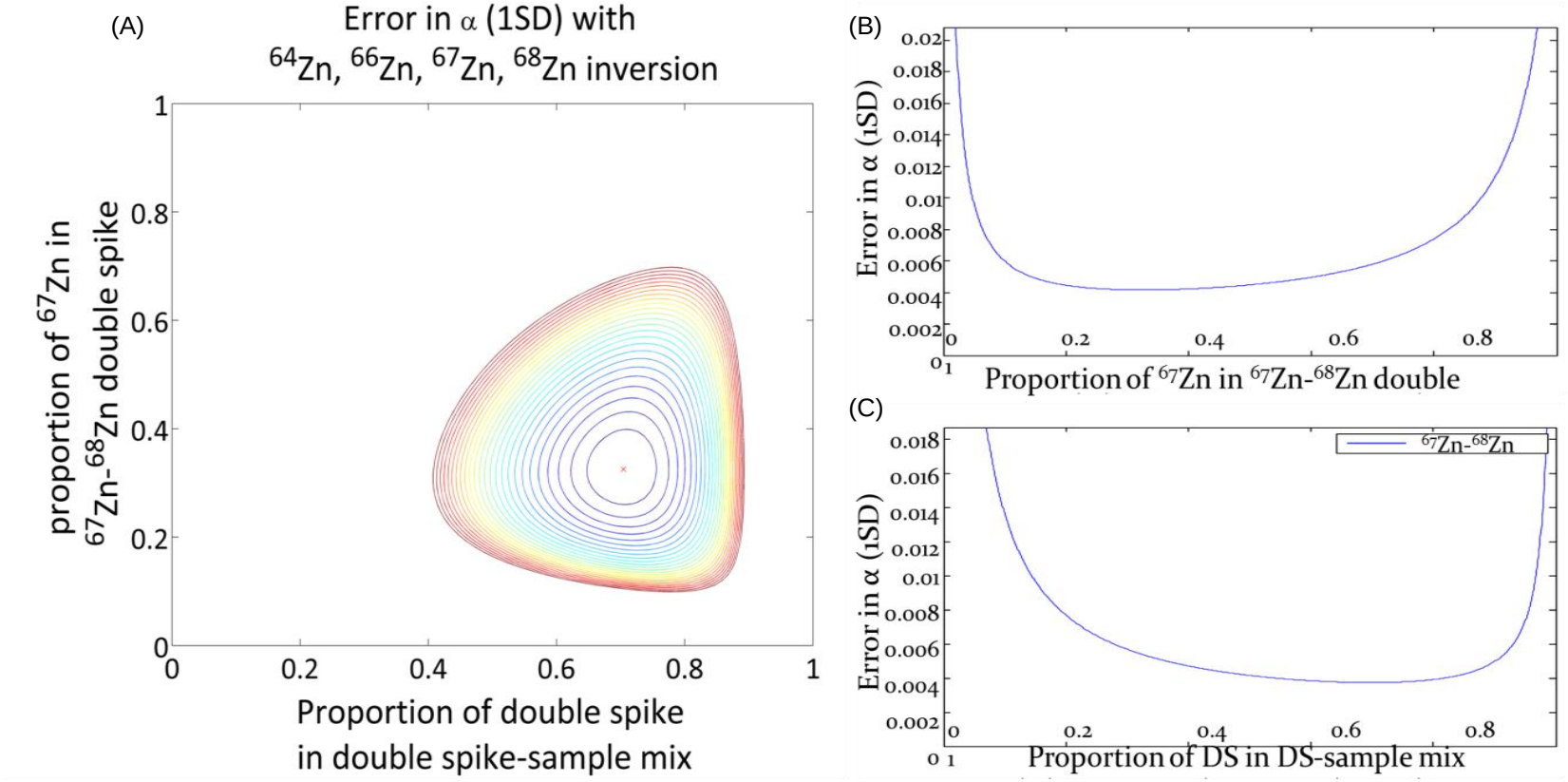

Figure 2.2: (A) Contour plot showing error magnification in calculating natural fractionation factor (α) associated with varying relative proportion of ^{67}Zn in ^{67}Zn-^{68}Zn DS, and DS in DS-sample mixture; The symbol (x) gives the proportions at which the uncertainty in estimation of α is at a minimum. Error in α (1SD) associated with different relative proportion of (B) ^{67}Zn in ^{67}Zn-^{68}Zn double spike and (C) double spike in double spike-sample mixture. Figures drawn using the MATLAB program by (Rudge et al. 2009)

2.1.2. Calibration of the double spike

In this study, the Zn DS was calibrated against the certified Zn standard IRMM-3702 utilising an in-house copper standard (Fluka, USA) to correct for mass dependent fractionation of Zn during the initial DS calibration. At the start of each analytical session mass dependent fractionation of the Zn standard in the MC-ICP-MS was corrected using copper by applying the exponential mass bias expression (Arnold et al. 2010).

$$R_{a/b} = r_{a/b}\left(\frac{m_a}{m_b}\right)^{P} \quad (1)$$

Where ($R_{a/b}$) is the true ratio of isotopes a and b, ($r_{a/b}$) is the measured ratio, m_a/m_b is ratio of the atomic masses for a and b and P is the exponential mass fractionation factor.

The following steps were undertaken to calibrate the DS solution at the start of each session:

1. An IRMM-3702 Zn standard solution (100 µg L^{-1}) containing copper (50 µg L^{-1}) was measured by MC-ICP-MS.

2. Based on the measured copper isotope values, the exponential fractionation factor (P') was determined and used to calculate instrumental mass bias

$$P' = \frac{\ln\left(\frac{^{63}Cu}{^{65}Cu}\text{true} \Big/ \frac{^{63}Cu}{^{65}Cu}\text{measured}\right)}{\ln(62.9296/64.9280)} \quad (2)$$

3. The newly calculated P' was then used to correct the measured $^{66}Zn/^{64}Zn$ isotope. If the mass bias corrected $^{66}Zn/^{64}Zn$ isotope was not equal to the certified value

IRMM-3702 ratio, P' was adjusted until they agreed. This new fully corrected exponential fractionation factor was termed P.

4. Using the new P factor the copper isotope composition in the IRMM-3702 standard solution was recalculated.

5. Next a DS solution (100 µg L^{-1}) containing the same copper standard (50 µg L^{-1}) was measured by MC-ICP-MS.

6. Based on the newly calibrated copper isotope composition and the measured copper isotope value for the DS solution, a fractionation factor was calculated and used to correct measured Zn isotope ratios ($^{64}Zn/^{68}Zn$, $^{66}Zn/^{68}Zn$, $^{67}Zn/^{68}Zn$ and $^{66}Zn/^{64}Zn$) for the DS.

This procedure of calibrating the DS was undertaken at the beginning of each analytical session (Arnold et al. 2010). The Zn isotope composition of natural samples was determined using the DS method and solved iteratively. The mass balance equations and how they were used and solved are detailed below.

2.1.3. Isotope dilution equation

If we consider a standard (Std) or a sample (Sa) – spike (Sp) mixture (Mix), the Zn isotope composition of the mixture will be equal to the total amount of Zn in the sample plus the spike.

Whereby,

$$^{67}\mathrm{Zn}_{\mathrm{Mix}} = {}^{67}\mathrm{Zn}_{\mathrm{Sa}} + {}^{67}\mathrm{Zn}_{\mathrm{Sp}} \quad (3)$$

And

$$^{68}Zn_{Mix} = {}^{68}Zn_{Sa} + {}^{68}Zn_{Sp} \quad (4)$$

Thus

$$^{67}Zn_{Sp} = {}^{68}Zn_{Sp} \times {}^{67}Zn_{Sp}/{}_{68}Zn_{Sp} \quad (5)$$

$$^{67}Zn_{Sa} = {}^{68}Zn_{Sa} \times {}^{67}Zn_{Sa}/{}_{68}Zn_{Sa} \quad (6)$$

Combing equations 3 and 4 we can write following equation:

$$\frac{^{67}Zn_{Mix}}{^{68}Zn_{Mix}} = \frac{^{67}Zn_{Sa}+{}^{67}Zn_{Sp}}{^{68}Zn_{Sa}+{}^{68}Zn_{Sp}} \quad (7)$$

Rearranging equation 7 we get:

$$\frac{^{67}Zn_{Mix}}{^{68}Zn_{Mix}} \times ({}^{68}Zn_{Sa} + {}^{68}Zn_{Sp}) = {}^{67}Zn_{Sa} + {}^{67}Zn_{Sp} \quad (8)$$

Combining equation 8 with equations 5 and 6 gives:

$$\frac{^{67}Zn}{^{68}Zn}\,Mix \times {}^{68}Zn_{Sa} + \frac{^{67}Zn}{^{68}Zn}Mix \times {}^{68}Zn_{Sp} = {}^{68}Zn_{Sa} \times \frac{^{67}Zn}{^{68}Zn}Sa + {}^{68}Zn_{Sp} \times \frac{^{67}Zn}{^{68}Zn}Sp$$

(9)

This can be rearranged and simplified to give:

$$^{68}Zn_{Sa}\left(\frac{^{67}Zn}{^{68}Zn}Mix - \frac{^{67}Zn}{^{68}Zn}Sa\right) = {}^{68}Zn_{Sp}\left(\frac{^{67}Zn}{^{68}Zn}Sp - \frac{^{67}Zn}{^{68}Zn}Mix\right) \quad (10)$$

Equation 10 can also be written as:

$$\frac{^{68}Zn_{Sp}}{^{68}Zn_{Sa}} = \frac{\left(\frac{^{67}Zn}{^{68}Zn}Mix - \frac{^{67}Zn}{^{68}Zn}Sa\right)}{\left(\frac{^{67}Zn}{^{68}Zn}Sp - \frac{^{67}Zn}{^{68}Zn}Mix\right)} = Q \quad (11)$$

We can write a similar equation whereby,

$$\frac{^{68}Zn_{Sp}}{^{68}Zn_{Sa}} = \frac{\left(\frac{^{66}Zn}{^{68}Zn}Mix - \frac{^{66}Zn}{^{68}Zn}Sa\right)}{\left(\frac{^{66}Zn}{^{68}Zn}Sp - \frac{^{66}Zn}{^{68}Zn}Mix\right)} = Q \quad (12)$$

Combining equations 11 and 12 gives:

$$\frac{\left(\frac{^{66}Zn}{^{68}Zn}Mix - \frac{^{66}Zn}{^{68}Zn}Sa\right)}{\left(\frac{^{66}Zn}{^{68}Zn}Sp - \frac{^{66}Zn}{^{68}Zn}Mix\right)} = \frac{\left(\frac{^{67}Zn}{^{68}Zn}Mix - \frac{^{67}Zn}{^{68}Zn}Sa\right)}{\left(\frac{^{67}Zn}{^{68}Zn}Sp - \frac{^{67}Zn}{^{68}Zn}Mix\right)} \quad (13)$$

If we generalise equation 13, the following isotope dilution equation can be written:

$$\frac{(Mix1 - Sa1)}{(Sp1 - Mix1)} = \frac{(Mix2 - Sa2)}{(Sp2 - Mix2)} \quad (14)$$

Where, 1 and 2 denotes isotopic ratios with the same denominator.

Rearranging equation 14 the Sp1 ratio can be expressed as follows:

$$Sp1 = Mix1 - \frac{(Sa1 - Mix1) \times (Mix2 - Sp2)}{(Sa2 - Mix2)} \quad (15)$$

And the Sa1 ratio in equation 14 can be expressed as:

$$Sa1 = Mix1 + \frac{(Mix1 - Sp1) \times (Sa2 - Mix2)}{(Mix2 - Sp2)} \quad (16)$$

Following equation 15, we can express equation 13 as:

$$\frac{^{67}Zn}{^{68}Zn}Sp = \frac{^{67}Zn}{^{68}Zn}Mix - \frac{\left(\frac{^{67}Zn}{^{68}Zn}Sa - \frac{^{67}Zn}{^{68}Zn}Mix\right) \times \left(\frac{^{66}Zn}{^{68}Zn}Mix - \frac{^{66}Zn}{^{68}Zn}Sp\right)}{\left(\frac{^{66}Zn}{^{68}Zn}Sa - \frac{^{66}Zn}{^{68}Zn}Mix\right)} \quad (17)$$

And if we consider the ratios 1 and 2 to be $^{66}Zn/^{64}Zn$ and $^{68}Zn/^{64}Zn$ respectively, equation 16 can be written as:

$$\frac{^{66}Zn}{^{64}Zn}Sa = \frac{^{66}Zn}{^{64}Zn}Mix + \frac{\left(\frac{^{68}Zn}{^{64}Zn}Sa - \frac{^{68}Zn}{^{64}Zn}Mix\right)\times\left(\frac{^{66}Zn}{^{64}Zn}Mix - \frac{^{66}Zn}{^{64}Zn}Sp\right)}{\left(\frac{^{68}Zn}{^{64}Zn}Mix - \frac{^{68}Zn}{^{64}Zn}Sp\right)} \quad (18)$$

This equation can be further manipulated to give:

$$\frac{^{66}Zn}{^{64}Zn}Sa = \frac{^{66}Zn}{^{64}Zn}Mix + \frac{\left(\frac{1}{^{64}Zn/^{68}Zn}Sa - \frac{1}{^{64}Zn/^{68}Zn}Mix\right)\times\left(\frac{^{66}Zn}{^{64}Zn}Mix - \frac{^{66}Zn}{^{64}Zn}Sp\right)}{\left(\frac{1}{^{64}Zn/^{68}Zn}Mix - \frac{1}{^{64}Zn/^{68}Zn}Sp\right)} \quad (19)$$

2.1.4. The iterative solution method for calculation of $\delta^{66}Zn$ of a sample

To calculate the $\delta^{66}Zn$ composition of samples spiked with the DS, we used an iterative process. The traditional iterative solution method to calculate the natural isotope ratios of the sample can be used to review the calibration of the DS. It also allows us to see the propagation of an error through each iterative cycle. For a standard- or sample-DS mixture, the $^{67}Zn/^{68}Zn$ ratio of the double spike ($^{67}Zn/^{68}Zn_{DS}$) in each measurement cycle was estimated using isotope dilution equation 17. Once an estimate of $^{67}Zn/^{68}Zn_{DS}$ ratio was obtained, the mass fractionation factor (P_{Mix}) was calculated using equation 2 but recomposed for the $^{67}Zn/^{68}Zn_{DS}$ ratio. This P_{Mix} factor was then used to correct the measured Zn ratios for $^{64}Zn/^{68}Zn_{mix}$, $^{66}Zn/^{68}Zn_{mix}$, $^{67}Zn/^{68}Zn_{mix}$, and $^{66}Zn/^{64}Zn_{mix}$. Using these corrected ratios, the $^{66}Zn/^{64}Zn_{sample}$ ratio was calculated using equation 19. Based on this newly calculated ratio a second mass fractionation factor (P_{sample}) was calculated using equation 2 but recomposed for the $^{66}Zn/^{64}Zn_{sample}$ ratio. For the first loop, we initially assigned the $^{66}Zn/^{64}Zn_{sample}$ as being

equal to the measured IRMM-3702 standard (but without added DS) along with the other measured isotope ratios required in equation 19. Using this P_{sample} value, the ratios for $^{64}Zn/^{68}Zn_{sample}$, $^{66}Zn/^{68}Zn_{sample}$, $^{67}Zn/^{68}Zn_{sample}$ were all corrected. This procedure constituted one sample loop. These steps were then repeated until the corrected mixture and samples isotope ratios converge to a constant value. Most isotope ratios converged within 3 to 5 iterations (Figure 2.3). Finally, the $^{66}Zn/^{64}Zn$ ratio was expressed in delta notation using the following equation:

$$\delta^{66}\mathrm{Zn} = \left(\frac{^{66}\mathrm{Zn}/^{64}\mathrm{Zn}_{\mathrm{sample}}}{^{66}\mathrm{Zn}/^{64}\mathrm{Zn}_{\mathrm{IRMM-3702}}} - 1\right) \times 1000 \qquad (20)$$

All Zn isotope measured in the study are relative to the standard reference material IRMM-3702. This standard has an offset of -0.30 ± 0.01 (‰) from the Johnson Matthey (JMC) Lyon Zn standard, the traditional Zn isotope reference material (Archer et al. 2017; Cloquet et al. 2008; Moeller et al. 2011; Moynier et al. 2017).

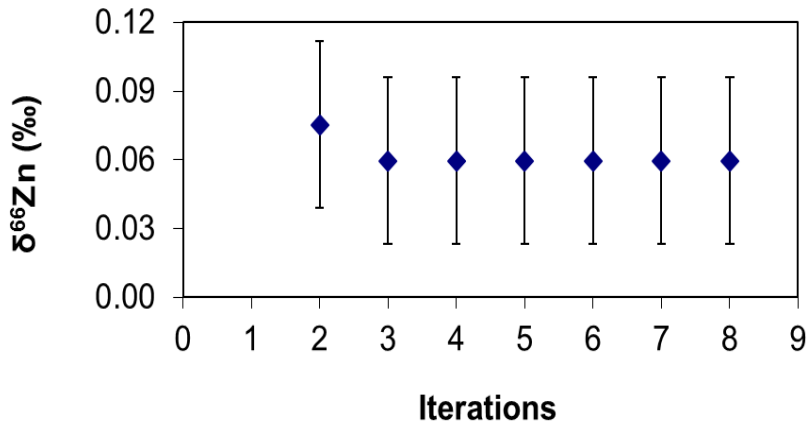

Figure 2.3: Calculated $\delta^{66}Zn$ values (w.r.t. IRMM-3702) of a sample with iteration steps. Error bars represent instrumental 2 SE (standard error of the mean for one block of 30 cycles) for each iteration step.

2.1.5. Pre-concentration of trace metals from seawater

Three different Zn pre-concentration techniques to separate seawater matrix from trace metals have been reported.

The solvent extraction method involves the addition of a hydrophilic chelating agent, usually a dithiocarbamate-based molecule, to the seawater which becomes hydrophobic when bound to a transition metal. The hydrophobic metal-dithiocarbamate species is then extracted from the hydrophilic phase by partitioning it into a hydrophobic solvent (Bruland et al. 1979; Danielsson et al. 1982). The organic phase is collected and nitric acid is added to decompose the metal-dithiocarbamate complex. Upon decomposition of the complex, the free uncomplexed trace metal ions are partitioned back into the hydrophilic nitric acid phase. Though this technique has the advantage of being quick and easy to undertake, the major disadvantage is the potential interference of sulphur ($^{32}S_2$) from the dithiocarbamate molecule on measurement of ^{64}Zn.

The co-precipitation technique involves the addition of a base (e.g. ammonium hydroxide) to the seawater to form a precipitate of magnesium hydroxide. As the precipitate forms, other trace elements are co-precipitated from the seawater matrix. The precipitate is separated from the supernatant liquid and further processed to separate Zn from magnesium by ion exchange chromatography. The main disadvantage of this process is the potential interference of the polyatomic species $^{24}Mg^{40}Ar$ on ^{64}Zn if magnesium is not fully removed (Bermin et al. 2006). Recently this method was modified to precipitate Zn along with aluminium hydroxide rather than magnesium hydroxide in order to process surface seawater samples with low dissolved

Zn concentration. However, the major drawbacks are relatively low recovery (70-90 %) and Zn blanks from aluminium solution (Zhao et al. 2014).

The solid phase extraction technique is an ion exchange chromatographic process whereby transition metals are complexed to a cation exchange resin, usually with iminodiacetate functional group, which forms a strong bond with polyvalent metal ions. When pH buffered seawater is passed across the resin the major elements are eluted out while transition metal ions are retained. These metal ions are eluted from the column at low pH. The extraction efficiency of Zn from seawater using this technique is reported to be 100.8 ± 0.7 % (n = 5) (Bermin et al. 2006). A major disadvantages of this technique is that it retains a large amount of calcium and magnesium on the resin along with the trace metal of interest (Bermin et al. 2006; Bruland et al. 1979). In recent past, development of new generation resins with quantitative recovery and low blank have made it possible to pre-concentrate Zn from large volumes of seawater (Conway et al. 2013; Takano et al. 2017).

2.1.6. Ion exchangecChromatography for Zn separation

After the preconcentration of Zn from seawater, it needs to be separated from other elements that could potentially interfere within the mass spectrometer. The procedure proposed by Maréchal and Albarède (2002) for the purification and separation of Zn from other trace elements involves use of a strong basic anion exchange resin, with a styrene divinylbenzene copolymer matrix and R-CH_2N-$(CH_3)_3$ functional group (Maréchal and Albarède 2002; Maréchal et al. 1999). Samples are loaded onto the resin, contained with a chromatographic column, in a hydrochloric acid matrix. Under

these conditions Zn forms an anionic chlorocomplex ($ZnCl_x^{2-x}$) that reversibly exchanges Cl^- ions bound to the positively charged quaternary ammonium group, R-$CH_2N^+H(CH_3)_3$, of the resin. Elements are eluted from the resin by passing hydrochloric acid at varying concentrations after which Zn is eluted from the column using dilute nitric acid.

2.2. Experimental

2.2.1. Reagents

All work for sample preparation was done in class 100 HEPA filtered clean hoods in a clean laboratory. All labware was rigorously cleaned by soaking in *aqua regia* for one week before rinsing with Milli-Q water (Millipore, Australia). Labware was soaked for a further week in distilled dilute acid before rinsing and use. Nitric acid (HNO_3) (AR grade) was purified by sub-boiling distillation in a Teflon still (Savillix, USA). Hydrochloric acid (HCl) (AR grade) was diluted to 8 mol L^{-1} before sub-boiling distillation in a Teflon still (Savillex, USA). An ammonium acetate buffer (12 mol L^{-1}) was prepared by dissolving ammonium acetate (Sigma Aldrich) in Milli-Q water. The buffer was purified by solvent extraction using chloroform and ammonium 1-pyrrolidinedithiocarbamate and diethyl dithio-carbamate as chelating agent. It was then stored in a Teflon bottle. A dilute ammonium acetate buffer was prepared by 10-fold dilution of the concentrated buffer and then adjusting the pH to 5.5. A 50% (v/v) ammonium hydroxide solution was made by diluting a high purity ammonium solution (Seastar chemical Inc.) with an equal volume of Milli-Q water.

2.2.2. Preparation of the Double Spike

To make the DS, artificially enriched high purity isotopes of ^{67}Zn (ZnO, Chemgas) and ^{68}Zn (Metal, ORNL, Batch 205940) was prepared in 2% HNO_3 and mixed together such that the percentage of Zn in the DS from the ^{68}Zn spike was 65.6%. The Zn-DS was then stored in a Teflon bottle (Table 2.6; Chapter Appendix). Mixtures of the DS in different relative proportions to the Zn standard IRMM-3702 were made and measured in the

MC-ICPMS. We know the DS is well calibrated when the calculated $^{66}Zn/^{64}Zn$ ratio of IRMM is same as the copper corrected IRMM ratios of the measurement session over a sufficiently wide range of mixtures. The working range of the DS sample mixture was also checked for in-house Zn standard 8834h, which has an offset of -0.70 ± 0.09 ‰ (± 2SD; measured over a course of 3 years) from IRMM-3702. It was observed that for both the standards the calculations work quite well when the percentage of Zn from DS in the DS-sample mix was within approximately 54% to 91%, which gave a $^{68}Zn/^{64}Zn_{intensity}$ ratio between 2 and 10.

2.2.3. Pre-concentration of trace metals

To pre-concentrate trace metals and separate from the seawater matrix we performed ion exchange chromatography using Toyopearl AF-Chelate 650M, an iminodiacetate resin with a macroporous methacrylate backbone (Willie et al. 1998b). A suitable amount of the DS was added to acidified seawater (~ pH 1.8) such that the percentage of spike in the sample-spike mixture was ~ 83 ± 3 % and was allowed to equilibrate overnight. Clean ammonium acetate buffer and ammonium hydroxide were added to adjust the pH of the seawater to around 5.5 ± 0.5. The seawater sample was loaded onto Toyopearl AF-Chelate 650M chromatographic columns (0.5 mL of resin) fitted to a 500 mL reservoir. Prior to use, the resin was first cleaned with 1 mol $L^{-1}HNO_3$, followed by 1 mol L^{-1} HCl and lastly Milli-Q water. The resin in each column was then equilibrated in dilute ammonium acetate at pH 5.5 before loading with seawater. Once the entire volume of seawater was passed over the resin, it was rinsed with dilute

ammonium acetate (pH 5.5) to remove interfering cations such as calcium, magnesium and sodium (Willie et al. 1998b). Full details the method is outline in Table 2.1a.

The solvent extraction technique using chelating agents ammonium pyrrolidinedithiocarbamate (APDC) and sodium diethyldithiocarbamate (DDC) and the use of the MOPS (Morpholinepropanesulfonic acid) buffer was also tested using the procedure outlined by (Ellwood 2008).

2.2.3.1. Optimising loading pH and elution efficiency

The optimum loading pH for extraction of Zn from seawater was tested across a range varying between 3.2 and 8.2 for a deep seawater sample with a dissolved Zn concentration of 6.55 ± 0.15 nmol L^{-1}. Three litres of the sample was split equally into 6 parts and adjusted to pHs of 3.2, 4.0, 5.1, 5.9, 6.9 and 8.2 using ammonium acetate and ammonium hydroxide. Zn was pre-concentrated from each aliquot following the steps in Table 2.1a. An equal amount of the DS (DS-sample mix = 4) was then added to each of the HCl extracts before the samples were dried down and the interfering elements separated by performing anion exchange chromatography.

Another seawater sample collected from the Tasman Sea (46◦18'S; 160◦00'E) from a depth of 3500 m with dissolved Zn concentration of 6.24 nmol L^{-1} was spiked with appropriate amount of the DS. The sample was buffered to a pH of 5.5 and split into 14 aliquots. Each aliquot was passed over a separate column containing 0.5 ml of Toyopearl AF-Chelate 650M resin and then rinsed with the diluted buffer. Six of columns were eluted with 3 mL 1 mol L^{-1} HNO_3 and 6 were eluted with 3 mL 1 mol L^{-1} HCl. Anion exchange chromatography was performed on 12 of the eluates to separate

Zn from other trace metals. Recovery of Zn after chemistry (pre-concentration and separation) was analysed by monitoring the voltage on ^{68}Zn and the $^{64}Zn/^{68}Zn$ ratio of the aliquots during mass spectrometry. A standard-DS mixture of similar ^{68}Zn intensity and $^{64}Zn/^{68}Zn$ ratio (assuming 100% recovery of Zn after chemistry) was measured after each aliquot measurement to compare recovery and monitor instrumental drift.

The other two aliquots were used to investigate the minimum amount of acid required to elute Zn completely from Toyopearl AF-Chelate 650M. One aliquot was extracted with 4 mL of 0.5 mol L^{-1} HCl and every 1 mL was collected and the other aliquot was extracted with 8 mL of 0.5 mol L^{-1} HNO_3 with every 2 mL collected and tested for recovery of Zn.

2.2.4. Ion exchange chromatography for Zn separation

The separation of Zn from other trace elements was undertaken using a modified form of the ion exchange chromatography procedure outlined by Marechal and Albarede (Maréchal and Albarède 2002). Teflon columns containing 0.15 mL of the AG1X8 resin supported by with polyethylene (PE) frits were first cleaned with 0.5 mol L^{-1} HNO_3 followed by rinsing with Milli-Q water (Table 2.1b). The resin in each column was then equilibrated in 0.5 mol L^{-1} HCl before loading with 0.3 mL of sample (dissolved in 0.5 mol L^{-1} HCl). Because Zn has a high distribution coefficient and remains adsorbed to the resin in 0.5 mol L^{-1} HCl, each column was rinsed with 0.5 mol L^{-1} HCl to remove potentially interfering elements. After a suitable volume has been passed Zn is eluted from the resin with 0.5 mol L^{-1} HNO_3.

To check the efficiency of the ion exchange chromatography process, an artificial sample was prepared. After loading the sample onto the column containing the AG1X8 resin each millilitre of eluent acid passed was collected and stored for elemental determination. Prior analysis each column cut was dried-down and taken up in 2% HNO_3 for analysis by quadrapole ICP-MS (Varian, Australia).

The efficiency of both new and used AG1X8 resin was tested. Loading the sample directly by dripping the 3 mL of 1 mol L^{-1} HCl eluate from the Toyopearl AF-Chelate 650M resin to AG1X8 instead of drying the eluate and loading it separately to the AG1X8 resin was also tested.

Table 2.1: Procedural steps involved in (a) extraction and (b) purification of dissolved Zn from seawater.

	Step	Reagents
(a)	1) Cleaning Toyopearl AF Chelate 650M resin	8 mL of 1 mol L^{-1} HNO_3 8 mL of 1 mol L^{-1} HCl
	2) Milli-Q rinsing	8 mL of Milli-Q H_2O
	3) Column conditioning	1 mL of dil. $CH_3COO^-NH_4^+$ @ pH 5.5
	4) Sample loading	Spiked seawater @ pH 5.5
	5) Eluting interfering elements	~ 3 mL of dil. $CH_3COO^-NH_4^+$ @ pH 5.5
	6) Eluting trace metals	3 mL of 1 mol L^{-1} HCl
(b)	7) Drying-down HCl extract and re-dissolving	0.3 mL in 0.5 mol L-1 HCl
	8) Cleaning AG1X8 resin	2 mL of 0.5 mol L^{-1}M HNO_3
	9) Milli-Q rinsing	1 mL of Milli-Q H_2O
	10) Column conditioning	1.5 mL of 0.5 mol L^{-1} HCl
	11) Sample loading	0.3 mL in 0.5 mol L^{-1} HCl (from Step 7)
	12) Eluting interfering elements	3.5 mL of 0.5 mol L^{-}1 HCl
	13) Eluting Zn	2.5 mL of 0.5 mol L^{-1} HNO_3

2.2.5. Isotope mass spectrometry

Zn isotope measurements were made on a MC-ICP-MS (Thermo Scientific Neptune Plus) at the Research School of Earth Sciences, Australian National University. The instrument was operated in low resolution mode with a standard Ni sampler cone and a Ni X-skimmer cone. Samples were introduced into the MC-ICP-MS via a desolvating system consisting of Quartz flow path (Apex IR, Elemental Scientific Inc.) and a Teflon micro-flow nebuliser (Elemental Scientific Inc.) operated at an uptake rate of 50 µL per minute. Intensities on mass ^{62}Ni, ^{63}Cu, ^{65}Cu, ^{64}Zn, ^{66}Zn, ^{67}Zn and ^{68}Zn were monitored during each blank, standard and sample measurement. The configuration for the Faraday cups is given in Table 2.3.

At the start of each measurement session, a 15 minute Gain and 5 minute Baseline calibration was undertaken. Each sample was peak centred on ^{64}Zn at the start of the measurement. All blank, standard and sample measurements were made as 1 block of 30 cycles with a 4 second integration time.

All measured ratios were corrected for the interference of ^{64}Ni on ^{64}Zn by monitoring the intensity of ^{62}Ni and subtracting the calculated intensity for ^{64}Ni, based on the natural ^{62}Ni/^{64}Ni ratio, from the measured intensity of ^{64}Zn. However, the Ni correction was insignificant as the contribution of ^{64}Ni on ^{64}Zn was < 0.01 %.

The interference corrected data was then blank corrected. Blank correction is done by subtracting the average intensity of the 30 cycle measurement for each isotope from the intensities measured for the blank. The ^{66}Zn/^{64}Zn ratio of the sample for each measurement cycle is calculated iteratively for each of the 30 cycles to give a ^{66}Zn/^{64}Zn ratio for the sample. The δ^{66}Zn for the sample was calculated with respect to IRMM-

3702. Calculation of the instrumental standard error (2x S.E.) was based on the corrected $^{66}Zn/^{64}Zn$ ratio of the 30 cycles.

Samples were analysed in groups of three bracketed with a standard-DS mixture to check for instrumental drift. A 2% (v/v) HNO_3 wash was undertaken between sample and standards. Intensities on Zn isotopes during wash was monitored and the wash was continued till intensities reached background levels.

The Zn concentration for each sample is also calculated in each workbook from the mass values for the sample and the spike. This calculation is based on isotope dilution using known proportion of ^{68}Zn in the ^{67}Zn-^{68}Zn double spike and its concentration.

All isotopic measurements were made in low resolution mode by MC-ICP-MS, although medium resolution mode was also tested. While it can help resolve interferences (Table 2.2) the signal size is greatly diminished. Since measuring in the medium resolution did not have any significant effect in the measured ratios, low resolution mode was preferred.

Both the ESI Apex-IR and the CETAC Aridus –II sample introduction systems were tested and we observed no appreciable difference in the isotopic ratios for the Zn standard IRMM-3702. The Apex-IR sample introduction system was preferred since the Aridus tended to generate an $^{40}Ar^{28}N_2$ interference on ^{68}Zn. Large mass bias variation have also been reported for the Aridus sample introduction system (Archer and Vance 2004; John et al. 2008). We did not test the Stable Introduction System (SIS) consisting of Scott-double pass quartz cyclonic spray chamber (Thermo Scientific) even though it is less prone to mass bias during sample introduction as compared to desolvating

systems, because it has a lower sensitivity compared to that of the Apex-IR and the CETAC Aridus –II.

The X-cone with a different aperture configuration to the standard H-cone was used for samples with very low Zn concentrations. To check for nickel and copper interferences from the nickel cones, aluminium cones were also tried with no appreciable difference observed between cone materials.

Table 2.2: Isobaric, doubly-charged and polyatomic interferences on Zn isotopes of interest

Mass Number	**Analytical Isotope (Natural Abundance)**	**Isobaric Interferences (Natural Abundance)**	**Doubly-charged Ions**	**Polyatomic Species**
64	^{64}Zn (48.63 %)	^{64}Ni (0.93%)		$^{24}Mg^{40}Ar^{+}$; $^{47}Ti^{16}O^{1}H^{+}$; $^{48}Ti^{16}O^{+}$; $^{48}Ca^{16}O^{+}$; $^{32}S^{16}O^{2+}$; $^{32}S^{2+}$
66	^{66}Zn (27.90 %)		$^{132}Ba^{2+}$; $^{132}Xe^{2+}$	$^{26}Mg^{40}Ar^{+}$; $^{50}Ti^{16}O^{+}$; $^{50}V^{16}O^{+}$; $^{50}Cr^{16}O^{+}$; $^{34}S^{16}O^{2+}$; $^{32}S^{34}S^{+}$
67	^{67}Zn (4.10 %)		$^{134}Ba^{2+}$; $^{134}Xe^{2+}$	$^{27}Al^{40}Ar^{+}$; $^{51}V^{16}O^{+}$; $^{35}Cl^{16}O^{2+}$
68	^{68}Zn (18.75 %)		$^{136}Ba^{2+}$; $^{136}Ce^{2+}$; $^{136}Xe^{2+}$	$^{28}Si^{40}Ar^{+}$; $^{52}Cr^{16}O^{+}$; $^{36}S^{16}O^{2+}$; $^{40}Ar^{12}C^{16}O^{+}$; $^{40}Ar^{14}N^{2+}$; $^{32}S^{36}S^{+}$

Table 2.3: The cup configuration of the Thermo Finnigan Neptune Plus for Zn isotope determination.

Cup	L3	L2	L1	C	H1	H2	H3
Mass	^{62}Ni	^{63}Cu	^{64}Zn	^{65}Cu	^{66}Zn	^{67}Zn	^{68}Zn

2.3. Results and Discussion

2.3.1. Solid phase extraction versus the solvent extraction technique

Large variations in the $\delta^{66}Zn$ values were obtained for samples extracted using solvent extraction technique involving the chelating agents ammonium pyrrolidinedithiocarbamate (APDC) and sodium diethyldithiocarbamate (DDC) (Table 3). These variations likely result from the interference of $^{32}S_2$ from the dithiocarbamate group on ^{64}Zn during isotope analysis. This problem was exacerbated for surface seawater samples with a low Zn concentration. We also noted a similar problem when using the morpholinepropanesulfonic acid (MOPS) to buffer the sample pH prior pre-concentration of the sample (Table 2.4).

2.3.2. Optimising loading pH for extraction and elution efficiency

2.3.2.1. Testing the use of HCl over HNO_3

During the pre-concentration stage, we noted that the recovery of Zn from the Toyopearl AF-Chelate 650M resin was significantly lower (50-75%, n = 6) if the resin was eluted with 1 mol L^{-1} HNO_3 compared to elution with 1 mol L^{-1} HCl (Figures 2.4). Full recovery of Zn (99 ± 2%, n = 6) was obtained when the resin was eluted with HCl. This result is similar to what Warnken et al. (2000) observed for cadmium elution from the Toyopearl AF-Chelate 650M resin, although other papers have reported 90 ± 10% recovery of Zn with 1 mol L^{-1} of HNO_3 with Toyopearl AF-Chelate 650M resin (Milne et al. 2010; Veguería et al. 2013; Willie et al. 1998b). The variations we observe may be specific to the batch of resin used. Multiple extraction of a deep water eluted with 1 mol L^{-1} HCl yielded an average $\delta^{66}Zn$ value of 0.60 ± 0.02 ‰ (n = 6), while those eluted

with 1 M HNO_3 yielded an average $\delta^{66}Zn$ value of 0.45 ± 0.05 ‰ (n = 6) (Figure 2.4 b), suggested isotope fraction of the samples upon elution. For subsequent work HCl was preferred over HNO_3 for eluting Zn from the Toyopearl AF-Chelate 650M resin because it allowed full recovery of Zn.

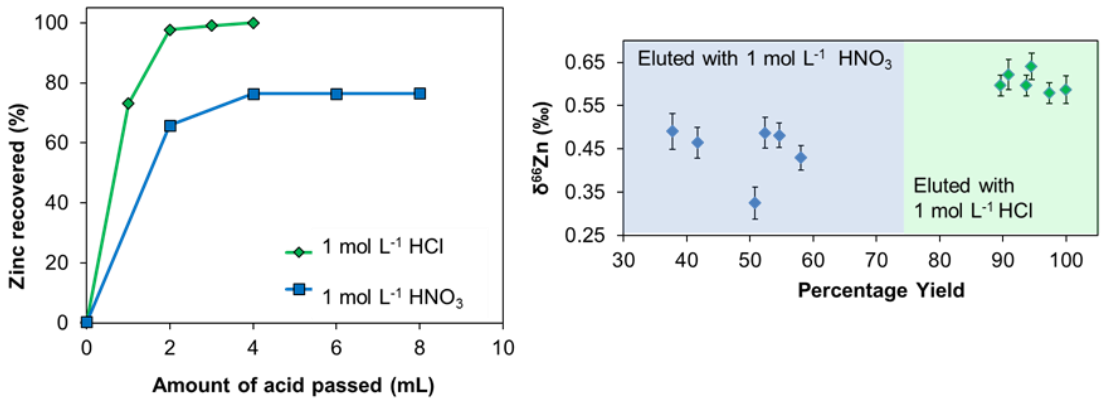

Figure 2.4: (a) Relative percentage recovery of Zn from the Toyopearl AF Chelate 650M resin for a deep seawater sample eluted with either 1 mol L^{-1} HCl or 1 mol L^{-1} HNO_3. (b) $\delta^{66}Zn$ values (w.r.t. JMC-Lyon) and percentage yield of dissolved Zn for replicates of a deep seawater sample eluted from Toyopearl AF Chelate 650M resin using 1 mol L^{-1} HCl and 1 mol L^{-1} HNO_3. Error bars represent instrumental 2 SE (standard error of the mean for one block of 30 cycles).

Table 2.4: (a) Comparing variations in $\delta^{66}Zn$ (‰) for a deep seawater sample (3500 m) preconcentrated by Solvent extraction (using APDC and DDC as chelating agent) and Solid phase extraction (using Toyopearl AF Chelate 650M resin); (b) Comparing variations in $\delta^{66}Zn$ (‰) for another deep seawater sample (1500 m) loaded onto Toyopearl AF Chelate 650M resin using different sample loading buffers, MOPS buffer and ammonium acetate plus ammonium hydroxide buffer. $\delta^{66}Zn$ (‰) values are with respect to JMC-Lyon. Errors represent SD (standard deviation of the mean).

		Depth (m)	Average $\delta^{66}Zn \pm 2$ SEM (‰)	$\delta^{66}Zn$ (‰) of replicate measurements							
(a)	Solvent extraction using chelating agents APDC and DDC	3500	0.08 ± 0.19	0.26	0.13	0.48	-0.24	0.23	0.26	-0.20	-0.23
	*True value		0.60 ± 0.02	0.58	0.64	0.62	0.60	0.60	0.59		
(b)	Sample buffered using MOPS buffer	1500	-1.66 ± 0.31	-1.83	-1.80	-1.35					
	#True value		0.44 ± 0.05	0.49	0.42	0.42					

* Solid phase extraction using Toyopearl AF Chelate 650M resin; #Sample buffered using ammonium acetate and ammonium hydroxide buffer.

2.3.2.2. Recovery versus pH

The optimum loading pH for the pre-concentration of Zn from seawater on to the Toyopearl AF-Chelate 650M resin was found to be between pH 5 and 8 (Figure 2.5). This finding is consistent with literature data (Milne et al. 2010; O'Sullivan et al. 2013; Veguería et al. 2013; Willie et al. 1998b) for pre-concentration of Zn from seawater by in-line flow-injection analysis by ICP-MS using the same resin. At lower pH values, Zn yields were significantly reduced with recoveries of 1% and 15% at pH 3.2 and 4.0, respectively. A significant variation in the δ^{66}Zn composition was also noted at low pH with δ^{66}Zn values of 1.17 ± 0.45 ‰ and 0.66 ± 0.07 ‰ at a pH of 3.2 and 4.0, respectively, when compared to a of 0.44 ± 0.03 at higher pH values (Figure 2.5) (Please note that the deep seawater samples used for optimising loading pH for extraction and that used for testing eluting acids are different, and thus have different Zn concentrations and δ^{66}Zn values). We also noted that the instrumental error (± 0.45 ‰, 2SE) was significantly high at pH 3.2 because of the low signal intensity.

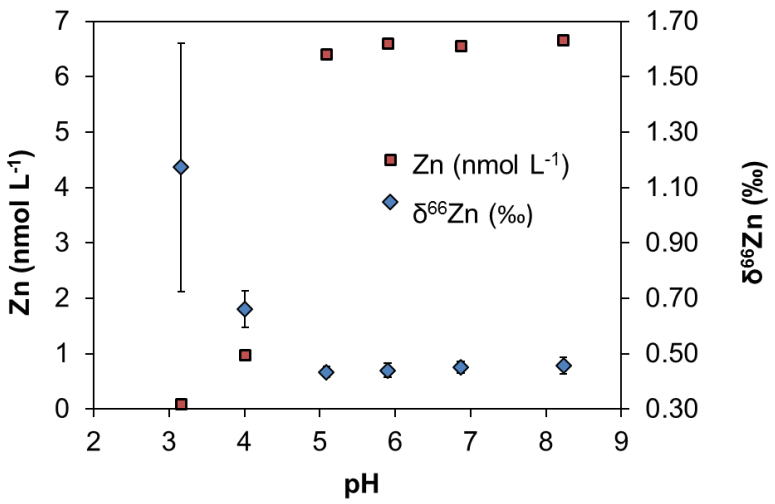

Figure 2.5: δ^{66}Zn values and concentration of dissolved Zn for replicates of a deep seawater sample ([Zn] = 6.55 ± 0.15 nmol L^{-1}) buffered at different pH before solid phase extraction. Error bars on δ^{66}Zn values represent instrumental 2 SE (standard error of the mean for one block of 30 cycles).

2.3.3. Anion exchange chromatography

The elution curves for major and minor elements passed through the anion exchange column are presented in Figure 2.6. Using the elution scheme detailed in Table 2.1b, almost all of the major and minor elements were eluted within the first 2 mL of the HCl passed over the column. Zn was only eluted from the anion exchange column when HNO_3 was passed over it. It was noted that cadmium also elutes with Zn, upon HNO_3 addition. However, for open ocean seawater samples the concentration of cadmium is 1-2 orders of magnitude lower than that of Zn, thus it is unlikely to interfere during Zn isotope determination. The recovery of Zn was greater than 99 ± 5 % (n = 8) for the ion exchange chromatography process. No difference in efficiency of anion exchange resin was observed between new and used resin. The major consideration for Zn isotope determination is the potential interference of chloride from the HCl ($^{40}Ar^{37}Cl$) on the measurement of ^{67}Zn. This can be eliminated by drying samples down and re-dissolving in 2% HNO_3.

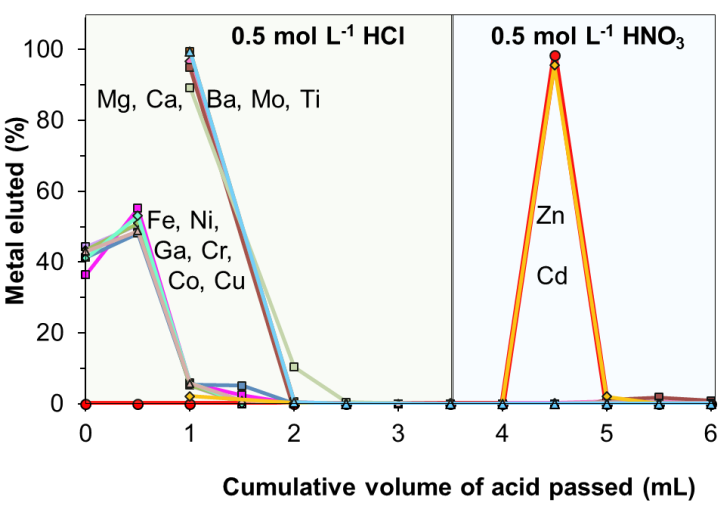

Figure 2.6: Elution curve of different elements (percentage of metal eluted) for anion exchange chromatography (using AG1X8 resin) loaded and washed with 0.5 mol L^{-1} HCl followed by elution with 0.5 mol L^{-1} HNO_3.

2.3.4. Method Blanks

The processing blank, i.e. the combined extraction and purification blank, following the steps described in Table 2.1 (a and b), ranged between 0.05 ng and 0.13 ng. This is similar to the procedural blank of 0.1 ng reported by Conway et.al (Conway et al. 2013). The main Zn blank for the overall extraction and purification procedure comes from the reagents used to buffer the sample pH prior to sample pre-concentration. The Zn concentration of the ammonium acetate was 4-5 nmol L^{-1}, which translates to an addition of 0.32 ng of Zn based on a 1 mL addition. The concentrated ammonium hydroxide solution had a Zn blank of less than 1 nmol L^{-1}, which translates to addition of 0.06 ng of Zn based on a 1 mL addition. Typically for a 500 mL sample the blank contribution was less than 0.5 ng.

2.3.5. Reproducibility

As a test of the method reproducibility, a shallow water ([Zn] = 0.05 ± 0.01 nmol L^{-1}) and a deep seawater sample ([Zn] = 6.55 ± 0.34 nmol L^{-1}) were preconcentrated and analysed on several days spanning a year. The isotopic composition reproducibility for the two samples analysed across this period were 0.08 ± 0.02 ‰ (n = 3) and 0.59 ± 0.02 ‰ (n = 9), respectively relative to the JMC Lyon isotope standard. The value obtained for the deep water sample is consistent with other data published for waters with a Southern Ocean origin (Conway and John 2014; Little et al. 2014).

2.3.6. Inter-calibration samples

To test the accuracy of the method we also ran samples obtained from GEOTRACES North Atlantic IC1 BATS inter-calibration station (Boyle et al. 2012) and from the SAFe inter-calibration station, which was located in North Pacific Ocean. The Zn isotopic results for samples analysed with our method were in excellent agreement with previously published data (Table 2.5) suggesting that method is both accurate and robust.

Table 2.5: Concentration and isotopic composition of Zn inter-calibration samples. Errors represents 2 SE for replicate extractions.

Sample Name	**Depth (m)**	**δ^{66}Zn (‰) ± 2 SEM**			**Zn (nmol L^{-1}) ± 2 SEM**	
		w.r.t IRMM-3702	w.r.t. JMC-Lyon			
		This study	This study	Literature data	This study	Literature data
GPrI 24 2680/81 GT09-02	500	-0.04 ± 0.04	0.26 ± 0.04	0.31 ± 0.01^	0.67 ± 0.01	0.68^, 0.52^, 0.66*
GPrI 2 2671 GT09-17	3500	0.07 ± 0.02	0.37 ± 0.02		2.21 ± 0.00	
SAFe D1	1000	0.15 ± 0.04	0.45 ± 0.04	0.48 ± 0.03*	8.44 ± 0.00	7.4 ± 0.35*
SAFe D2	1000	0.15 ± 0.03	0.45 ± 0.03	0.49 ± 0.03*	7.83 ± 0.25	7.19 ± 0.70[#]
Deep N. Atlantic	1500	0.11 ± 0.02	0.41 ± 0.02		2.03 ± 0.00	

[#] Data from (Milne et al. 2010), * data from (Conway et al. 2013), ^ data from (Boyle et al. 2012).

2.4. Conclusions

Here we present an accurate and precise procedure for determining the dissolved Zn isotope composition of seawater. The method makes use of the DS technique in conjunction with the pre-concentration of Zn from seawater utilising Toyopearl AF-Chelate 650M resin. The method has a high extraction efficiency (~99%), is very reproducible (0.59 ± 0.02 ‰, n = 9), and has a low processing blank. The method is well suited to analysis of surface seawater samples with low dissolved Zn concentrations. The identification of Zn isotope variability in the upper ocean will provide a useful tool to understanding the biogeochemical cycling of Zn in the ocean and thus highlights the value of this technique.

Acknowledgements

Thanks to Leslie Kinsley, Steve Eggins and Claire Thompson for their help and advice. We extend our gratitude to the captain and crew of RV Southern Surveyor for help with seawater sample collection during the PINTS voyage. Funding from Australian Research Council (DP110100108) and Australian Antarctic Division (project 3120) is appreciated. ANU and RSES scholarships to the lead author are also appreciated. Finally, we would like to thank Ed Boyle for providing the GEOTRACES IC1 BATS, Micha Rijkenberg for the North Atlantic Sample and Geoffrey Smith and Ken Bruland for the SAFe samples.

Appendix

Table 2.6: Preparation of ^{67}Zn-^{68}Zn Double Spike.

^{67}ZnO Chemgas Spike **^{67}Zn STOCK**		^{68}Zn Metal ORNL Spike (Batch 205940) **^{68}Zn STOCK**		Final **Zn-DS**	
^{67}ZnO	0.01266 g	^{68}Zn	0.00355 g	^{67}Zn STOCK	3.1163 g
Final Solution	99.63754 g	Final Solution	101.0235 g	^{68}Zn STOCK	17.6282 g
Zn	1.5326 µmol g^{-1}	Zn	0.5174708 µmol g^{-1}	Final Solution	498.42 g
Zn	102.5 µg g^{-1}	Zn	35.140339 µg g^{-1}	Zn	27.9 nmol g^{-1}
^{67}Zn	1.3884 µmol g^{-1}	^{68}Zn	0.5140555 µmol g^{-1}	Zn	1884 ng g^{-1}

Chapter 3:

Dissolved zinc isotope cycling in the Tasman Sea, SW Pacific Ocean

Moneesha Samanta, Michael J. Ellwood, Marie Sinoir, Christel S. Hassler[2]

Abstract

The trace metal micronutrient zinc (Zn) act as a cofactor in several essential enzymes within phytoplankton. The uptake of Zn by phytoplankton is complex and depends on the concentration and chemical speciation of dissolved Zn; both of which affect Zn bio-availability. In some parts of the surface ocean dissolved Zn concentrations are sufficiently low, in the picomolar range, to potentially limit the growth of certain phytoplankton species. Here we investigated the relationship between Zn availability and primary production using the dissolved Zn isotopic composition of samples collected across high and low productivity waters in the Tasman Sea, SW Pacific Ocean. Maximum variability in the isotope composition of dissolved Zn was observed in the upper ocean (0-200 m) at two stations where productivity was dominated by eukaryotic phytoplankton. At these stations, heavier δ^{66}Zn values tended to coincide with the chlorophyll maxima indicating preferential uptake of lighter Zn isotopes by phytoplankton. A significant correlation was obtained between the dissolved Zn isotopic composition and the relative fluorescence in the upper 200 m strengthening the observation that isotope fractionation occurs during Zn uptake by phytoplankton.

[2] Authors' contribution: M. Samanta analysed the dissolved Zn isotope data and drafted the manuscript with contribution from M.J.E., M. Sinoir analysed the Zn speciation data and C.S.H. analysed the biological data.

Immediately below the chlorophyll maxima, the isotope composition of dissolved Zn became lighter indicating the preferential regeneration of isotopically lighter Zn from sinking particulate organic material. A seasonal change in the Zn isotope signal was observed for a north Tasman Sea station with heavier Zn isotope values appearing to be coupled to an increase in biological production during the austral autumn. Based on the biological data, the ligand data (from a companion study) and the δ^{66}Zn values, we suggest that the composition of the resident phytoplankton community controls Zn isotope fractionation and Zn speciation in the upper water column for the Tasman Sea.

3.1. Introduction

Marine phytoplankton being primary producers, form the base of the food chain. Phytoplankton account for about more than 40 % of the total primary productivity on earth; thus playing an important role in moderating the climate through the sequestration of carbon dioxide by photosynthesis followed by its transfer to the deeper ocean via export (Falkowski 1994; Field et al. 1998). Trace metal micronutrient zinc (Zn) act as cofactors in several important enzymes including: carbonic anhydrase which catalyses the reversible hydration of CO_2 and hence plays an important role in CO_2 transport and fixation by phytoplankton (Morel et al. 1994); alkaline phosphatase which helps in the acquisition of organic phosphorous (Kuenzler and Perras 1965) by phytoplankton. However, the Zn requirement of phytoplankton species varies, as does their response to Zn limitation and toxicity (Brand et al. 1983; Sunda and Huntsman 1992). Nonetheless, Zn plays an important biological role in the marine food web (Morel and Price 2003), and hence the global carbon cycle.

In seawater, the profile of dissolved Zn concentration versus depth is nutrient like with depletion in surface waters and higher concentrations at depth. The structure of the Zn profile is similar to that of silicic acid (Si) with deeper regeneration relative to that other macro (nitrate and phosphate) and micro nutrients, suggesting that Zn may be involved in either the uptake or the formation biogenic silica structures (opal) (Bruland et al. 1994; Hunter and Boyd 1999). However, it is interesting to note that biogenic silica does not appear to be a significant export vector of Zn from the surface to the deep ocean as the diatom frustule only contain 1-3 % of the total Zn associated with the cell (Ellwood and Hunter 2000). Zhao et al. (2014) argued that Zn, which has a strong affinity for amino and carboxylic group, is associated with the polysaccharide

and/or protein coating of the diatom frustule (Gelabert et al. 2006; Zhao et al. 2014). Thus, this organic phase, which is intimately associated with the opal phase, is oxidised only after dissolution of the opal phase occurs, which could potentially result in a deeper Zn regeneration profile, similar to that of Si. John and Conway (2014) proposed that the deeper regeneration of Zn at a depth similar to Si might be due to the scavenging of Zn onto the surface of sinking phytoplankton.

Zinc has five naturally occurring stable isotopes ^{64}Zn, ^{66}Zn, ^{67}Zn, ^{68}Zn and ^{70}Zn (Rosman 1972). Mass dependent Zn isotope fractionation, the processes whereby there is partitioning of isotopes between two substances or phases resulting in different proportion of isotopes (Hoefs 2009), can be physical, biological or chemical in nature (Bermin et al. 2006; Johnson et al. 2004; Pichat et al. 2003; Rosman 1972). These isotope fractionation processes can be under kinetic or equilibrium control (Stewart 1975). Zinc isotope fractionation is expressed in delta notation, where, $\delta^{66}Zn$ is the relative deviation of the ^{66}Zn:^{64}Zn ratio of the sample with respect to a Zn standard. Zinc isotope fractionation is expressed in parts per 1000 due to small variability of Zn isotope composition in nature (Cloquet et al. 2008).

An example of biological processes leading to Zn isotope fractionation has been reported for the marine diatom *Thalassiosira oceanica* and the chlorophyte *Dunaliella tertiolecta* (John and Conway 2014; John et al. 2007) where, during Zn uptake, lighter isotopes were preferentially taken up leading to a lower Zn isotope composition within the cells relative to the media. Zinc isotope fractionation in diatom *T. oceanica* was found to be dependent on the free Zn^{2+} ion concentration in the growth media (John et al. 2007). When *T. oceanica* was grown at a low free Zn^{2+} ion concentration, Zn isotope fractionation was low and when grown at high free Zn^{2+} ion concentration, Zn

isotope fractionation was larger with the cells being ~ 0.6 ‰ lighter (John et al. 2007). Diffusion uptake of Zn also results in a light isotope composition within cells whereas surface adsorption of Zn on the cell surface leads to a heavier isotope (Gelabert et al. 2006; John et al. 2007).

Quantum mechanical calculations suggest that more strongly bounded species prefer heavier isotopes (Criss 1999); therefore tetrahedral complexes with shorter bonds would have heavier δ^{66}Zn values as compared to octahedral complexes. The carboxylate species in the external polysaccharide layer of the diatom cell wall or protein side chains which form tetrahedral complexes with Zn^{2+} was shown, using 'FITEQL thermodynamic modelling', to be the dominant group in Zn^{2+} adsorption to the diatom cell surface which explains the preferential adsorption of isotopically heavy Zn from the aqueous solution in which Zn^{2+} forms octahedral complexes with H_2O molecules with longer Zn-O bond (Gelabert et al. 2006). Modelling of Zn isotope fractionation for co-existing Zn inorganic complexes in solution shows that Zn carbonate and bicarbonate complexes are isotopically heavy, whereas, Zn chloride complexes tend to be isotopically light (Fujii et al. 2014). However, Zn isotope fractionations of Zn hydroxide and sulfate complexes are negligible at pH ≥ 8.1. This leads to an estimated negative δ^{66}Zn value for the free Zn^{2+} relative to the bulk solution, though isotope fractionation is small (Fujii et al. 2014). In open ocean waters >98% of dissolved Zn is bound to strong organic ligands, so from the discussion above we could speculate that the remaining dissolved inorganic Zn available for uptake by phytoplankton would be isotopically light relative to organically bound Zn. (Bruland 1989; Ellwood 2004; Ellwood and Van den Berg 2000; Jakuba et al. 2012; Sinoir et al. 2016b). (Peel et al. 2009) reported that in a eutrophic lake, the Zn isotope composition

of the settling particles are the lightest in the productive period and this Zn is chiefly associated with organic matter. This observation suggests that isotopically light Zn is preferentially taken up by phytoplankton (Peel et al. 2009).

Measuring the dissolved Zn isotope composition is challenging due to contamination issues associated with the collection and handling of samples and the low Zn concentrations in surface waters (Bruland et al. 1978). Advancements in analytical technique along with the advent of the multi-collector inductively coupled plasma mass spectrometry (MC-ICPMS) have made it possible to measure the isotope composition of dissolved Zn. Recent studies have shown that the Zn isotope composition of the deep water is remarkably homogeneous with a mean δ^{66}Zn value of 0.50 ± 0.15 ‰ (2SD, depth ≥ 1000 m, n = 242, 2 SE = 0.01; combining data from (Bermin 2006; Conway and John 2014; Conway and John 2015; Samanta et al. 2016; Zhao et al. 2014). However, the δ^{66}Zn seawater values near hydrothermal plumes and continental margins are isotopically lighter compared to the deep ocean (Conway and John 2014). In the oxygen minimum zones of the ocean heavier δ^{66}Zn values of dissolved Zn were attributed to removal of lighter Zn as sulphide precipitates (Conway and John 2014). Compared to the deep ocean, a wider range of δ^{66}Zn values have been observed in the surface 100 m of the ocean (between -1.1‰ and +0.9‰) (Conway and John 2014). These variations in δ^{66}Zn values of the surface waters could result from a variety of process, including complexation with organic ligands (Jouvin et al. 2009), biological uptake (Gelabert et al. 2006; John et al. 2007), particle scavenging (John and Conway 2014) and input from rivers and aerosols (Conway and John 2014; Little et al. 2014).

The aim of this chapter is to investigate the relationship between Zn availability and primary production using the dissolved Zn isotopic composition of samples collected across the north-south transect of the Tasman Sea, from oligotrophic waters north of the Tasman Front to mesotrophic waters in the mid Tasman sea through to the highly productive water in the subantarctic zone (SAZ).

3.2. Experimental

3.2.1 Cleaning

All equipment used in this study had been extensively acid-cleaned. Typically, sample bottles were soaked for 1 week in a 15% aqua regia (HCl:HNO_3 3:1) AR grade, rinsed and then soaked for a further week in 2% HNO_3. Water used to rinse bottles was purified using an ion-exchange water purification system (Milli-Q water) (Millipore, Australia). The final step in the process was to fill bottles with 0.5% (w/w) Teflon-distilled (designated here as t-acid, Savillex, USA) HNO_3 (Mattinson, 1972) and doubly bagged. Laboratory plastic-ware was acid-cleaned by heating in aqua regia followed heating with 0.5% t-HNO_3.

3.2.2. Sampling

The majority of the seawater samples for dissolved Zn isotopic analyses were collected during the PINTS (Primary productivity induced by Iron and Nitrogen in the Tasman Sea) voyage in the austral summer (January-February) of 2010 (Hassler et al. 2014). Three process stations (P1, P2 and P3) were located along a north-south transect within the Tasman Sea region (Figure 1). Station P1 was reoccupied in May 2011 as part of the GP13 zonal section. Re-occupation of this station allow us to compare seasonal changes and the chemical and biological characteristics of this north Tasman Sea region.

PINTS samples were collected on board the R.V. *Southern Surveyor* as a GEOTRACES Process study following similar protocols recommended by GEOTRACES (Cutter et al.

2014). The procedures followed for seawater sample collection, and data analysis for salinity, temperature, fluorescence, oxygen, pigments concentration and composition, photophysiology, primary productivity, N_2 fixation rate and macronutrient concentration (reactive phosphorus, PO_4; Si; nitrate-plus-nitrite, NO_x) are reported in 'Primary productivity induced by iron and nitrogen in the Tasman Sea: an overview of the PINTS expedition' (Hassler et al. 2014). For the dissolved Zn isotope work, seawater samples were collected across a range of depths (from 15m to 3000 m or 3500 m) at GEOTRACES process stations P1 (30°S, 165°E), P2 (39.6°S, 162.1°E) and P3 (46.2°S, 159.5°E).

Seawater samples were collected using a trace-metal clean autonomous rosette (Model 1018, General Oceanics, USA) equipped with 12 × 10 L Teflon-coated Niskin X-1010 bottles deployed using a 6 mm Dynex cable (Hampidjan). Samples were then filtered through 0.2 µm acid-washed capsule filter cartridges (Pall, AcroPak 200) into acid washed low density polyethylene bottles under HEPA filtered air (ISO Class 5 conditions). Samples were stored double bagged in plastic tubs after acidification with Teflon-distilled nitric acid to pH 1.6 (Hassler et al. 2014; Thompson and Ellwood 2014)

Water collected from Niskin bottles on the calibrated standard conductivity-temperature-depth (CTD) rosette (SeaBird SBE11) was used to obtain salinity, temperature, fluorescence, oxygen data and samples for pigments and nutrient analysis. Automated flow-injection analyser (Lachat QuickChem 300, Lachat Instruments, Loveland, CO, USA) and colorimetric techniques were used by CSIRO Hydrochemistry to determine macronutrients (reactive phosphorus, PO_4; Si; nitrate-plus-nitrite, NO_x) at sea.

3.2.3 Biological measurements

Phytoplankton biomass was determined from the concentrations of chlorophyll *a*; while the phytoplankton community structure for the three Tasman Sea stations was determined by analysing the biomarker pigments (Jeffrey and Vesk 1997; Jeffrey and Wright 2006). Analysis was undertaken by High Performance Liquid Chromatography (Alliance, Waters) and a photo-diode array detector following a modified version of (Van Heukelem and Thomas 2001). The concentrations of chlorophyll *a* and chlorophyll *b* were determined by comparing with Sigma standards and that of the other biomarker pigments, Fucoxanthin (Fuco), 19-Butanoyloxyfucoxanthin (But-Fuco), 19 Hexanoyloxyfucoxanthin (Hex-Fuco), Zeaxanthin (Zea), Peridinin (Perid) and Divinyl Chlorophyll *a* (DVChl *a*), were determined from DHI (Denmark) standards. The method is described in detail by Hassler et al. (2012). Briefly, phytoplankton was collected by gently filtering seawater through a Whatman GF/F filter and stored until use in liquid nitrogen in cryovials. To extract the pigments, sonication was done in two stages in 100% methanol in the dark and on ice. The pigment extract, kept at 4◦C overnight, was then separated from the filter debris by centrifugation for analysis. Chlorophyll *a* and the different biomarker pigment concentrations were integrated from 30 to 125 m depth for P1, 15 to 70 m depth for P2 and from 15 to 80 m depth for P3 to determine the biomass and estimation of the community structure of the phytoplankton assemblage.

3.2.4. Procedure for dissolved Zn isotope analysis

Analysis of dissolved Zn isotope was done following the procedure described in Chapter 2. Purification and separation of Zn from the seawater matrix was by solid phase extraction utilising chelating ion chromatography followed by anion exchange chromatography. Samples were spiked with a ^{67}Zn-^{68}Zn double spike (DS) 12 hours prior to processing to correct for any mass dependent fractionation that might occur during sample preparation and measurement. After letting the sample-DS mixture equilibrate overnight, the pH was adjusted to around 5.5 using ammonium hydroxide and buffer ammonium acetate. This pH adjusted seawater-DS mixture was passed through a Teflon column containing 0.5 mL of cleaned and conditioned Toyopearl AF-Chelate 650M resin for pre-concentration of trace metals. Interfering alkali metals and alkaline earth metals were removed by flushing with the dilute ammonium acetate (pH 5.5) (Willie et al. 1998a). Zinc was then eluted from the column with 1 mol L^{-1} HCl, dried and taken up in 0.5 mL of HCl for anion exchange chromatography. This was loaded onto a Teflon column containing 0.15 mL of cleaned and conditioned AG1X-8 resin, 200-400 mesh. The column was rinsed with 0.5 mol L^{-1} HCl to remove potentially interfering elements. After a suitable volume of HCl had been passed over the column, Zn was eluted from the resin with 0.5 mol L^{-1} HNO_3.

Zinc isotope measurements were made by Multicollector-ICPMS (Thermo Scientific Neptune Plus) with a desolvating sample introduction system (Apex IR, Elemental Scientific Inc.) at an uptake rate of ~ 50 µL per minute. A standard Ni sampler cone and a Ni X-skimmer cone were used to enhance instrument sensitivity. At the start of each measurement session, the instrument was tuned for intensities on masses ^{62}Ni, ^{63}Cu, ^{65}Cu, ^{64}Zn, ^{66}Zn, ^{67}Zn and ^{68}Zn. Samples were analysed in low resolution mode in groups

of three, bracketed with a standard-DS mixture with a 2% (v/v) HNO_3 blank measurement before each sample or standard measurement. All measurements were made as 1 block of 30 cycles with a 4 second integration time. Measured isotopes intensities were on-peak blank corrected. The results were processed using the procedures outlined in Chapter 2.

All Zn isotope ratios were measured relative to the standard reference material IRMM-3702, which is isotopically indistinguishable from the new Zn standard AA-ETH Zn (Archer et al. 2017) and has an offset of 0.30 ± 0.05 (‰) with respect to the Johnson Matthey (JMC) Lyon standard (Archer et al. 2017; Cloquet et al. 2008; Moeller et al. 2011). The $\delta^{66}Zn$ values in this chapter are reported with respect to JMC-Lyon Zn standard using the following the equation:

$$\delta^{66}Zn_{JMC_Lyon} = \left(\frac{^{66}Zn/^{64}Zn_{sample}}{^{66}Zn/^{64}Zn_{IRMM_3702}} - 1\right) \times 1000 + \delta^{66}Zn_{IRMM_3702 \quad - JMC_Lyon} \quad (1)$$

Uncertainties associated with $\delta^{66}Zn_{IRMM_3702 - JMC_Lyon}$ were not propagated into the Zn isotope values as the analytical uncertainty in most cases is greater than the error introduced by this simplification (Archer et al. 2017). The error bars for the majority of the samples presented represent 2 x standard error (2 SE) of multiple ($n \geq 2$) extractions. Where sample volumes limited us to a signal extraction, error bars represent 2 standard error of the mean for a measurement block consisting of 30 cycles. As a check on the accuracy of our Zn concentration data, we compared our data to Zn concentrations obtained by the CSIRO trace metal group for samples collected at station P1 (Edward Bulter, personnel communication). The overall correlation between the two datasets was excellent: Zn_{CSIRO} = [0.96 ± 0.02] Zn_{ANU} + [0.02 ± 0.12] (r^2 = 0.997,

n = 7; note that the limit of detection for the CSIRO dataset was 0.1 nmol kg^{-1} so concentrations below this value were not included in the comparison).

The reproducibility of the procedure, described in Chapter 2, for a deep seawater sample is 6.55 ± 0.34 nmol L^{-1} and 0.59 ± 0.02 ‰ (n = 9) and a shallow seawater sample is 0.05 ± 0.01 nmol L^{-1} and 0.08 ± 0.02 ‰ (n = 3) analysed over a period of one year.

Samples collected during reoccupation of station P1, as part of the GEOTRACES GP13 transect were analysed for Zn isotopes at the Department of Earth Sciences in ETH Zurich.

3.3. Results and Discussion.

In this study, we compare and contrast the dissolved Zn isotopic composition for high and low productive waters in three chemically distinct oceanographic regimes with the aim of determining the processes that potentially influence Zn isotope fractionation in the upper water column. We then explore the role of seasonal variability in primary productivity has on δ^{66}Zn fractionation at process station P1 in the north Tasman Sea. This is followed by a discussion on the Zn and Si relationship in the South Pacific Ocean where we speculate on the mechanism(s) controlling the coupling of dissolved Zn and Si relationship in the deeper ocean.

3.3.1. Hydrography

The three Process stations P1, P2 and P3 represent chemically distinct oceanographic regions in the Tasman Sea (Figure 3.1) (Hassler et al. 2014). Station P1, located north of the Tasman front (33-34°S) in the New Caledonia Basin, is an oligotrophic site with nitrate concentrations typically less than 0.05 µmol L^{-1} (Figure 3.1B)(Ellwood et al. 2013; Law et al. 2011). This site is influenced by the East Australian Current (EAC) which is associated with warm, saline, low oxygen water originating from the Coral Sea region (Figure 3.2) (Ridgway and Dunn 2003). At station P1, Subtropical Lower Water (SLW) overlies significantly modified intermediate waters: Subantarctic Mode Water (SAMW) and Antarctic Intermediate Water (AAIW) (Figure 3.9) (Bostock et al. 2013). SLW is formed in the central Tasman Sea where there is excess of evaporation over

precipitation. It has a shallow summer mixed layer and a deeper winter mixed layer due to strong cooling by the atmosphere (Sokolov and Rintoul 2000).

Station P2 is located in the mesotrophic mid Tasman Sea, between the Tasman Front to the north and the Subtropical Front (STF) to the south. The Tasman Front is displayed by a subsurface frontal region between 50 m and 250 m in both temperature (*T*) and salinity (*S*). The Subtropical Front is marked by a sharp transition between cool, fresh, high oxygen subantarctic waters of the south and warm, saline, low oxygen subtropical waters in the north which was expressed in both *T* and *S* in the upper 400 m (Figure 3.2).

Station P3 is located in the highly productive South Tasman Sea, in subantarctic waters south of the STF. The surface waters at this site are characterised by cool, fresh, oxygen rich waters with a Southern Ocean origin (Figure 3.2).

SAMW, formed by deep winter convection in the Sub Antarctic Zone (SAZ), is characterised by an oxygen maxima (between 200 m and 600 m; Figure 3.9) (Sokolov and Rintoul 2000) and a low Si to nitrate ratio ($Si:NO_3$) (Sarmiento et al. 2004; Wyatt et al. 2014). SAMW enters the Tasman Sea from the south and also from the north via the EAC (Sokolov and Rintoul 2000). SAMW is identified by a negative Si* (which is the dissolved Si concentration minus the dissolved nitrate concentration) and a high oxygen pycnostad; the thickness and the oxygen content of which decreased from south to north from station P3 to station P1 (Figure 3.2). Negative Si* values are observed between 125 m and 750 m for stations P1 and P2 and from the surface to 750 m for station P3. The Si to nitrate ratio decrease and Si* becomes more negative from north to south in the Tasman Sea. The most negative Si* values are observed

between 80 m and 750m at the SAZ station P3 and between 500m and 750m at the northern station P1 (Figure 3.2D).

At station P3, AAIW is characterised by a salinity minimum (<34.4) and enters the Tasman Sea from the south (Figure 3.2) (Bostock et al. 2013; Ridgway and Dunn 2003). AAIW at this station is thought to originate from the Indian sector of the Southern Ocean ((Bostock et al. 2013) and references therein). In contrast, AAIW at station P1 appears to be a modified variety of AAIW (salinity ~ 34.45) formed through the mixing of AAIW within the subtropical gyre with shallower high salinity, warm thermocline waters from the north Tasman Sea (Bostock et al. 2013). AAIW originating from the north flows beneath the EAC. At station P2, AAIW has a salinity minima intermediate of that observed at station P1 and P3 and is formed by mixing of these two varieties of AAIW (Figures 3.2 and 3.9).

Below AAIW is Circumpolar Deep Water (CDW). Upper Circumpolar Deep Water (UCDW) is influenced by low oxygen waters from the Pacific and Lower Circumpolar Deep Water (LCDW), between 2500 and 3000 m, is influenced by a weak salinity maximum of North Atlantic Deep Water (Figure 3.9). The thickness of the oxygen minimum layer of UCDW (between 1500 and 2000 m) decreases from the North Tasman Sea to the South Tasman Sea as the oxygen content increases (Sokolov and Rintoul 2000). Below 3000 m lies cool fresh modified Antarctic Bottom Water (AABW) (Figure 3.9).

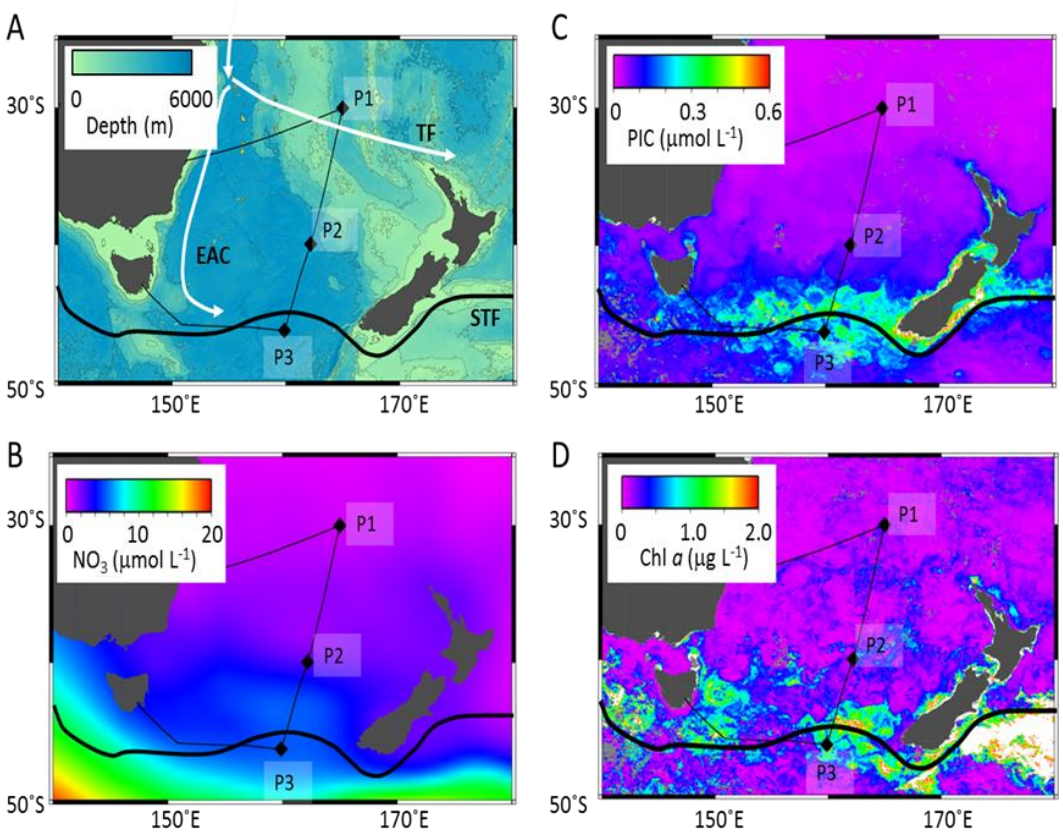

Figure 3.1: Maps of **A**. Seafloor bathymetry; **B.** Surface nitrate concentration; **C.** Particulate inorganic carbonate (PIC) concentration and; **D.** Chlorophyll *a* concentration. Nitrate concentration data was extracted from the electronic version of the World Ocean Circulation Experiment database compiled by Schlitzer (2006). Surface chlorophyll and PIC data were extracted from the Aqua MODIS dataset via ERDDAP at NOAA (upwell.pfeg.noaa.gov/erddap/). The chlorophyll and PIC datasets cover the January-February sampling period during the 2010 PINTS voyage. P1, P2 and P3 denote the three process stations from which samples were collected for the dissolved Zn isotope work. The abbreviations EAC, TF and STF correspond to East Australian Current, Tasman Front and Subtropical Front, respectively.

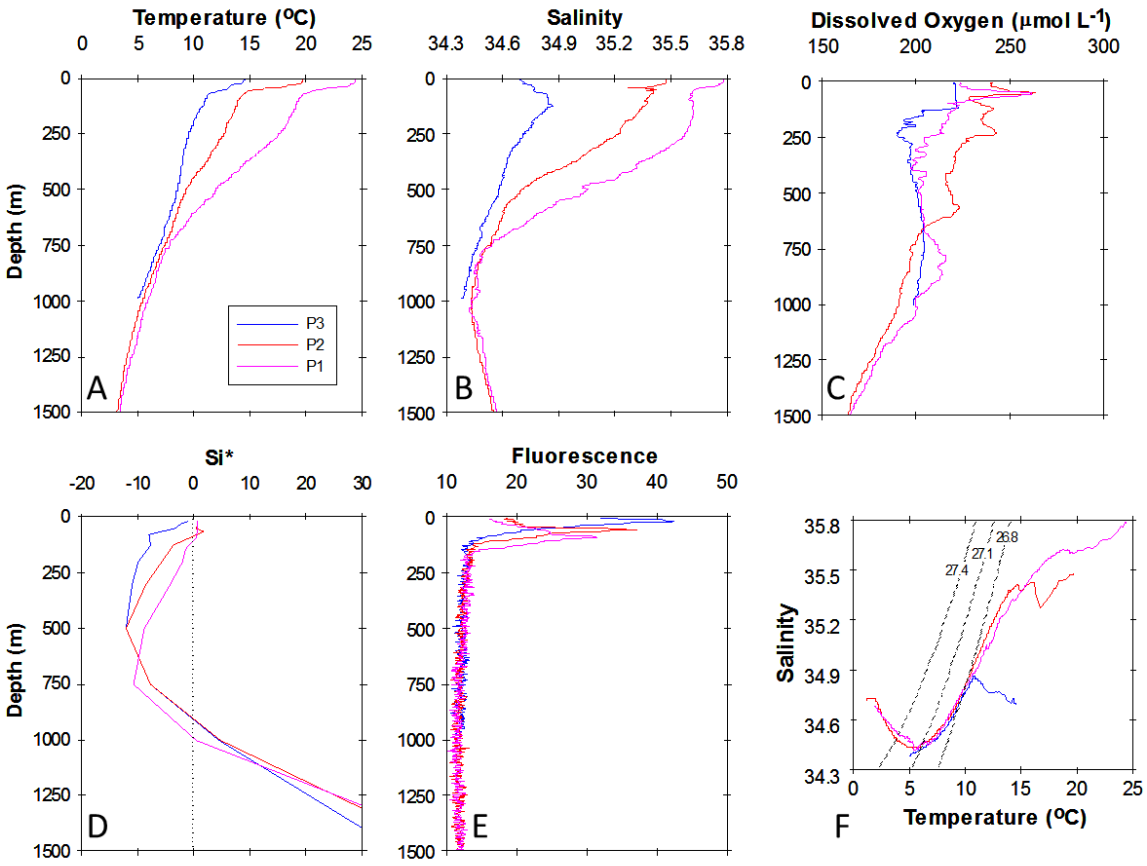

Figure 3.2. Profiles to 1500 m of: **A.** Temperature, **B.** Salinity, **C.** Dissolved oxygen, **D.** Si*, **E.** raw CTD fluorescence and **F.** a property-property plot of temperature versus salinity for process stations P1, P2 and P3. The density lines are for sigma-t of 26.8, 27.1 and 27.4. SAMW typically occurs between a density of 26.8 and 27.1 and AAIW occurs between a density between 27.1 and 27.4.

3.3.2. Biological data

The biological data for the three process stations sampled here have been previously reported (Hassler et al. 2014; Sinoir et al. 2016b). The fluorescence data from the CTD and the total chlorophyll *a* concentration at each station are well correlated across the depth 0 to 100 m (p = <0.01 stn P1; <0.01 stn P2; <0.01 Stn P3). The total water column integrated chlorophyll *a* concentration increased in a southward direction. The depth of the Deep Chlorophyll Maximum (DCM) also shoaled with depth from north (P1) to

south (P3) (Figure 3.2). Station P1 had the lowest chlorophyll *a* concentration (0.12 to 0.36 µg L^{-1}), especially in the top 50 m, with a maximum chlorophyll *a* found between 90 and 110 m. Cyanobacteria (*Prochlorococcus and Synechococcus)* (22%), along with haptophytes (24%) and other tropical species (23%) are present at this station (Figure 3.3A and 3.4). A peak in *Prochlorococcus* abundance coincided with the depth of the DCM (~ 95m). High N_2 fixation rates (maximum N_2 fixation at 50 m), due to the presence of diazotrophs, are also noted for this station (Law et al. 2012; Law et al. 2011).

The total chlorophyll *a* concentration at P2 ranged between 0.16 and 0.69 µg L^{-1} with a maximum chlorophyll *a* concentration found between 40 and 60 m. The dominant phytoplankton groups at this site are haptophytes (27%), cyanobacteria (15 %) and chlorophytes (11 %) (Figure 3.3B).

Station P3 had the highest chlorophyll *a* concentrations (0.18 to 0.92 µg L^{-1}) of all the stations with most of the biomass present in the top 30 m. The dominant phytoplankton group at this station are haptophytes (44%), which is corroborated by the MODIS calcite map (Figure 1C), which shows a coccolithophorid bloom at P3 during the time of sampling. Other phytoplankton groups found at P3 are chlorophytes (14%) and cyanobacteria (5%; dominated by *Synechococcus*) (Figure 3.3C). The abundance of diatoms increased from P1 to P3 and dinoflagellates are also present (less than 5%) in all stations.

Reoccupation of Station P1 in late autumn 2011 revealed high biological production at this station compared to summertime sampling during January 2010. During the summertime occupation of this station, a distinct DCM is observed at 95 m whereas

during the autumn occupation no DCM is observed; rather production is high throughout the upper water column (0-100 m) as reflected in the raw fluorescence data for this station and the cyanobacterial and picoeukaryotic cell counts (Figure 3.4). AQUA MODIS satellite observations of the site also highlighted higher surface chlorophyll *a* concentrations during autumn sampling period (data not presented). Macro-nutrient concentrations within the upper water were also elevated during the reoccupation of P1 in May 2011, which is indicative of an increased vertical supply of nutrients across the pycnocline in the euphotic zone. This increased nutrient supply is the main factor leading to the increased phytoplankton production during this period.

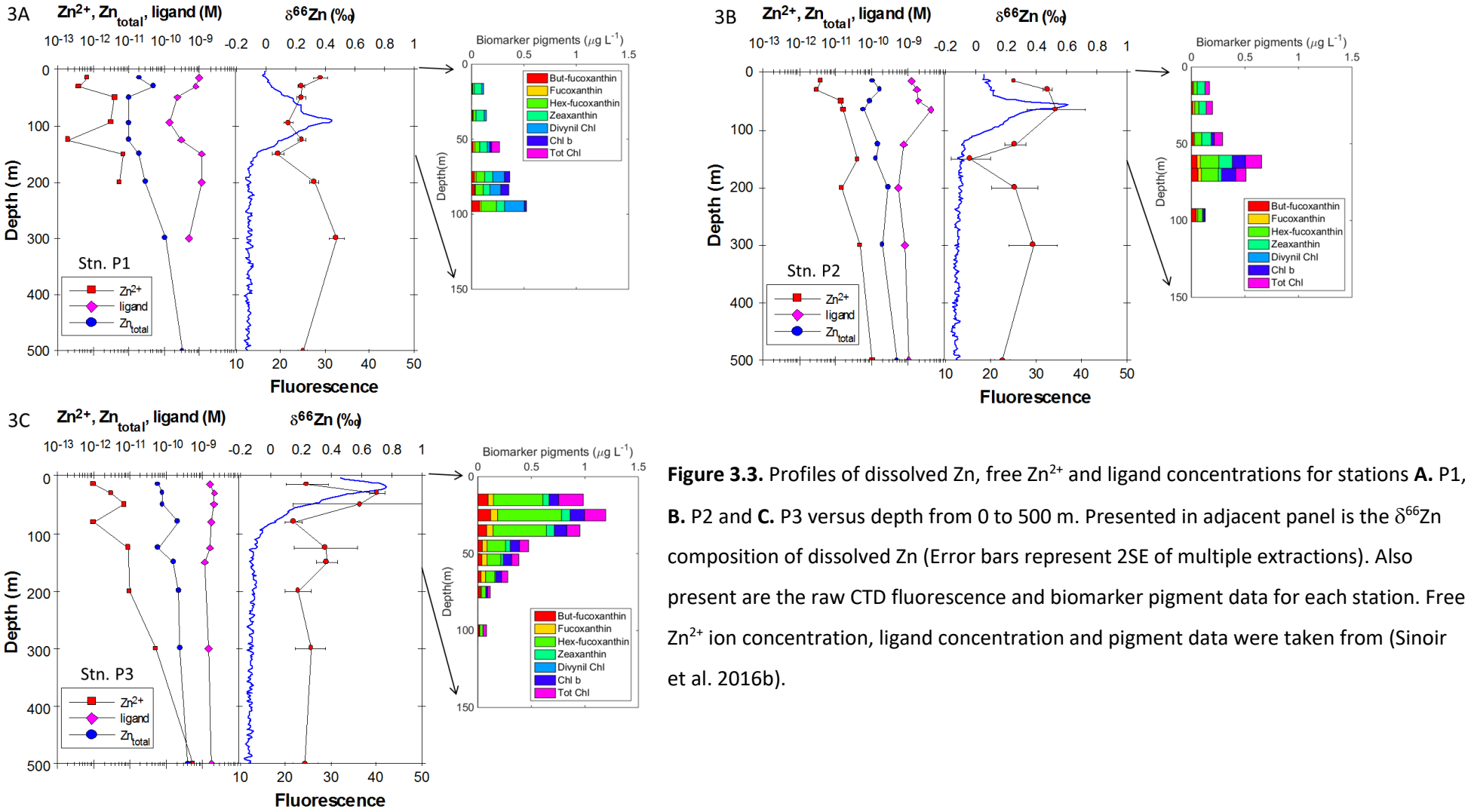

Figure 3.3. Profiles of dissolved Zn, free Zn^{2+} and ligand concentrations for stations **A.** P1, **B.** P2 and **C.** P3 versus depth from 0 to 500 m. Presented in adjacent panel is the $\delta^{66}Zn$ composition of dissolved Zn (Error bars represent 2SE of multiple extractions). Also present are the raw CTD fluorescence and biomarker pigment data for each station. Free Zn^{2+} ion concentration, ligand concentration and pigment data were taken from (Sinoir et al. 2016b).

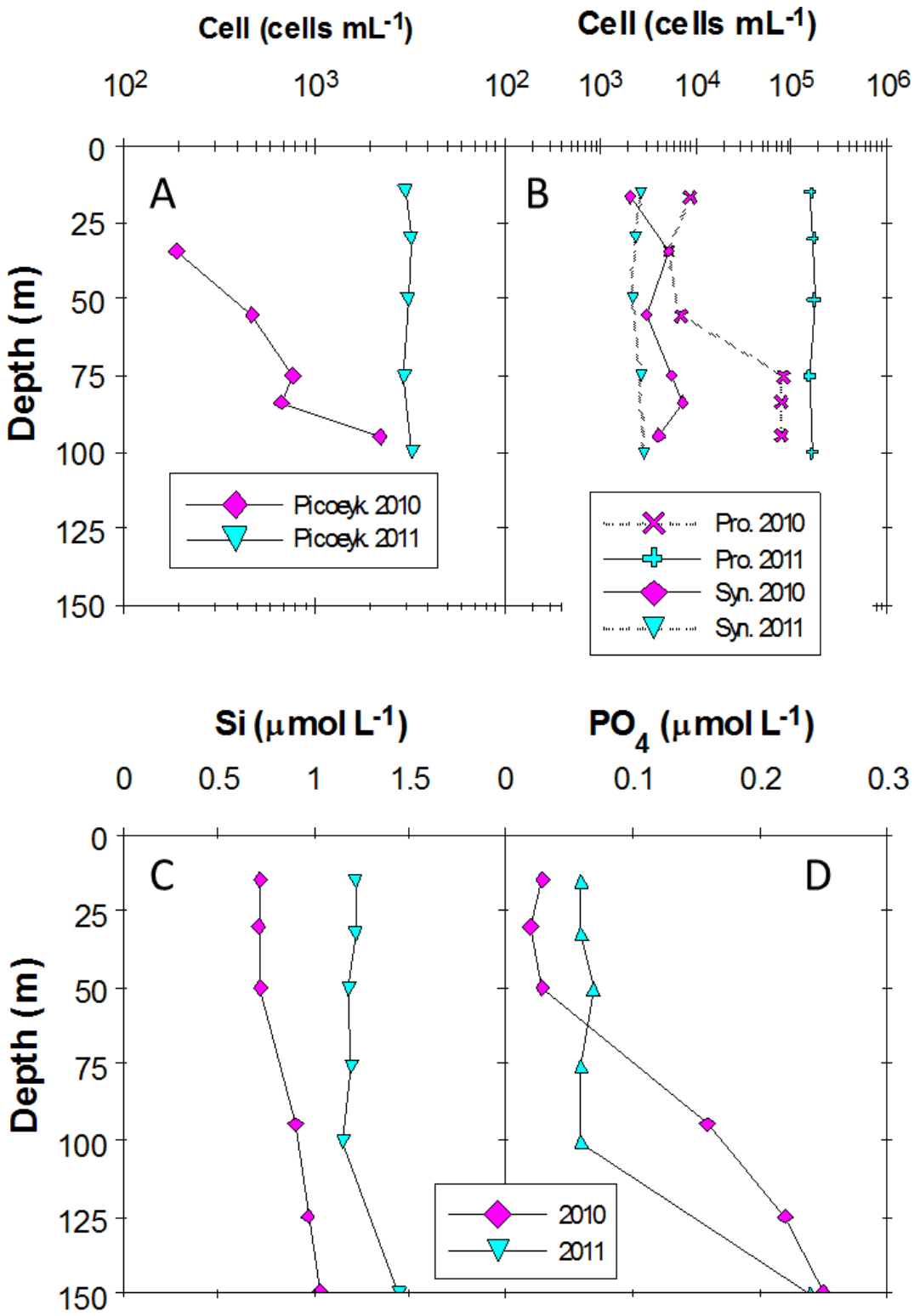

Figure 3.4. Seasonal variations in **A.** Picoeukaryotic (Picoeuk.) **B.** Synechococcus (Syn.) and Prochlorococcus (Pro.) cell abundance, **C.** Silicic acid concentration and **D.** Phosphate concentration, versus depth for process station P1.

3.3.3. Dissolved Zn concentration and isotope results

Profiles of Zn concentration and isotopic composition measured at the three process stations are presented in Figures 3.3 and 3.5 and Table 3.2. The dissolved Zn concentrations versus depth profiles for all three stations are nutrient like and similar to that of Si (Figure 3.5). There is a strong correlation (R^2=0.99, p< 0.001) between the dissolved Zn concentration and Si concentration, which is consistent with other data from the Southwest Pacific Ocean (Figure 3.5) (Ellwood 2008). The concentration of Zn and Si in surface waters is higher at station P3 compared to stations P2 and P1, whilst at depth (>1500 m) the concentration of Zn and Si is greater at P1 relative to stations P2 and P3 (Figure 3.5).

The isotope composition for dissolved Zn (δ^{66}Zn) varied between -0.03 ‰ and 0.71 ‰ with most of the variability occurring in the upper water column at each of the stations (Table 3.2). Below 750 m the δ^{66}Zn composition varied between 0.37 ‰ and 0.60 ‰ which is comparable to the deep ocean mean δ^{66}Zn value of 0.50 ± 0.14 ‰ (2SD, depth ≥ 1000 m, n = 252; (Conway and John 2014; Zhao et al. 2014) present study) (Figure 3.5C). There is good agreement in the δ^{66}Zn below 750 m for samples collected at station P1 during summer 2010 (PINTS) and late autumn in 2011 (GP13) with deep water values averaging 0.44 ± 0.02 ‰ (1SD) and 0.49 ± 0.05 for PINTS and GP13, respectively. The variability in δ^{66}Zn in the deep ocean for the summer and autumn profiles could be attributed to error in external reproducibility associated with measurements in different laboratories (John et al. 2017a).

At station P3, the heaviest δ^{66}Zn value (0.71 ± 0.05 ‰) is associated with the DCM (30 m) (Figures 3.3C and 3.5C). Similarly, at station P2 a heavy δ^{66}Zn value is associated

with the DCM (65 m), though the extent of $\delta^{66}Zn$ fractionation is lower (0.53 ± 0.03 ‰; Figures 3.3B and 3.5C). Below the DCM, the dissolved Zn becomes isotopically lighter, by approximately 0.55 ‰, with values of 0.16 ± 0.06 ‰ at 80 m for station P3 and -0.03 ± 0.19 ‰ at 150 m for station P2 (Figures 3.3 and 3.5C). A significant correlation ($p \leq 0.01$, $r^2 = 0.63$) is obtained between $\delta^{66}Zn$ and the relative fluorescence data for the upper 200 m for stations P2 and P3 (Figure 3.6A). We observed a negative correlation between $\delta^{66}Zn$ and the dissolved Zn concentration (30 -200 m) whereby the heaviest $\delta^{66}Zn$ values correspond to the lowest dissolved Zn concentrations within the DCM (for station P3, $r^2 = 0.66$). Below the DCM, the dissolved Zn concentration increases and $\delta^{66}Zn$ becomes lighter (Figure 3.6B). The heavier $\delta^{66}Zn$ values observed at depth of the DCM for stations P2 and P3 suggest that eukaryotic phytoplankton preferentially accumulate lighter Zn isotopes, which is consistent with the culture work of John et al. (2007). Based on the extent of Zn isotope fractionation ($\Delta^{66}Zn_{DCM\text{-}surface} \approx$ 0.5 ‰ (P3); 0.3 ‰ (P2)), phytoplankton in the South Tasman Sea do not appear to be Zn-limited even though free Zn^{2+} ion concentrations are in the low picomolar concentration range (0.4 to 22 pmol L^{-1}; surface to 200 m) (Figure 3.3)(Sinoir et al. 2016b). If phytoplankton in the south Tasman Sea are Zn-limited, the degree of $\delta^{66}Zn$ fractionation within the DCM is expected to be smaller, although this idea needs to be tempered with the realisation that dissolved Zn maybe cycled multiple times within the DCM by cells, which may amplify the degree fractionation observed.

Below the DCM at stations P2 and P3, a shift to lighter $\delta^{66}Zn$ values along with an increase in Zn concentration suggests shallow remineralisation of Zn associated with cellular debris. This observation is consistent with other studies (Bermin et al. 2006; Boyle et al. 2012; Conway and John 2014; Croot et al. 2011; Zhao et al. 2014) although

the scavenging of heavy Zn from solution would also produce light dissolved Zn isotope composition (John and Conway 2014).

At station P1, the variability in $\delta^{66}Zn$ is low between the surface and 200 m, with values ranging between 0.08 ‰ and 0.37 ‰, with no apparent correlation between $\delta^{66}Zn$ and relative fluorescence, even across the depth of DCM. At this station the DCM was dominated by the prokaryotic cyanobacteria *Prochlorococcus* which has low Zn requirement (Brand et al. 1983; Saito and Goepfert 2008). In a companion study to this one (Sinoir et al. 2016b)reported significant negative correlation between biomarker pigments Zeaxanthin (indicating the presence of cyanobacteria) and free Zn^{2+} ion concentration across all stations (Sinoir et al. 2016b). They also reported a significant negative correlation between Divinyl Chlorophyll *a* (indicating the presence of tropical species like cyanobacteria *Prochlorococcus*) and Zn concentration across all Tasman Sea stations; which they suggested that low Zn availability favoured prokaryotes production over eukaryote production (Sinoir et al. 2016b). These results indicate that different classes of organisms may exhibit different Zn isotope fractionation factors, which is hitherto unknown.

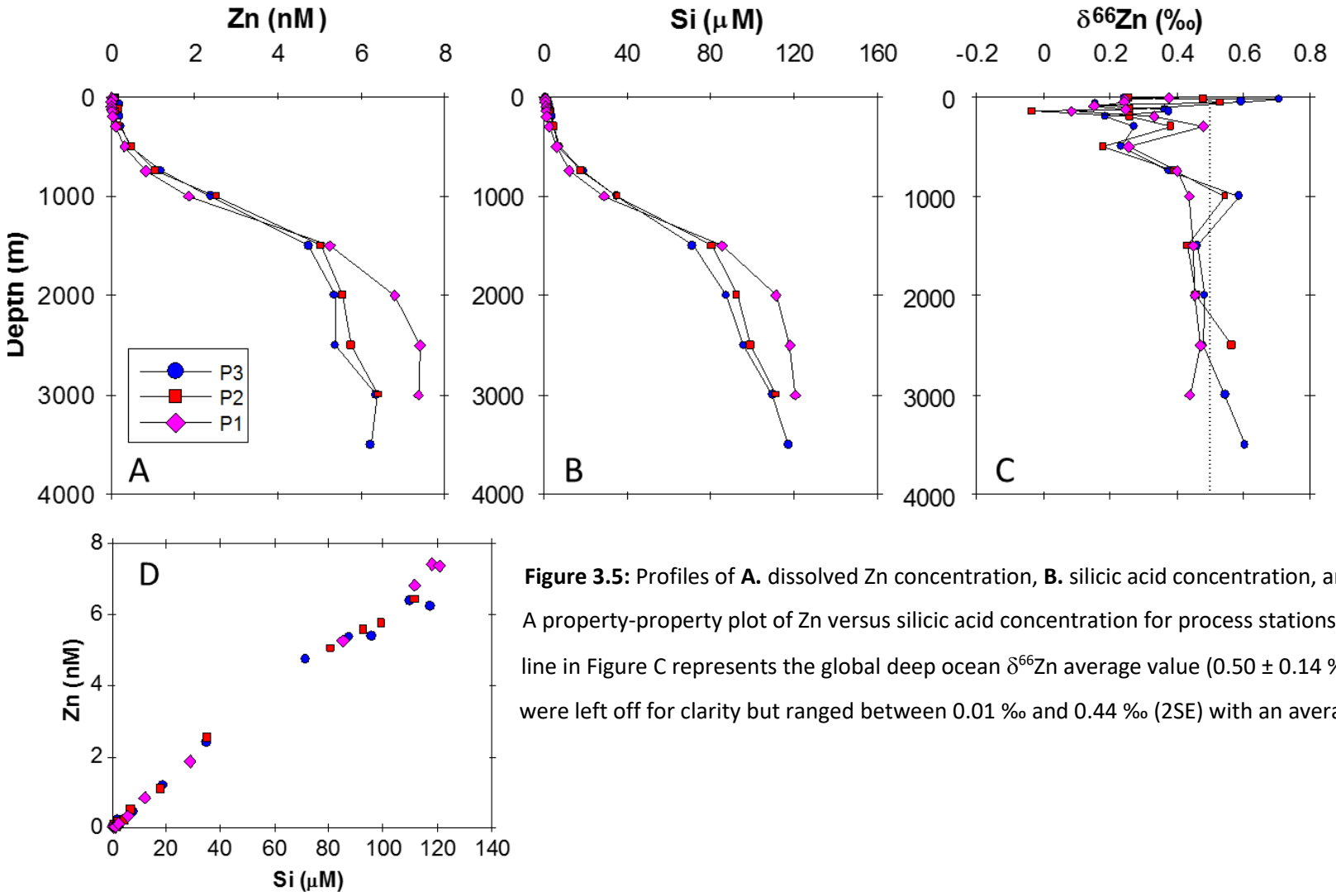

Figure 3.5: Profiles of **A.** dissolved Zn concentration, **B.** silicic acid concentration, and **C.** δ^{66}Zn versus depth. **D.** A property-property plot of Zn versus silicic acid concentration for process stations P1, P2 and P3. The dotted line in Figure C represents the global deep ocean δ^{66}Zn average value (0.50 ± 0.14 ‰). The error bars for δ^{66}Zn were left off for clarity but ranged between 0.01 ‰ and 0.44 ‰ (2SE) with an average of 0.10 ‰.

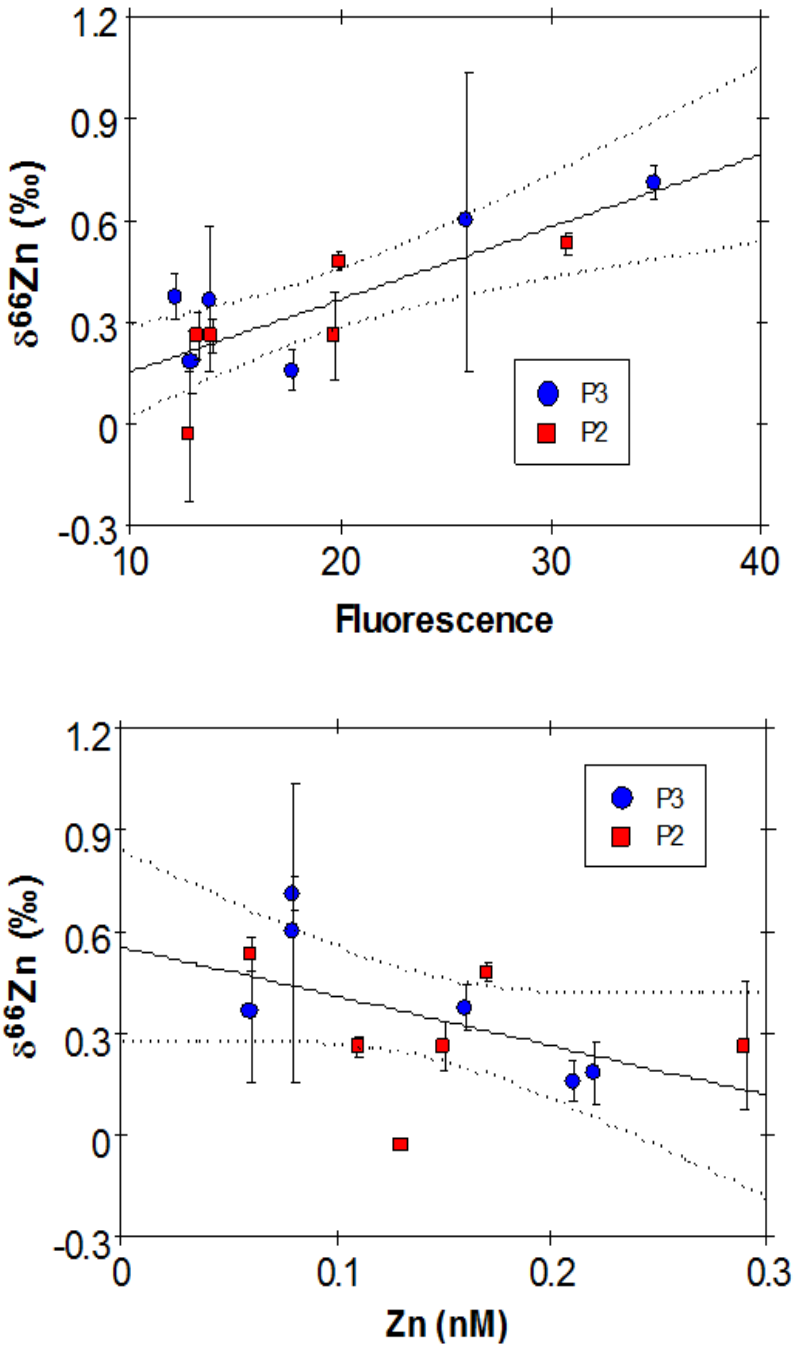

Figure 3.6: Property-property plots of δ^{66}Zn versus A. raw CTD fluorescence and B. dissolved Zn concentration for process stations P2 and P3 between 0 and 200 m. Dotted lines represent the 95% confidence intervals for the regression.

Table 3.1: Zinc isotope and concentration data for the stations P1, P2 and P3 of the Tasman Sea. Error represents 2 SE for complete replicates, i.e. repeated extraction and isolation of Zn followed by mass spectrometry.

Depth (db)	Average $\delta^{66}Zn_{IRMM-3702}$ (‰)	$\delta^{66}Zn_{JMC-Lyon}$ (‰)$^{\#,\Psi}$	$\delta^{66}Zn_{IRMM-3702}$ (‰) replicates						Average Zn (nmol kg^{-1})	Zn (nmol kg^{-1}) replicates					
			1	2	3	4	5	6		1	2	3	4	5	6
Station P3 (46.2 °S; 159.5 °E) – 8 February 2010															
15	-0.05 ± 0.14	0.25 ± 0.14	-0.12	0.01					0.06 ± 0.01	0.07	0.06				
30	0.41 ± 0.05	0.71 ± 0.05	0.43	0.38					0.08 ± 0.00	0.08	0.08				
50	0.29 ± 0.44	0.59 ± 0.44	0.08	0.51					0.08 ± 0.00	0.07	0.08				
80	-0.14 ± 0.06	0.16 ± 0.06	-0.12	-0.17					0.21 ± 0.00	0.21	0.20				
125	0.07 ± 0.21	0.37 ± 0.21	0.17	-0.04					0.06 ± 0.00	0.06	0.06				
150	0.07 ± 0.07	0.37 ± 0.07	0.04	0.11					0.16 ± 0.00	0.16	0.16				
200	-0.12 ± 0.18	0.18 ± 0.09	-0.16	-0.07					0.22 ± 0.03	0.23	0.20				
300	-0.03 ± 0.10	0.27 ± 0.10	0.02	-0.08					0.24 ± 0.01	0.24	0.23				
500	-0.07 ± 0.08	0.23 ± 0.08	-0.06	-0.18					0.40 ± 0.02	0.40	0.39				
750	0.07 ± 0.01	0.37 ± 0.01	0.07	0.08					2.12 ± 0.02	2.13	2.11				
1000	0.29 ± 0.02	0.59 ± 0.03	0.27	0.30					2.39 ± 0.00	2.40	2.39				
1500	0.16 ± 0.05	0.46 ± 0.05	0.19	0.12	0.22	0.12			4.74 ± 0.03	4.78	4.73	4.73	4.72		

2000	0.18 ± 0.07	0.48 ± 0.07	0.22	0.15					5.37 ± 0.10	5.32	5.42				
2500	0.18 ± 0.06	0.48 ± 0.04	0.14	0.20	0.20				5.39 ± 0.00	5.39	5.39	5.39			
3000	0.25 ± 0.11	0.55 ± 0.11	0.19	0.30					6.38 ± 0.00	6.38	6.38				
3500	0.30 ± 0.02	0.60 ± 0.02	0.28	0.34	0.32	0.30	0.30	0.29	6.24 ± 0.02	6.23	6.22	6.26	6.22	6.22	6.28

Station P2 (39.6 °S; 162.1 °E) – 4 February 2010

15	-0.04 ± 0.13	0.26 ± 0.13	-0.17	-0.02	0.05				0.11 ± 0.02	0.10	0.14	0.10			
30	0.18 ± 0.03	0.48 ± 0.03$^{\psi}$	0.18						0.17	0.17					
65	0.23 ± 0.03	0.53 ± 0.03$^{\psi}$	0.23						0.06	0.06					
125	-0.04 ± 0.05	0.26 ± 0.05	-0.06	-0.01					0.15 ± 0.04	0.17	0.14				
150	-0.33 ± 0.19	-0.03 ± 0.19	-0.24	-0.43					0.13 ± 0.00	0.13	0.13				
200	-0.04 ± 0.07	0.26 ± 0.07	-0.01	-0.07					0.29 ± 0.03	0.30	0.28				
300	0.08 ± 0.13	0.38 ± 0.13	0.15	0.02					0.20 ± 0.00	0.20	0.20				
500	-0.12 ± 0.15	0.18 ± 0.15	-0.19	-0.05					0.50 ± 0.00	0.50	0.50				
750	0.09 ± 0.16	0.39 ± 0.16	0.12	0.28	0.08	-0.10			1.07 ± 0.00	1.07	1.07	1.07	1.07		
1000	0.25 ± 0.05	0.55 ± 0.05	0.22	0.27					2.54 ± 0.02	2.55	2.54				
1500	0.13 ± 0.02	0.43 ± 0.02	0.12	0.14					5.05 ± 0.05	5.07	5.03				
2000	0.16 ± 0.03	0.46 ± 0.03	0.14	0.17					5.56 ± 0.02	5.55	5.57				
2500	0.27 ± 0.07	0.57 ± 0.07	0.30	0.23					5.76 ± 0.02	5.75	5.77				
3500	0.19 ± 0.02	0.49 ± 0.02	0.18	0.20					6.96 ± 0.07	6.93	7.00				

Station P1 (30.0 °S; 165.0 °E) – 28 January 2010

15	0.07 ± 0.05	0.37 ± 0.05$^{\psi}$	0.07		0.02	0.02	
30	-0.06 ± 0.02	0.24 ± 0.02$^{\psi}$	-0.06		0.05	0.05	
50	-0.06 ± 0.03	0.24 ± 0.03$^{\psi}$	-0.06		0.01	0.01	
95	-0.15 ± 0.03	0.15 ± 0.03$^{\psi}$	-0.15		0.01	0.01	
125	-0.05 ± 0.03	0.25 ± 0.03$^{\psi}$	-0.05		0.01	0.01	
150	-0.22 ± 0.04	0.08 ± 0.04$^{\psi}$	-0.22		0.02	0.02	
200	0.03 ± 0.03	0.33 ± 0.03$^{\psi}$	0.03		0.03	0.03	
300	0.18 ± 0.05	0.48 ± 0.05$^{\psi}$	0.18		0.11	0.11	
500	-0.04 ± 0.03	0.26 ± 0.03$^{\psi}$	-0.04		0.33	0.33	
750	0.10 ± 0.05	0.40 ± 0.05	0.13	0.08	0.84 ± 0.01	0.83	0.84
1000	0.14 ± 0.01	0.44 ± 0.01	0.14	0.14	1.87 ± 0.00	1.87	1.87
1500	0.15 ± 0.00	0.45 ± 0.00	0.15	0.15	5.26 ± 0.04	5.24	5.28
2000	0.15 ± 0.01	0.45 ± 0.01	0.16	0.15	6.82 ± 0.02	6.81	6.82
2500	0.17 ± 0.04	0.47 ± 0.04	0.15	0.19	7.43 ± 0.02	7.44	7.42
3000	0.14 ± 0.01	0.44 ± 0.01	0.14	0.14	7.38 ± 0.01	7.39	7.38

Station P1 (30.0 °S; 165.0 °E) – 20 May 2011

15	0.31 ± 0.05	0.61 ± 0.05$^{\Psi}$	0.31	0.04	0.04
75	0.27 ± 0.04	0.57 ± 0.04$^{\Psi}$	0.27	0.05	0.05
100	0.55 ± 0.07	0.85 ± 0.07$^{\Psi}$	0.55	0.03	0.03
125	0.32 ± 0.04	0.62 ± 0.04$^{\Psi}$	0.32	0.04	0.04
150	0.50 ± 0.04	0.80 ± 0.04$^{\Psi}$	0.50	0.08	0.08
200	0.23 ± 0.04	0.53 ± 0.04$^{\Psi}$	0.23	0.06	0.06
300	0.72 ± 0.03	1.02 ± 0.03$^{\Psi}$	0.72	0.17	0.17
500	0.10 ± 0.03	0.40 ± 0.03$^{\Psi}$	0.10	0.26	0.26
750	0.14 ± 0.03	0.44 ± 0.03$^{\Psi}$	0.14	0.76	0.76
1000	0.10 ± 0.04	0.40 ± 0.04$^{\Psi}$	0.10	1.92	1.92
1250	0.14 ± 0.03	0.44 ± 0.03$^{\Psi}$	0.14	3.93	3.93
1500	0.25 ± 0.02	0.55 ± 0.02$^{\Psi}$	0.25	5.29	5.29
1750	0.22 ± 0.02	0.52 ± 0.02$^{\Psi}$	0.22	6.34	6.34
2000	0.23 ± 0.03	0.53 ± 0.03$^{\Psi}$	0.23	6.93	6.93
2500	0.20 ± 0.08	0.50 ± 0.08$^{\Psi}$	0.20	7.57	7.57
3000	0.19 ± 0.09	0.49 ± 0.09$^{\Psi}$	0.19	7.50	7.50

[#] Here we added 0.30 ‰ to the $Zn_{IRMM\text{-}3702}$ calibrated data to put it onto the $Zn_{JMC\text{-}Lyon}$ scale.

[Ψ] Where a sample was extracted only once, the isotope error represents 2SE for a 30 cycle instrument measurement.

3.3.3.1. Biological control on Zn isotope fractionation and Zn speciation in the upper water column

Zinc speciation in the Tasman Sea is dominated by its complexation to natural organic ligands in the upper water column across all three process stations (Sinoir et al. 2016b) (Figure 3.3). At stations P2 and P3 a peak in ligand production and a minimum in Zn concentration are noted for the DCM; however, at station P1 a decrease in ligand concentration is observed across the depth of the DCM (Sinoir et al. 2016b). This minimum in Zn concentration at stations P2 and P3 also coincided with the peak in δ^{66}Zn. The coupling between the various Zn parameters (e.g. ligand concentration, minimum in Zn concentration, heavy δ^{66}Zn values) at the depth of the DCM of stations P2 and P3 suggests that eukaryotic phytoplankton control on both Zn ligand production and isotope fractionation. In the upper water column, this pattern of heavier δ^{66}Zn values followed by a shift to lighter values immediately below has been observed in other parts of the world ocean; the North Atlantic (Boyle et al. 2012; Conway and John 2014), the Atlantic Sector of Southern Ocean (Zhao et al. 2014) and the NE Pacific (Bermin et al. 2006) and was speculated to be associated with biological activity.

A significant correlation between biomarker pigment Fucoxanthin (indicating the presence of diatoms) and free Zn^{2+}, dissolved Zn, ligand concentration, excess ligand concentration and ligand strength was also reported for the three processes stations, which would be consistent with an immutable Zn requirement by diatoms, although this is speculative (Sinoir et al. 2016b). It was also observed that most eukaryotic biomarker pigments were correlated to the ligand and the excess ligand concentration. It is interesting to note here that we observed a strong and significant correlation

between δ^{66}Zn and the biomarker pigments 19-Hexanoyloxyfucoxanthin (R^2 = 0.97), 19-Butanoyloxyfucoxanthin (R^2 = 0.90), both pigments indicating the presence of diatoms and/or haptophytes, and Fucoxanthin (R^2 = 0.90) at the depth of maximum biomass (DCM) for P2 (30-65 m) and P3 (30-50 m). This suggests that eukaryotic phytoplankton may control Zn isotope fractionation and Zn speciation in the upper water column although, with only four points across this depth zone, this still remains speculative and needs further assessment.

We also explored whether seasonality occurs for δ^{66}Zn fractionation at station P1. At this station, heavier δ^{66}Zn values for upper water column (0-150 m) are observed during late autumn compared to summer. These heavier δ^{66}Zn values are also coupled to an increase in the water column fluorescence and cell counts, and are consistent with high phytoplankton productivity during late autumn compared to summer (see Section 3.3.2 above).

The increase in phytoplankton production is likely coupled with increased vertical mixing thereby increasing the supply of macro-nutrients into the euphotic zone. Dissolved Zn concentrations are also elevated by about 20 pmol L^{-1} between the two sampling periods (P1 January 2010, dissolved Zn = 20 ± 17 pmol L^{-1}, 15 to 125 m, n = 5; P1 May 2010, dissolved Zn = 40 ± 10 pmol L^{-1}, 15 to 125 m, n = 4).

Recently John and Conway (2014), have suggested that lighter δ^{66}Zn values observed for the shallow western Atlantic Ocean relative to deeper waters could be explained by scavenging of heavier Zn on particles. It is also worth mentioning that most input sources of Zn in the ocean have a light isotopic composition (Little et al. 2014). Thus, it could be speculated that the normal situation in the upper water column is for light Zn

isotope compositions to predominate. Heavy Zn isotope compositions observed close to the depth of the DCM at stations P2 and P3, where eukaryotic phytoplankton are abundant would suggest that they are dominating the cycling of Zn in this zone. Immediately below the DCM, there is an increase in the total dissolved Zn concentration associated with lighter δ^{66}Zn values which is suggestive of shallow degradation of phytoplankton and an associated release of isotopically light Zn.

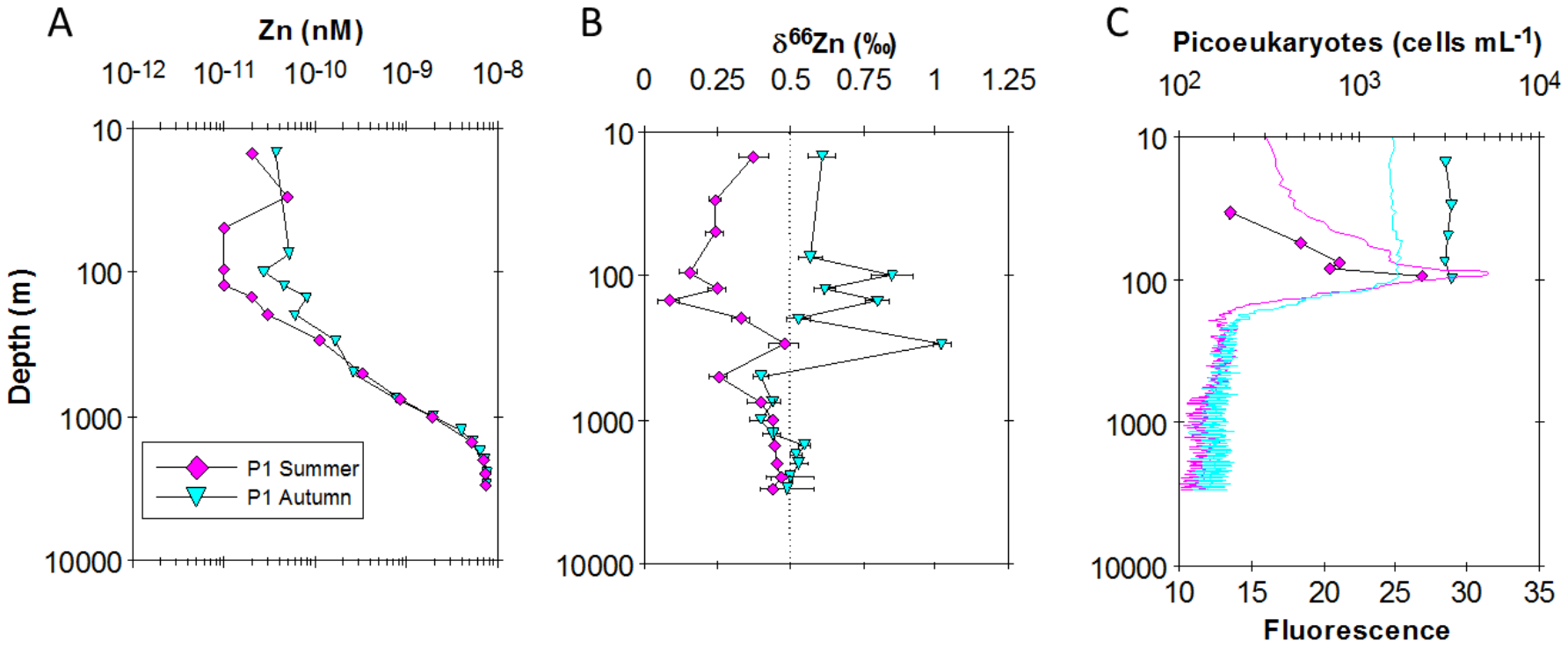

Figure 3.7: Profiles of **A.** dissolved Zn concentration, **B.** δ^{66}Zn, and C. Picoeukaryote and raw CTD fluorescence versus depth for process station P1 occupied in the 28-30 January 2010 (summer) and reoccupied on 20 May 2011 (late autumn).

3.3.4. Dissolved Zn and silicic acid

Profiles of dissolved Zn and Si concentration versus are similar in their shape (Bruland 1980; Bruland et al. 1978), which at face value would imply that a significant fraction of Zn is taken up and regenerated from phytoplankton in a manner similar to that of Si. However work examining the Zn content of biogenic silica found that it is not significant sink for Zn (Ellwood and Hunter 2000). In the sections below, we briefly re-examine the potential coupling between Zn and Si.

*3.3.4.1. Zn*and $\delta^{66}Zn$*

A strong correlation (R^2=0.99, p< 0.001) between the dissolved Zn and Si concentration is seen for all three process stations in the Tasman Sea. We also calculated Zn*, which is a measure of the coupling between dissolved Zn and Si, using the formula (Conway and John 2014; Wyatt et al. 2014):

$$Zn^* = [Zn] - (Zn/Si_{deep})x[Si] \quad (2)$$

where, Zn/Si_{deep} equals the Zn/Si ratio of the deep Tasman Sea. This value was set to 0.06 nmol:µmol based on our Zn/Si relationship for all three Tasman Sea stations.

The Zn* values at the three Tasman Sea stations remained close to 0.0 from the surface until about 750 m (-0.12 to +0.08) (Figure 3.8). Below 750m, the Zn* value at the north Tasman Sea station P1 ranged between 0.0 and 0.15 except for a distinct peak at 2500 m in both the summer and late autumn profiles (Figure 3.8). At stations P2 and P3, a positive bulge is observed between 750 m and 2000 m. At 1000 m, at the core of AAIW, the Zn isotopic composition at station P3 and P2 was distinctively heavier (δ^{66}Zn values of 0.59 ± 0.03 ‰ and 0.55 ± 0.05 ‰ respectively) than at station

P1 (δ^{66}Zn = 0.44 ± 0.01 ‰) for the same corresponding depth (Figure 3.9). The δ^{66}Zn values observed for AAIW for stations P2 and P3 are similar to that observed at the SAFe station in the NE Pacific (0.5 to 0.6 ‰) where a positive bulge in Zn* has also been observed (Figures 3.8 and 3.9) (Conway and John 2015). The positive bulge in Zn* associated with a heavy δ^{66}Zn value at intermediate depths could be due to the regeneration of an isotopically heavy Zn phase, as proposed by Conway and John (2015). Below 2000 m the Zn* values became negative for stations P2 (-0.01 to -0.28) and P3 (-0.22 to -0.81). The structure of the Zn* profiles of stations P2 and P3 are similar to that calculated for station PS71-104-2 (47°39.36'S, 4°15.7'E) from the South Atlantic Ocean utilising a deep water Zn/Si ratio of 0.067 (Zhao et al. 2014), and is consistent with a near homogenous deep Southern Ocean.

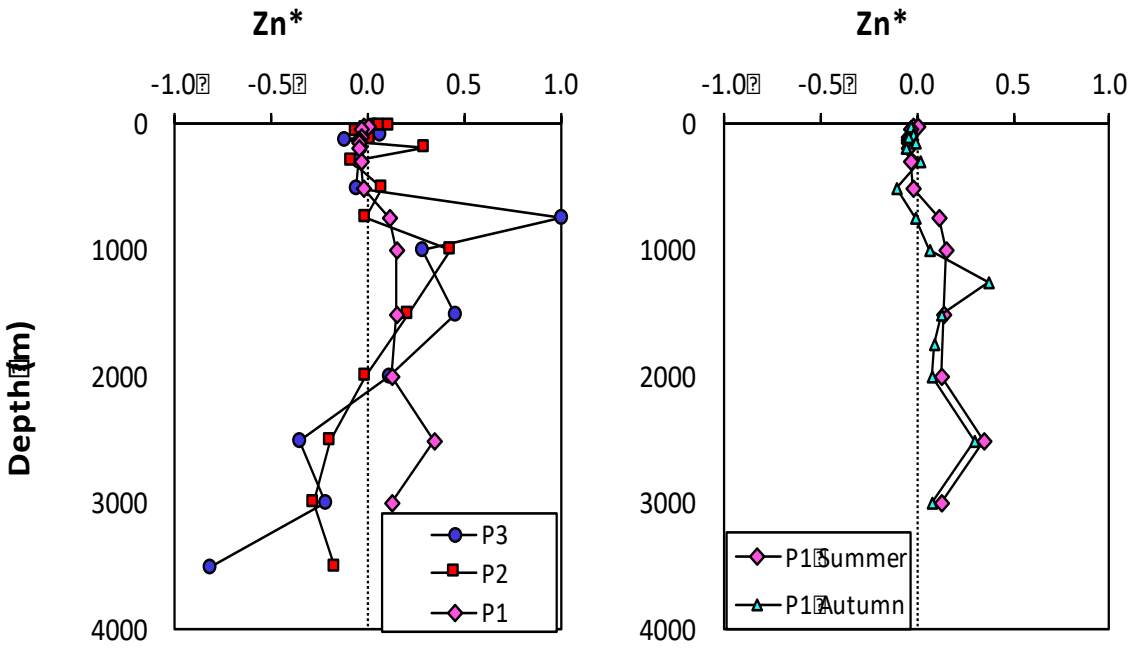

Figure 3.8: Profiles of Zn* versus depth for A. process stations P1, P2 and P3 and B. process station P1 occupied in the 28-30 January 2010 (summer) and reoccupied on 20 May 2011 (late autumn).

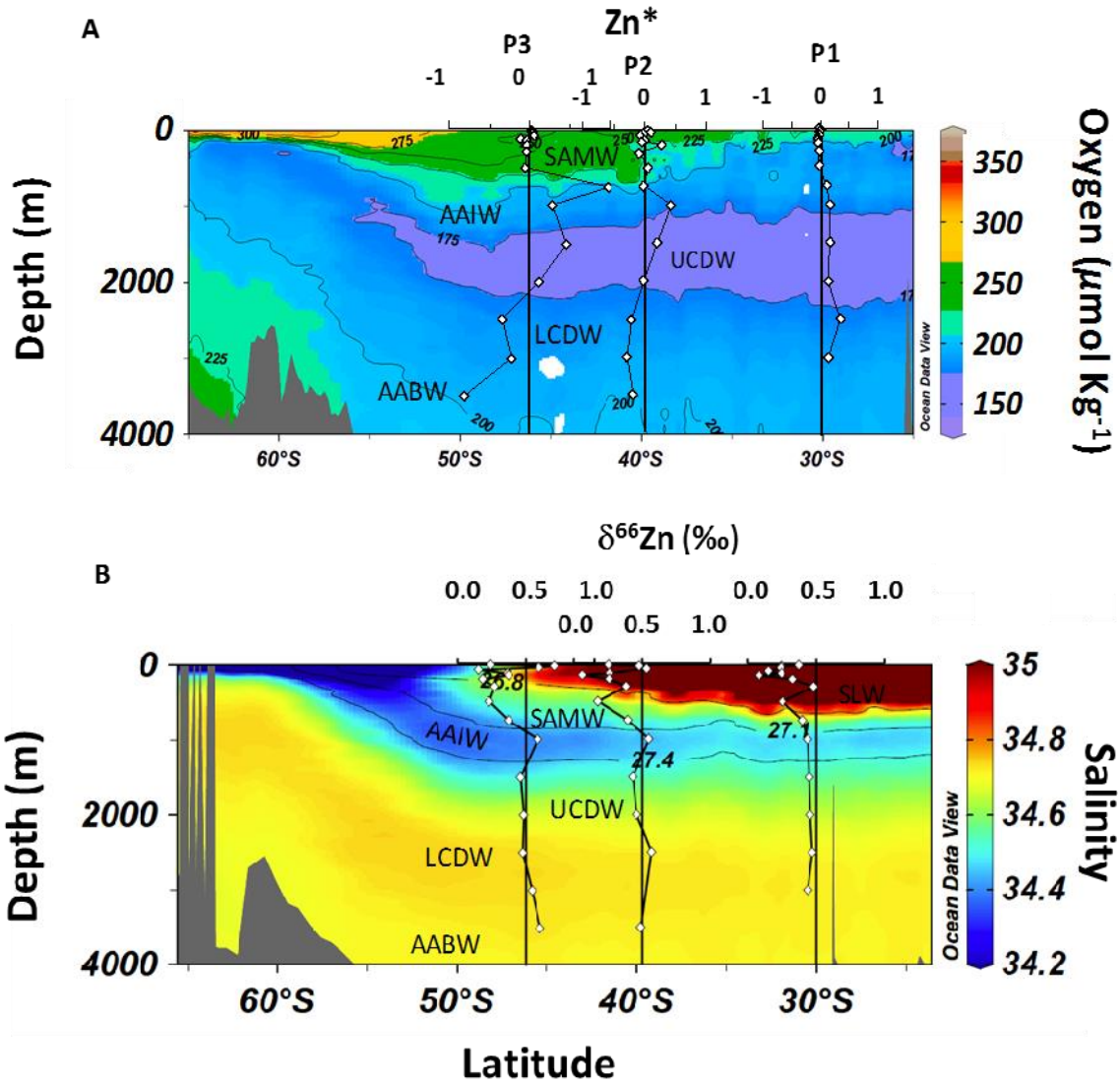

Figure 3.9: Section of **A.** oxygen and **B.** salinity along the P11S line which extends into the Tasman Sea along 155 ˚E showing the different water masses in the Tasman Sea. **A.** Overlaying the oxygen section are the Zn* profiles for stations P1, P2 and P3. **B.** Overlaying the salinity section are density lines with sigma-t of 26.8, 27.1 and 27.4 and Zn isotope profiles for stations P1, P2 and P3. SAMW occurs between a density of 26.8 and 27.1 and AAIW occurs between a density between 27.1 and 27.4.

3.3.4.2. $\delta^{66}Zn$ and $\delta^{30}Si$

We observed a strong coupling between the $\delta^{66}Zn$ for water collected from station P3 and the Si isotope composition ($\delta^{30}Si$) of waters of a near-by station also located in the SAZ. Below 200 m, the $\delta^{66}Zn$ of the station P3 (46.2°S, 159.5°E) and the $\delta^{30}Si$ of the nearby SAZ station CTD24 (48.8° S, 140°E-144°E) (Cardinal et al. 2005) are strongly negatively correlated ($R^2 = 0.77$, $p < 0.001$; Figure 3.10). Our Zn isotope data for stations P3 and P2 also couple to Si isotope values of stations further east (103°W; (De Souza et al. 2012) in the eastern Pacific Ocean, with a similar negative correlation between $\delta^{66}Zn$ and $\delta^{30}Si$ ($R^2 = 0.60$).

Why $\delta^{66}Zn$ and $\delta^{30}Si$ should be coupled is unknown. We speculate that the strong coupling observed between $\delta^{66}Zn$ and $\delta^{30}Si$ is suggestive of a deep regeneration cycle for these two elements, which would be consistent with concentration data for these two elements. The surface waters of the Southern Ocean in the SAZ region are relatively deficient in Zn and Si due to preferential biological uptake (by diatoms) compared to NO_3 and PO_4 due to Fe limitation of this region (Sunda and Huntsman 2000). Sarmiento et al. (2004) proposed that these water masses forms SAMW, advect northward and set the global distribution, for Si at least. Zhao et al. (2014) proposed that Zn regenerates deeper in the water column since it is associated intimately with the organic rich material of the silica frustule and is exposed to oxidation only after the dissolution of the opal phase. In contrast, John and Conway (2014) hypothesise that the Zn released from the disintegrating phytoplankton is scavenged back onto sinking particulate organic matter which is released at depth. The scavenged Zn is isotopically heavier which explains the heavier isotopic composition of the deep ocean (John and

Conway 2014). The inverse coupling between the isotope composition of dissolved Zn and Si and the strong coupling between dissolved Zn and Si concentrations would suggest that biogeochemical processing of these two elements in the Southern Ocean is the key to their coupling as hypothesised by Vance et al. (2017). This was further supported by model stimulations (Vance et al. 2017). These processes may be connected to Fe limitation of phytoplankton in the surface waters of this region (Sunda and Huntsman 2000); this will require further detailed studies to determine if Fe limitation propagates through the biogeochemical cycling of Zn in the ocean.

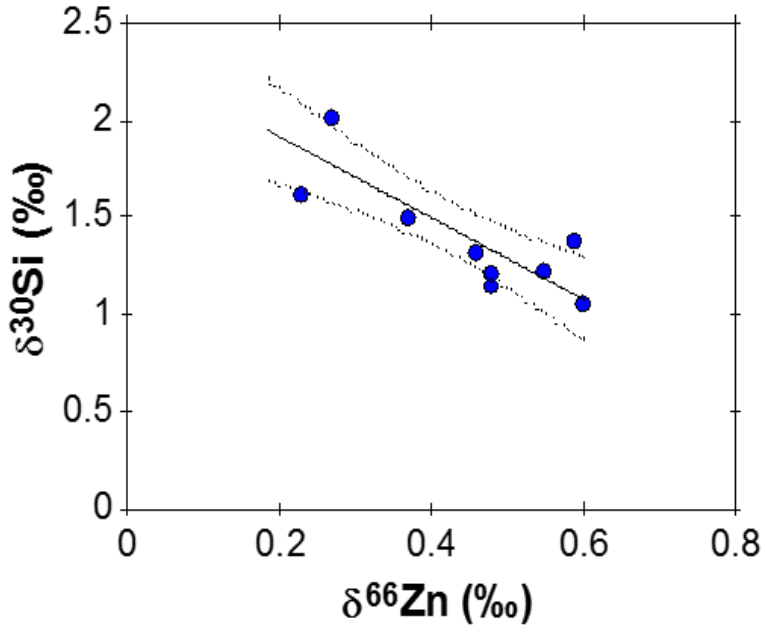

Figure 3.10: Property-property plots of δ^{66}Zn versus δ^{30}Si for samples collected between 200 and 3500 m for station P3. The δ^{30}Si data is based on δ^{29}Si values obtained by Cardinal et al (2005) for stations CTD17 and CTD24 located at the Subantarctic Zone at 46.9˚S and 48.8˚S, respectively at ~142˚E. The δ^{29}Si data was converted to δ^{30}Si by multiplying by the mass dependent fractionation factor of 1.96 (Reynolds et al. 2007) and then interpolating to common depths to the δ^{66}Zn samples.

3.4. Conclusions

In this study, we show that Zn isotope fractionation in the surface waters of the Tasman Sea is controlled by the composition of phytoplankton community, as evident from the significant correlation between δ^{66}Zn and the relative fluorescence at the mesotrophic station P2 and the highly productive SAZ station P3 while no coupling was observed at the oligotrophic station P1. We propose that at stations P2 and P3, lighter Zn isotopes is taken up by the eukaryotic phytoplankton at a slightly faster rate than their heavier counterparts resulting in a heavier δ^{66}Zn composition of the seawater. This is especially evident at the depth of the DCM for stations P2 and P3. Immediately below the DCM, there is degradation of phytoplankton and release of lighter Zn isotope which results in lighter δ^{66}Zn values as dissolved Zn concentration increases. The range of Zn isotope fractionation observed in the surface ocean (range ~0.55 ‰) is consistent with Zn isotope fractionation observed for biological uptake in culture work (John et al, 2007).

Based on our observations the dissolved Zn isotope composition in the upper water column appears to be controlled by uptake by eukaryotic phytoplankton and regeneration of sinking organic material. Below 500 m, there is vertical exchange with deep water and release of lighter Zn isotope as particulate organic matter sinks which results in gradual increase in dissolved Zn concentration and δ^{66}Zn getting heavier to reach the deep ocean value of 0.50 ± 0.14 ‰.

Acknowledgements

The authors would like to thank the two anonymous reviewers for their constructive comments. We thank the following people for help with sample collection and analysis of various supporting measurements to this chapter: Claire Thompson, Martina Doblin, Gabriel Shaw, Lesley, Sue Reynolds and Alicia Navidad. We also thank the Marine National Facility and the offices and crew of the RV Southern Surveyor for the PINTS and GP13 voyages. We thank Graham Mortimer and Leslie Kinsley for their help and advice. The Australian Research Council is also acknowledged for funding awarded to Ellwood and Hassler (DP110100108). Hassler was also funded by a UTS Chancellor Fellowship and a Swiss National Science Foundation Fellowship (PP00P2_138955).

Appendix

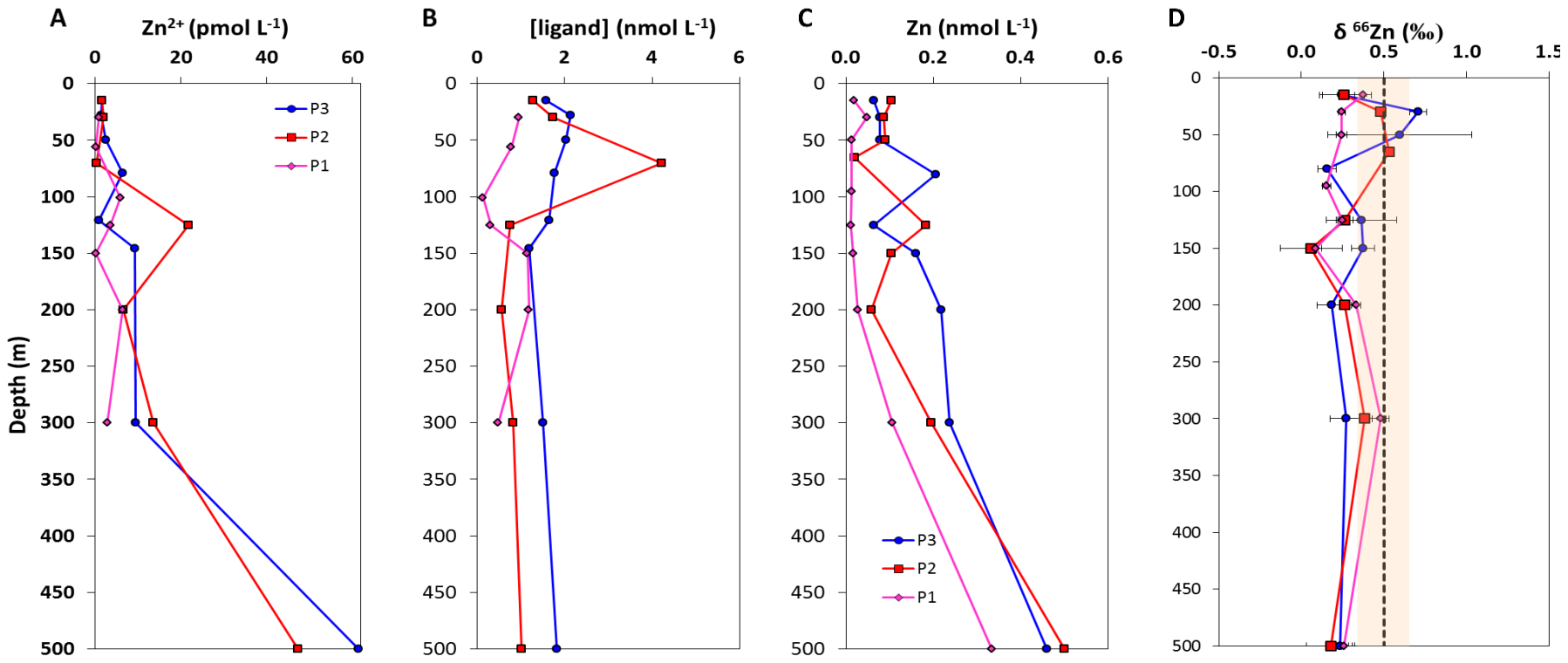

Figure 3.3. Profiles of (C) dissolved Zn, (A) free Zn^{2+} (B) ligand concentrations and (D) the $\delta^{66}Zn$ composition of dissolved Zn for stations P1, P2 and P3 versus depth from 0 to 500 m. Free Zn^{2+} ion concentration, ligand concentration and pigment data were taken from (Sinoir et al. 2016b). The shaded portion represents the deep ocean $\delta^{66}Zn$ composition with an average (dotted line) of 0.5 ± 0.14 ‰ and error bars represent 2SE of multiple extractions.

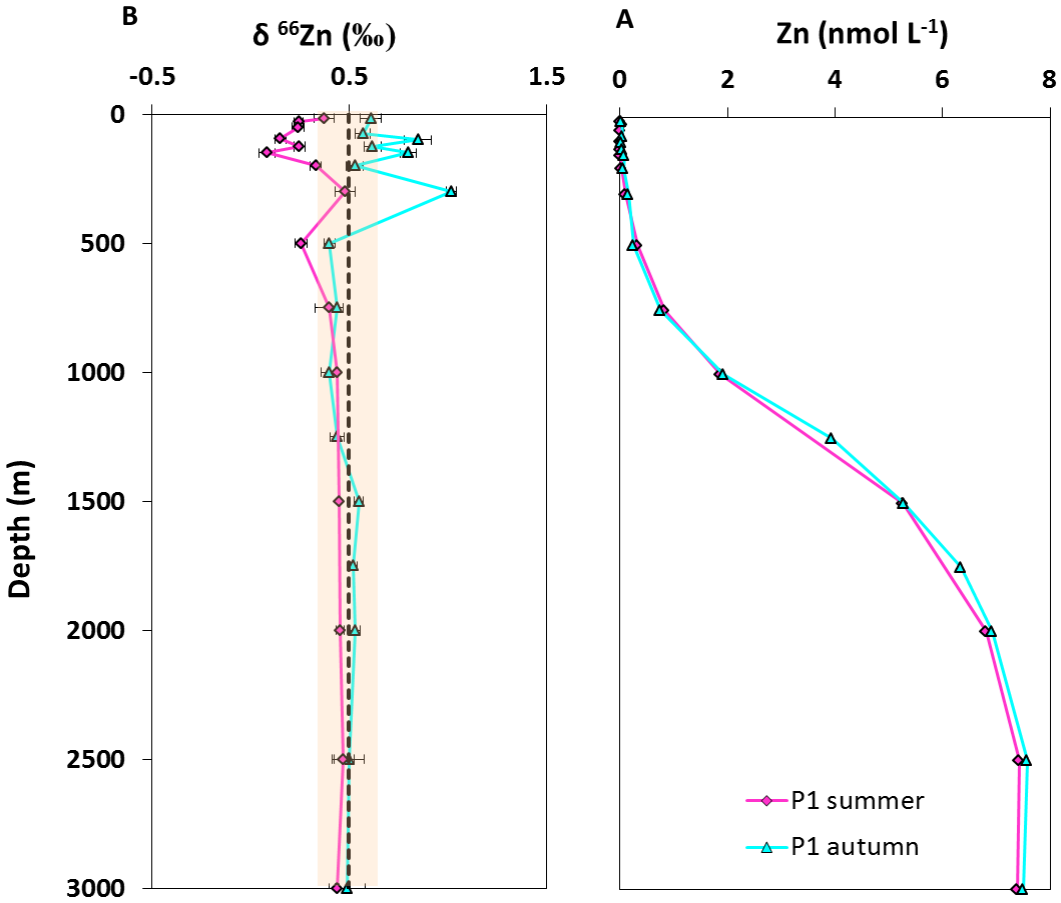

Figure 3.7: Profiles of **A.** dissolved Zn concentration and **B.** δ^{66}Zn verses depth for process station P1 occupied in the 28-30 January 2010 (summer) and reoccupied on 20 May 2011 (late autumn). The shaded portion represents the deep ocean δ^{66}Zn composition with an average (dotted line) of 0.5 ± 0.14 ‰ and error bars represent 2SE of 30 cycles instrument measurement.

Chapter 4:

Zinc isotope fractionation by *Emiliania huxleyi* cultured across a range of free Zn^{2+} ion concentrations

Moneesha Samanta, Michael J. Ellwood, Robert F. Strzepek[3]

Abstract

Zinc (Zn) isotope fractionation by the coccolithophore *Emiliania huxleyi* (a Tasman Sea isolate) was investigated by culturing it across a range of free Zn^{2+} ion concentrations (1.2 pmol L^{-1} to 3.2 nmol L^{-1}), which span the natural range observed in the global oceans. Across the range of free Zn^{2+} ion concentrations tested in this study, the amount of bio-available Zn did not have any appreciable influence on the specific growth rate or cell morphology of *E. huxleyi*. However, a suite of secondary physiological indicators reflected changes in Zn bioavailability. An increase in the photosynthetic efficiency of photosystem II (F_v/F_m) was observed with increasing free Zn^{2+} concentration. The time constants for electron transport from Q_A to Q_B and from Q_B to the plastoquinone (PQ) pool decreased as the free Zn^{2+} ion concentration increased, reflecting enhanced photosynthetic electron transport. The effect of Zn bioavailability on photosynthetic physiology was speculated to be due to increased activity of carbonic anhydrase with increasing bioavailable Zn. Zinc uptake by *E. huxleyi* resulted in Zn isotope fractionation and the $\Delta^{66}Zn_{cells\text{-}media}$ ranged between -0.6 ‰ and -0.2 ‰. The major finding from this work is that the lighter Zn isotope is taken up

[3] Authors' contribution: M.S. analysed the data and drafted the manuscript with contribution from M.J.E. and R.F.S.

preferentially by this coccolithophore, making the dissolved Zn composition of the surrounding seawater isotopically heavier.

4.1. Introduction

The isotopic fractionation of zinc (Zn) in natural waters can result from complexation with organic ligands, biological uptake and the partitioning between dissolved and particulate phases. In open ocean waters, except in the Southern Ocean where there is upwelling of nutrient-rich waters, approximately 98% of dissolved Zn is bound to strong organic ligands (Baars and Croot 2011; Bruland 1989; Ellwood and Van den Berg 2000; Jakuba et al. 2012; Sinoir et al. 2016b). The unbound dissolved Zn^{2+} is believed to be the main Zn species available for uptake by phytoplankton, although Zn complexation to weak complexing compounds are known to influence Zn bioavailably as well (Anderson et al. 1978; Xu et al. 2012). Quantum mechanical calculations suggest that heavier isotopes tend to form stronger bonds than their light isotope counterparts (Criss 1999). For Zn, this would mean that ^{66}Zn would be more strongly bound to the strong organic ligands present in seawater and more energy would be required to break a bond between ^{66}Zn and ligand than ^{64}Zn and ligand. This would imply that Zn available for uptake by phytoplankton should be isotopically light relative to the surrounding medium. The diffusion of the lighter ^{64}Zn isotope is also faster than that of the ^{66}Zn isotope, which will result in isotopic fractionation, i.e. enrichment of ^{64}Zn within the phytoplankton cell even when free Zn^{2+} ion concentrations are low (Bruland 1989; John et al. 2007; Rodushkin et al. 2004). In the south Tasman Sea, we observed that heavier dissolved Zn isotope values coincided with the deep chlorophyll maximum, which was dominated by coccolithophores (see Chapter 3). It has been speculated that in the upper waters of the ocean, lighter Zn isotopes are taken up by the resident phytoplankton at a slightly faster rate than their heavier counterparts, resulting in a heavier $\delta^{66}Zn$ composition of the seawater (Andersen et al. 2011; Conway

and John 2014; Hendry and Andersen 2013; Pichat et al. 2003; Zhao et al. 2014). However, till date only a few studies have investigated Zn isotope fractionation by phytoplankton (Gelabert et al. 2006; John and Conway 2014; John et al. 2007; Köbberich and Vance 2017). Lighter $\Delta^{66}Zn$ values within phytoplankton cells relative to the culture media have been reported for the chlorophyte *Dunaliella tertiolecta* and the diatom *Thalassiosira oceanica* (John and Conway 2014; John et al. 2007). During Zn uptake by *T. oceanica*, Zn isotope fractionation was systemically reduced when the free Zn^{2+} ion concentration of the media was reduced. This difference in isotope fractionation for *T. oceanica* grown at high and low free Zn^{2+} ion concentrations was attributed to the change in dominance of the two Zn transport pathways viz. the high and low affinity uptake pathways (John et al. 2007; Sunda and Huntsman 1992). In *T. oceanica*, the low affinity pathway dominates at free Zn^{2+} ion concentrations greater than ~10^{-9} mol L^{-1} with the shift from the low to the high affinity pathway occurring between $10^{-10.5}$ and $10^{-9.5}$ mol L^{-1} Zn^{2+} (Sunda and Huntsman 1992). In this chapter, we examined how Zn isotopes are fractionated by a clone of the coccolithophore *Emiliania huxleyi* isolated from the Tasman Sea, across a range of free Zn^{2+} ions concentrations observed in the global oceans.

Coccolithophores are a cosmopolitan marine phytoplankton group that produce calcium carbonate plates, which form ballast, enhancing the rates of organic matter sinking into the deep ocean (Klaas and Archer 2002) thereby making them important to the marine carbon cycle. The ratio of calcification to photosynthetic carbon fixation by coccolithophores depends on number of environmental factors, namely light intensity and the availability of nutrients and trace metals (Zondervan 2007). The formation of organic matter during photosynthesis reduces atmospheric partial

pressure of carbon dioxide (pCO_2), whereas calcium carbonate formation reduces seawater alkalinity, causing an increase in pCO_2. Thus coccolithophores play an important role in the marine carbon cycle by directly affecting the air-sea carbon dioxide (CO_2) exchange (Rost and Riebesell 2004). *E. huxleyi* is a globally significant coccolithophore species distributed throughout the marine realm but for the polar oceans (Buitenhuis et al. 2003). Its growth habitat is within the ~100 m of the surface ocean and it tends to bloom in highly stratified waters when irradiance is high (Nanninga and Tyrrell 1996).

Here, we measured a suite of physiological characteristics (specific growth rates, cell morphology, photophysiological parameters) alongside the Zn isotope compositions of *E. huxleyi* at different free Zn^{2+}ion concentrations, to assess Zn bioavailability and to better understand the physiological basis for the Zn isotope fractionation results.

4.2. Methods

4.2.1. Study organism and experimental design

The coccolithophore *Emiliania huxleyi* (CS-1016), a Tasman Sea isolate, was obtained from the Australian National Algal Culture Collection (ANACC), CSIRO, Hobart, Australia. The cultures were maintained in a 20^{o}C incubator under a continuous irradiance of ~120 μmol quanta m^{-2} s^{-1}. Irradiance was measured with a calibrated 4π quantum meter (model QSL-2101; Biospherical Instruments). Cultures were subjected to six treatments that differed in Zn concentrations (-log[Zn^{2+}] = pZn = 8.5, 9.5, 10.0, 10.8, 11.4 and 11.9, respectively), spanning the range of free Zn^{2+} ion concentrations observed in the ocean. Three replicates for each treatment were acclimated to growth conditions by maintaining them at exponential growth phase by dilution for at least two transfers (14–16 cell divisions) before inoculation into 1 L experimental bottles. Specific growth rates and photophysiological parameters, including the photochemical efficiency of the photosystem II (PSII) reaction centre (F_v/F_m), effective absorption cross section of PSII (σ_{PSII}), potential storage efficiency of the plastoquinone (PQ) pool, and of the time constants for electron transport from the mobile electron carriers Q_A to Q_B, from Q_B to the PQ Pool, and from the PQ Pool to photosystem I (PSI). Cultures were harvested by collection of cells on filters at the mid-exponential phase of growth and saved for measurements of Chlorophyll *a* (Chl *a*), Zn isotope composition (δ^{66}Zn), and Zn and phosphorous (P) content of cells. Cell size and cell concentration density measurements were conducted on unpreserved cells at the time of harvest.

4.2.2. Cleaning protocol

Precautions were taken to minimise trace metal and bacterial contaminations. All work was undertaken in a Class 100 HEPA filtered laminar flow hood that was sterilized with 90% (v/v) ethanol before each use. All labware used for Aquil preparation and culturing was rigorously cleaned and microwave-sterilised prior to use. Cleaning was done by soaking in soap (L900, Nalgene) for 2 days before rinsing with Milli-Q water (Millipore, Australia). This was followed by a further soak in 10% (v/v) AR grade hydrochloric acid (HCl) for a week before rinsing with Milli-Q water.

For the measurement of Zn isotope ratios, strict trace metal clean protocol was followed. All labware was soaked for a further week in distilled dilute (1 % v/v) acid before rinsing with Milli-Q water. Nitric acid (HNO_3) (AR grade) was purified by sub-boiling distillation in a Teflon still (Savellix, USA). Hydrochloric acid (HCl) (AR grade) was diluted to 8 mol L^{-1} before sub-boiling distillation in a Teflon still (Savillex, USA). O-rings of filtration gear were cleaned by thoroughly rinsing with Milli-Q after a light HCl soak (2 % v/v) and 2.0 µm polycarbonate membrane filters (Whatman Nuclepore) were cleaned by soaking in dilute (2 % v/v) distilled HCl for two days followed by Milli-Q water rinse prior to collection of cells for δ^{66}Zn measurement.

4.2.3. Medium preparation

Artificial seawater medium (Aquil) was used for culturing. Synthetic Ocean Water (SOW), made following the protocol described in Price et al. (1988), and nutrient stocks were eluted through a column containing Toyopearl AF-chelate-650M ion-exchange resin (Tosoh Biosciences, Japan) to remove trace metal contaminants. The

trace metal clean SOW was then microwave-sterilized before addition of filter-sterilized (0.2 μm Gelman Acrodisc PF) nutrients, vitamins and trace metal solution to it. The final concentration of nutrients and vitamins in Aquil were 10 μmol L^{-1} phosphate, 100 μmol L^{-1} silicate, 300 μmol L^{-1} nitrate, 0.55 μg L^{-1} vitamin B_{12}, 0.5 μg L^{-1} biotin and 100 μg L^{-1} thiamine. A filter-sterilized trace metal solution (without Zn) was added to the SOW such that the final media had 565 nmol L^{-1} of iron, 50 nmol L^{-1} of cobalt, 19.8 nmol L^{-1} of copper, 228 nmol L^{-1} of manganese, 9.96 nmol L^{-1} of selenium, 100 nmol L^{-1} of molybdenum and 100 μmol L^{-1} of ethylenediaminetetraacetic acid (EDTA) as the chelating agent. The Zn contamination in the SOW was measured to be 6 nmol L^{-1} and was accounted for in the calculations of pZn (-log $[Zn^{2+}]$). The Zn concentration of the SOW was measured by Multi-Collector Inductively Coupled Plasma Mass Spectrometry (MC-ICPMS) with ^{67}Zn-^{68}Zn double spike following the protocol for dissolved Zn analysis described in (Samanta et al. 2016). The pMetal, which is the negative logarithm of the free metal ion concentration, levels were calculated using the chemical equilibrium computer program Visual MINTEQ (version 3.0; default thermodynamic database) for Aquil media at 20°C and at pH 8.1. For the lowest Zn treatment, no extra Zn was added and the pZn was calculated to be 11.9. For the other five treatments, Zn was added as zinc sulphate solution such that the Zn concentrations were 17.3 nmol L^{-1}, 80.6 nmol L^{-1}, 0.48 μmol L^{-1}, 1.58 μmol L^{-1} and 14.2 μmol L^{-1} with pZn values of 11.4, 10.8, 10.0, 9.5 and 8.5, respectively. Changing the Zn concentrations of the media made insignificant changes in the pMetal values of other trace elements and thus should not affect the physiology of the cultured phytoplankton.

4.2.4. Growth rate measurement

Growth rates of cultures were determined from in vivo chlorophyll-a fluorescence using a Turner Designs Model 10-AU fluorometer (Sunnyvale, CA). Cultures were dark-acclimated for approximately 30 min. prior to daily measurement of fluorescence so that the PSII reaction centres are open and the photosynthetic apparatus is in a well-defined state (Kalaji et al. 2014). Blanking of the instrument was done with sterilised SOW before sample analysis. The specific growth rate (μ; d^{-1}) was then calculated by determining the slope of ln(fluorescence) versus cumulative time during the exponential growth phase.

4.2.5. Measurement of photophysiological parameters

The Light Induced Fluorescence Transients (LIFT) technique was used to examine the in vivo photosynthetic efficiency of PSII (F_v/F_m) using a LIFT- Fast Repetition Rate (FRR) fluorometer ((Kolber 2002; Kolber et al. 1998) Soliense, Inc., Shoreham, NY; http://soliense.com/LIFT_Marine.php). During the excitation phase of this technique, a sequence of light pulses (1.2 μs flashlets) was applied at a rate of excitation energy delivery to the PSII reaction center far exceeding the capacity of photosynthetic electron transport (saturation sequence), followed by a relaxation sequence where the time interval between flashlets increased exponentially. An excitation wavelength of 470 nm was used to manipulate the level of photosynthetic activity of PSII and record the resulting changes in fluorescence yield. Measurements of photosynthetic efficiency were conducted on cells collected during early- to mid-exponential growth phase. Cells were dark acclimated for 30 minutes prior to measurement. Maximum quantum yield

of PSII relates to the number of electrons extracted from water per quanta of light absorbed and is given by the amplitude of variable fluorescence, F_v, (where $F_v = F_m - F_o$; F_o = minimal fluorescence) normalised to maximum fluorescence, F_m, (i.e. F_v/F_m). F_v/F_m is widely used as an algal health indicator. The functional absorption cross section of PSII (σ_{PSII}) is a measure of the light-harvesting antennae size, and the efficiency of excitation energy transfer from pigments to the reaction centre, of PSII. The electrons extracted from water are transferred from PSII to PSI via a series of electron carriers, namely Q_A, Q_B, the PQ pool, the cytochrome b_6f complex and plastocyanin (PC). Light absorption at PSI transfers electrons to ferrodoxin, where they are redistributed for use in carbon fixation or cyclic electron transport around PSI. The relaxation portion of the fluorescence induction curve was fitted with a three-component exponential model (SEQ_3), which assumes three stages of electron transport from Q_A to Q_B, Q_B to the PQ Pool, and the PQ Pool to PSI with time constants τ_1, τ_2 and τ_3, respectively. Both the size of the oxidized portion of PQ and the time constant of PQ reoxidation can be calculated from the kinetics of relaxation of the fluorescence transient (http://soliense.com/LIFT_Method.php).

4.2.6. Cell sizing and cell density

Cell diameter (μm), cell volume (fL cell^{-1}; fL = femtolitre = 10^{-15} L) and cell density (no. of cells per mL) were measured using a Multisizer 4 Coulter Counter (Beckman Coulter) fitted with a 100 μm aperture using a spherical approximation for the *E. huxleyi* cells. The instrument was programmed to take 3 replicate measurements and detect particles within the 2 – 15 μm size range. Before every session a blank measurement

was made using a 0.45 μm-filtered 3.5 % sodium chloride (NaCl) solution. This solution was also used for flushing between samples and diluting cell suspensions. Cell density (cells mL^{-1}) and cell volume (fL $cell^{-1}$) data were collected from unpreserved subsamples of experimental cultures collected at the same time as samples for Chl *a*.

4.2.7. Scanning Electron Microscope imaging

High resolution images of *E. huxleyi* cells for the different treatments were taken using a Zeiss UltraPlus analytical Field Emission Scanning Electron Microscope (FESEM) located at the Centre for Advanced Microscopy at the Australian National University. About 5 mL of experimental culture in the mid-exponential growth phase was passed through 0.45 μm pore size polycarbonate membrane filter (Whatman Nuclepore) under a low vacuum (<200 mbar). The filter was then washed with a few drops of Milli-Q water (~ 0.5 mL) to remove salts and dried for 12 h at 60 ◦C. The filters were then attached to aluminium stubs using double-sided electrically-conductive, non-porous carbon tape, and coated with gold-palladium before acquiring images with the SEM.

4.2.8. Cellular chlorophyll a measurement

Cellular Chl *a* concentrations were determined by *in vitro* fluorometry using a Turner Designs Model 10-AU fluorometer (Parsons et al. 1984)calibrated with spectrophotometrically-measured spinach Chl *a* standards (Sigma-Aldrich) (Strzepek et al. 2012). For Chl *a* measurements, 20 mL of culture was collected during the mid-exponential growth phase and passed through 25mm glass fibre filters (Whatman

GF/F) under low vacuum. The filters were then stored in 15 mL centrifuge tube at -20°C in the dark until analysis. For analysis, 10 mL of 90 % acetone solution was added to each tube and vortexed for 30 s to extract pigments from cells. The extract was then allowed to sit in the dark at 3 ± 1°C for 18-24 hrs, after which it was re-vortexed to homogenise the solution (Arar and Collins 1997). The solution was brought to room temperature in the dark before measurement. The solution was measured before and after the addition of 0.5 mL of 10% HCl. Blanking of the instrument was done with a 90% acetone solution prior to sample analysis. Chl *a* concentrations were calculated by the following equation

$$[\text{Chl } a]\ (\mu g\ L^{-1}) = 2.117 \times 1.0188(F_O - F_A) \times (v/V) \quad \ldots (1)$$

Where, F_O is fluorescence before acidification and F_A is fluorescence after acidification; v is the volume of acetone extract (mL), V is the volume of sample filtered (mL) and 2.117 is the acid ratio correction factor. Coulter counter data were used to normalize Chl *a* concentration to per cell (pg Chl *a* $cell^{-1}$) and to cell volume (mmol Chl *a* L^{-1}_{CV}).

4.2.9. Cell harvesting, Zn:P and Zn isotope determination

Emiliania huxleyi cultures were harvested in the mid-exponential phase of growth onto trace metal-cleaned filters for elemental and Zn isotope measurements. To determine if there was significant Zn adsorption onto the surface of cells and the isotopic composition of adsorbed Zn, an oxalate-EDTA wash was used for some of the cultures following the protocol described by (John et al. 2007). About 900 mL of experimental culture in the mid-exponential growth phase was split into two equal volumes and passed through 2 μm polycarbonate membrane filters (Whatman Nuclepore) under a

low vacuum. One of the filters was rinsed twice for 5 min with 5 mL of oxalate-EDTA wash (prepared following the method described by Tovar-Sanchez et al. (2003)) to remove extracellular Zn adsorbed to the cell surface. This was followed by three 5 min 5 mL rinses with trace metal-free SOW to wash away excess oxalate-EDTA. For the second aliquot, cells were only washed with trace metal-free SOW. The filters were then transferred to 5 mL acid-cleaned Teflon beakers. To oxidise organics, the cells were digested with 0.5 mL of concentrated nitric acid (HNO_3), 0.5 mL of 8 mol L^{-1} HCl and 1 mL of Milli-Q water. The solution was refluxed for several hours at ~90 °C. After cooling, 0.1 mL of solution was removed, taken to dryness and then taken up in 2 mL of 2 (v/v) % HNO_3 for elemental (Zn and P) determination. The specific cellular Zn uptake rate was calculated by multiplying the specific growth rate by the cellular Zn:P ratio of the cultures.

Zinc and P concentrations were determined by high resolution Inductively Coupled Plasma Mass Spectrometry (ICPMS; Element XR) based at the University of Canberra. Five calibration standards were made from a Multi-Element (ME; containing Zn) and P concentration standard and measured at the beginning of the session and after every ten samples. Iridium and Ytterbium were added to standards and samples and used as an internal standard to correct for instrumental drift. Blank measurements were made on 2% HNO_3. Zinc and P concentrations of samples were calculated by comparing the measured intensities of the samples with the intensities of measured standards.

The remaining 1.9 mL of the solution was used for measurement of $\delta^{66}Zn$ utilising the ^{67}Zn-^{68}Zn Double Spike (DS) technique by MC-ICPMS (Thermo Scientific Neptune Plus). Once the Zn concentration of the same digest was known, ^{67}Zn-^{68}Zn DS was added such that the concentration of the DS in the DS-sample mixture was 80 %. The

theoretical working range for the DS-sample mix for our double spike is 55% to 91% (see Chapter 2). The sample-DS solution was taken to dryness and taken up in 0.5 ml of distilled 0.5 mol L^{-1} HCl for purification and isolation of Zn by anion exchange chromatography. For this purpose, 0.15 mL of AG1X8 resin was used. The resin was pre-cleaned (using 0.5 mol L^{-1} HNO_3 followed by Milli-Q water rinse) and pre-conditioned (with 0.5 mol L^{-1} HCl) before loading of sample onto the column. After loading, the column was rinsed with 3 mL of 0.5 mol L^{-1} HCl to remove potentially interfering elements. Zinc was eluted from the column with 2.5 ml of 0.5 mol L^{-1} HNO_3 into another trace metal clean Teflon beaker. The solution was dried and taken up in appropriate volume of 2% HNO_3 for measurement of δ^{66}Zn.

Zinc isotope measurements were made using the MC-ICPMS Neptune Plus (Thermo Scientific) based at the Australian National University following the method described in Chapter 2. A desolvating sample introduction system (Apex IR, Elemental Scientific Inc.) with an uptake rate of ~ 50 μL per minute and a standard Ni sampler cone and a Ni X-skimmer cone were used. The instrument was operated in low resolution mode and each sample measurement was bracketed with the measurement of a standard-DS mixture. A 2% (v/v) HNO_3 solution was measured as a blank before every sample and standard measurement. This was preceded by a 2% HNO_3 wash. Intensities on mass ^{62}Ni, ^{63}Cu, ^{65}Cu, ^{64}Zn, ^{66}Zn, ^{67}Zn and ^{68}Zn were monitored and measured as 1 block of 30 cycles with a 4 second integration time.

The Zn isotopic composition was expressed in delta notation using the following equation:

$$\delta^{66}\mathrm{Zn} = \left(\frac{^{66}\mathrm{Zn}/^{64}\mathrm{Zn}_{\mathrm{sample}}}{^{66}\mathrm{Zn}/^{64}\mathrm{Zn}_{\mathrm{standard}}} - 1\right) \times 1000 \quad \ldots (2)$$

In the study, IRMM-3702 was used as the standard reference material. The isotopic composition of the Zn added to Aquil was 0.06 ± 0.01 (± 2 x SD) ‰. Since the isotopic composition of the Zn added is similar to the standard reference material, no correction was made on the $\delta^{66}Zn$ measurement and values reported here are with respect to the Zn standard IRMM-3702. Thus, in this study, $\Delta^{66}Zn_{cells\text{-}media}$ (Zn isotope composition of the cells relative to the media) is essentially $\delta^{66}Zn_{cells}$ (Zn isotope composition within cells measured relative to the standard IRMM-3702); The error bar reported for each treatment is 2 times the standard deviation of the replicates for that treatment. It should also be noted that the isotopic composition of the Zn added is similar to the lithogenic value (Little et al. 2016), thus any Zn contamination should not have a significant effect on $\Delta^{66}Zn_{cells\text{-}media}$.

4.2.10. Statistical analysis

The influence of Zn on *E. huxleyi* (CS-1012), particularly its effect on growth rates, cell size, cellular Chl *a*, photophysiological responses, Zn:P ratio and Zn isotope fractionation are discussed below. Significant results are reported at the 95% confidence level ($p < 0.05$) calculated using regression analysis and/or two-tailed t-test assuming unequal variances in Excel (2010 version). Paired two sample t-test for means at 95 % confidence interval was used to test for differences in $\delta^{66}Zn$ between oxalate-EDTA washed and unwashed cells.

4.3. Results and Discussion

4.3.1. Specific growth rates and cell morphology

Changes in the concentration of bioavailable Zn did not have any significant influence on the cell size of *E. huxleyi*. The cell volume ranged between 42 fL cell^{-1} and 55 fL cell^{-1} and was comparable to that reported for another Tasman Sea isolate of *E. huxleyi* (CS-812) (Figure 4.1, Table 4.1) (Sinoir et al. 2016a). In both Tasman Sea isolates of *E. huxleyi* (CS-1012 and CS-812), Zn concentration had a minor influence on specific growth rates (μ; d^{-1}). The growth rate of our clone at pZn 11.4 was 0.67 ± 0.02 d^{-1}, which is higher than that reported for the other Tasman Sea isolate at a similar free Zn^{2+} ion concentration (Figure 4.1, Table 4.1) (Sinoir et al. 2016a) but within the range reported for other strains of *E. huxleyi* (Schulz et al. 2004; Sinoir et al. 2016a; Xu et al. 2007). Sunda and Huntsman (1992) also reported no appreciable effect of the free Zn^{2+} concentrations on the specific growth rate of *E. huxleyi* (clone BT6) at pZn values ranging between 12.2 and 7.0. At the highest free Zn^{2+} ion concentrations tested in this study (pZn = 8.5 and 9.5) the growth rates (μ = 0.62 ± 0.03 d^{-1}) were reduced relative to intermediate free Zn^{2+} ion concentrations, pZn = 10.8; which seemed to be the optimal free Zn^{2+} ion concentration for the species as it sustained the highest growth rates ($\mu = \mu_{max}$ = 0.68 ± 0.02 d^{-1}). The significantly lower growth rates (μ:μ_{max} = 0.91; p = 0.01) observed at very high free Zn^{2+} concentrations could be due to Zn toxicity although we did not observe any significant increase in cell volume (p> 0.05), which has previously been associated with Co deficiency induced by Zn toxicity (Sunda and Huntsman 1995a). At the lowest free Zn^{2+} ion concentrations in this study, pZn = 11.9, the growth rates (μ = 0.66 ± 0.03 d^{-1}; μ:μ_{max} = 0.97) were only slightly reduced

compared to higher Zn treatments (pZn =10.8). This apparent lack of effect ($p > 0.05$) of low Zn^{2+} ion concentrations on growth rates could be due to substitution of Zn by cobalt (Co). Zn-Co substitution has been observed in *E. huxleyi*, for which an absolute requirement for Co has been shown (Sunda and Huntsman 1995a; Xu et al. 2007).

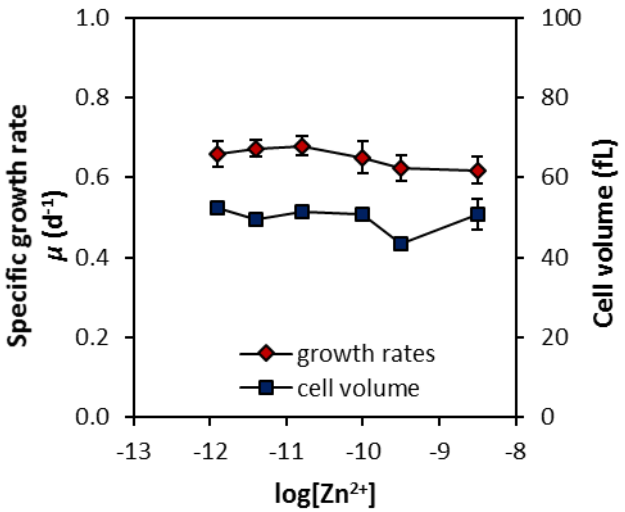

Figure 4.1: Variation in growth rate (diamonds) and cell size (squares) of *E. huxleyi* at different free Zn^{2+} concentration. Error bars represent 1x SD of the replicate treatments.

Table 4.1: Effect of Zn on specific growth rates and cell morphology of *E. huxleyi* cultured across a range of free Zn^{2+} ion concentrations. (Errors represent ± 1 x S.D)

pZn = -log [Zn^{2+}]	8.5	9.5	10.0	10.8	11.4	11.9
Specific growth rate μ (d^{-1})	0.62 ± 0.03	0.62 ± 0.03	0.65 ± 0.04	0.68 ± 0.02	0.67 ± 0.02	0.66 ± 0.03
μ:μ_{max}	0.91	0.92	0.96	1	0.99	0.97
cell volume (fL)	50.76 ± 3.86	43.47 ± 1.16	50.67 ± 0.63	51.40 ± 0.12	49.42 ± 0.58	52.22 ± 1.33
surface area/vol (μm^{-1})	1.31 ± 0.04	1.38 ± 0.01	1.31 ± 0.01	1.30 ± 0.00	1.32 ± 0.01	1.29 ± 0.02

The production of calcium carbonate plates (coccoliths) by coccolithophores results in reduction in seawater alkalinity and a consequent increase in pCO_2 while formation of organic matter during photosynthesis reduces atmospheric pCO_2 (Rost and Riebesell 2004). Overall, there is a net decrease of pCO_2 in seawater due to coccolithophore growth, however the relative rates of photosynthesis and calcification determine how much CO_2 is absorbed and sequestered to the deep ocean. (Schulz et al. 2004) reported that under Zn limitation the growth rates of *E. huxleyi* were significantly reduced, but the rate of $CaCO_3$ production remained the same, which led to a higher $CaCO_3$ to organic carbon ratio ($CaCO_3$/org-C). In other words, Zn limited cells were more heavily calcified (Schulz et al. 2004). In this study, we did not observe heavy calcification of *E. huxleyi* even at the lowest free Zn^{2+} ion concentrations studied (Figure 4.2). This is supported by the growth rates and cell size results where variations in pZn did not have any significant effect ($p > 0.05$) on growth rates or cell size. This discrepancy in the two studies could be due to substitution of Zn by Co. In this study *E. huxleyi* was grown at an ambient Co concentration (pCo) of 10.88, whereas in the study by Schultz et al. (2004) the cells were grown at limiting Co concentrations pCo = 12.7 (Schulz et al. 2004). *E. huxleyi* has a primary requirement for Co (Sunda and Huntsman 1995a; Xu et al. 2007); hence the growth limitation observed by (Schulz et al. 2004) could be due to Zn and Co co-limitation, which may have led to more heavily calcified cells. If this is the case, the $CaCO_3$/org-C ratio of *E. huxleyi* would be dependent on the bioavailability of both Zn and Co.

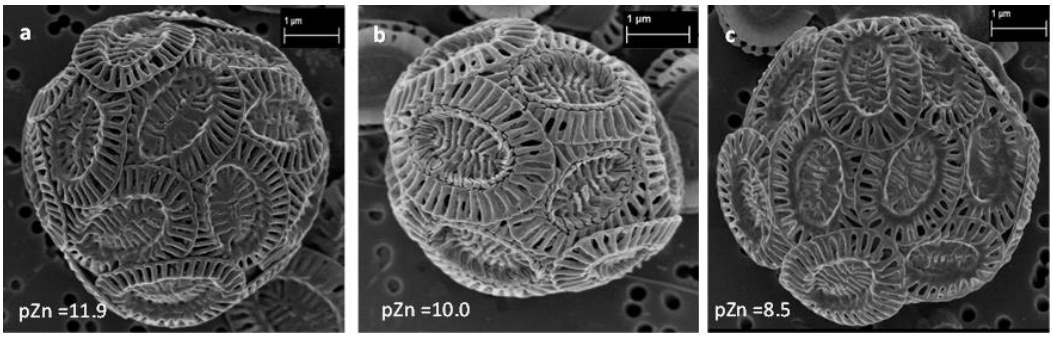

Figure 4.2: Scanning electron microscope images of *E. huxleyi* cultured at different free Zn^{2+} concentrations; (a) pZn = 11.9, (b) pZn = 10.0 and (c) pZn = 8.5.

4.3.2. Photophysiology and cellular chlorophyll a concentration

In contrast to growth rates, a small but significant effect of free Zn^{2+} ion concentrations on photophysiology was observed, whereby the photosynthetic efficiency of *E. huxleyi* significantly decreased as the free Zn^{2+} ion concentration decreased (r^2= 0.87, $p < 0.01$). The maximum quantum yield of PSII, F_v/F_m, decreased from 0.56 ± 0.02 at pZn = 8.5 to 0.50 ± 0.01 at pZn = 11.9 (Figure 4.3a, Table 4.2). The duration of electron transport from the electron carriers Q_A to Q_B, $\tau 1$, and from Q_B to the PQ Pool, $\tau 2$, increased ($p < 0.05$) with decreasing free Zn^{2+} ion concentration (Figure 4.3b, Table 4.2). However, no significant influence of Zn was observed on the proportion of oxidized PQ ($p > 0.05$). A trend of reduced cellular Chl *a* (both per cell and per cell volume) was observed with decreasing free Zn^{2+} concentrations, however, these were not statistically significant ($p > 0.05$; Figure 4.3, Table 4.2). In photosynthetic algae, a balance must be maintained in the sequentially linked photosynthetic and biosynthetic processes, which starts with light capture by Chl *a*, followed by electron transfer, CO_2 fixation and biomolecule synthesis. Many of these processes are affected by nutrient

(Zn) limitation, which would lead to downregulation of the photosynthetic system (Kana et al. 1997; Sunda and Huntsman 2004). One possible explanation for the effect of Zn bioavailability on the photochemical efficiency of PSII could be an increase in the activity of the Zn containing enzyme carbonic anhydrase (CA) with increasing free Zn^{2+} ion concentration. Carbonic anhydrase catalyses the reversible hydration of CO_2 and is therefore critical to CO_2 transport and fixation by phytoplankton (Morel et al. 1994). Since the concentration of CO_2 is low in seawater the extracellular CA when present converts abundant bicarbonate ion (HCO_3^-) to CO_2. It has been suggested that *E. huxleyi* (clone CS-812) relies primarily on CO_2 rather than HCO_3^- as an inorganic carbon source and that external CA helps but is not essential in C acquisition (Buitenhuis et al. 2003; Sinoir et al. 2016a). The internal CA is involved in the carbon concentrating mechanism in marine phytoplankton where the dehydration of HCO_3^- to CO_2 is facilitated by CA in the chloroplast (Hopkinson et al. 2011; Soto et al. 2006). This CO_2 could now be acted upon by the enzyme RubisCO and used for organic carbon production (Buitenhuis et al. 2003). This would suggest that at higher free Zn^{2+} ion concentrations, more CO_2 may be concentrated due to greater activity of CA. This greater CO_2 concentration would allow for greater RubisCO carboxylase activity during carbon fixation, therefore requiring more ATP. This increased demand for ATP may cause increased PSII electron transfer rates, reflected in decreased $\tau_1$and τ_2 with increasing free Zn^{2+} concentrations, and perhaps induce the synthesis of more chlorophyll molecules in the antennae of the Light Harvesting Complex of PSII.

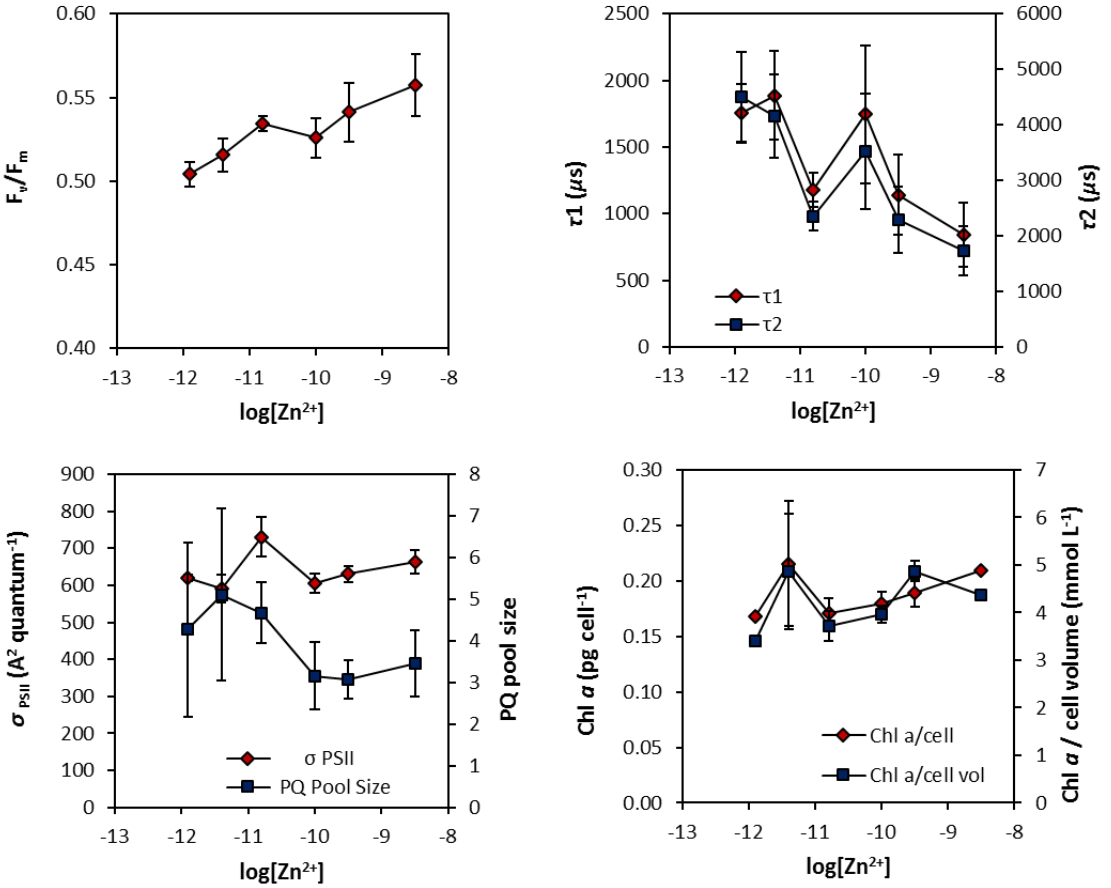

Figure 4.3: Variation in (a) the potential photochemical efficiency of PSII reaction centre (F_v/F_m); (b) duration of electron transport from QA to QB (τ1: diamonds) and from QB to PQ Pool (τ2 : squares); (c) the size of the functional absorption cross section of PSII (σ : diamonds) and the size PQ pool (squares); and (d) Variation in Chlorophyll *a* normalised per cell (diamonds) and per cell volume (squares) of *E. huxleyi* with increasing free Zn^{2+} concentration. Error bars represent 1x SD of the replicate treatments.

Table 4.2: Effect of Zn photophysiological parameters (± 1 x S.D.) of E. huxleyi cultured across a range of free Zn^{2+} ion concentrations.

pZn = -log [Zn^{2+}]	8.5	9.5	10.0	10.8	11.4	11.9
F_v/F_m	0.56 ± 0.02	0.54 ± 0.02	0.53 ± 0.01	0.53 ± 0.00	0.52 ± 0.01	0.50 ± 0.01
σ_{PSII} (Å^2 quantum^{-1})	664 ± 32	631 ± 22	606 ± 26	731 ± 54	591 ± 37	620 ± 8
PQ Pool Size	3 ± 1	3 ± 0	3 ± 1	5 ± 1	5 ± 2	4 ± 2
τ_1 (µs)	842 ± 242	1141 ± 300	1745 ± 520	1178 ± 128	1885 ± 333	1754 ± 220
τ_2 (µs)	1726 ± 445	2295 ± 596	3529 ± 1040	2356 ± 255	4152 ± 747	4501 ± 809
τ_3 (µs)	7738 ± 526	8838 ± 3313	8780 ± 3608	17088 ± 2117	10378 ± 4834	9992 ± 1096
Chl *a* (pg)/ cell	0.21	0.19 ± 0.01	0.18 ± 0.01	0.17 ± 0.01	0.22 ± 0.06	0.17
Chl *a*/cell volume (mmol L^{-1})	4.37	4.87 ± 0.22	3.96 ± 0.18	3.71 ± 0.32	4.87 ± 1.22	3.41

4.3.3. Zn:P ratio and Zn isotope fractionation

The relationship between cellular Zn:P ratio and free Zn^{2+} ion concentration had a hysteresis at pZn 9.5, with increasing slope between pZn values 11.9 to ~10.0, and above a pZn value of 9.5 (Figure 4.4, Table 4.3). This observation is similar to the sigmoidal relationship between cellular Zn:C ratios and free Zn^{2+} ion concentration reported by Sunda and Huntsman (1992), where minimal slopes were observed within the pZn range of 10.5 to 8.5. Overall, our data fit well with the cellular free Zn^{2+} ion concentration versus Zn:P ratio of *E. huxleyi* (clone BT6) reported by Sunda and Huntsman (1992; Figure 4.4). To convert between datasets, the Zn:P ratio of *E. huxleyi* (clone BT6) was obtained by multiplying the Zn:C ratio with the Redfield ratio (C:P = 106:1).

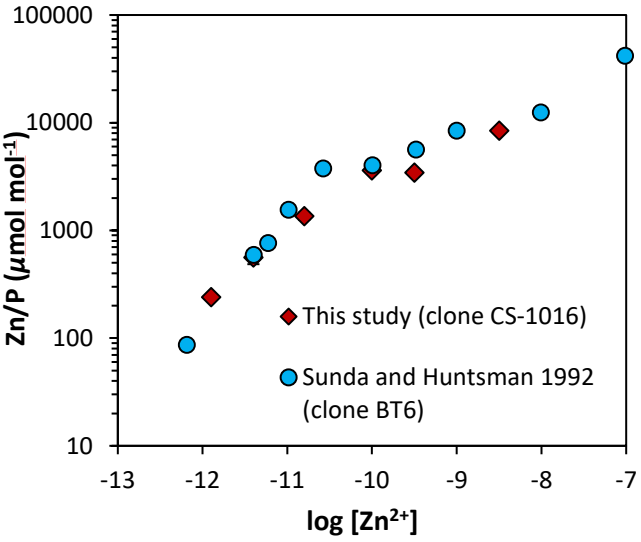

Figure 4.4: The cellular Zn normalised to the P content of the cells (μmol mol^{-1}) of *E. huxleyi* (clone CS-1016; diamonds) cultured across a range of free Zn^{2+} ion concentrations showing a sigmoidal relationship between Zn:P and the free Zn^{2+} ion concentration with minimum slope between pZn values of 10 and 9.5. The Zn:P ratio of another clone of *E. huxleyi* (clone BT6; circles) (Sunda and Huntsman 1992) is shown for comparison.

Table 4.3: Zn uptake (± 1 x S.D.) and Zn isotope fractionation (± 2 x S.D.) by *E. huxleyi* cultured at a range of free Zn^{2+} ion concentrations.

pZn = -log [Zn^{2+}]	8.5	9.5	10.0	10.8	11.4	11.9
Zn:P (µmol mol^{-1})	8473 ± 407	3452 ± 219	3608 ± 141	1357 ± 106	562 ± 76	241.34
$\Delta^{66}Zn$ (‰) SOW washed	-0.54 ± 0.06	-0.26 ± 0.06	-0.37 ± 0.02	-0.41 ± 0.07	-0.46 ± 0.00	-0.45 ± 0.07
$\Delta^{66}Zn$ (‰) oxalate - EDTA washed	-0.63 ± 0.09	-0.36 ± 0.09	-0.43 ± 0.09			

The Zn isotopic composition ($\Delta^{66}Zn$) of both oxalate-EDTA washed and unwashed cells of *E. huxleyi* were lighter relative to the media and varied between -0.66 ‰ and -0.22 ‰ across the range of free Zn^{2+} ion concentrations tested (Figure 4.5a, Table 4.3). Lighter $\Delta^{66}Zn$ values of oxalate-EDTA washed cells have also been reported for the chlorophyte *Dunaliella tertiolecta* and the diatom *Thalassiosira oceanica*, where the Zn isotope composition of the cells varied between -0.8 and -0.16 ± 0.1 (Figure 4.5a) at similar free Zn^{2+} ion concentrations (John and Conway 2014; John et al. 2007). For the diatom *T. oceanica*, measurements of Zn isotopes of unwashed cells showed a systematic enrichment of ^{66}Zn with increasing free Zn^{2+} ion concentrations (John et al. 2007). However, we did not observe any significant difference between the oxalate-EDTA washed and unwashed cells for the coccolithophore *E. huxleyi*. The oxalate-EDTA washed cells had a slightly lighter isotopic composition than the unwashed cells $\Delta^{66}Zn_{washed\text{-}unwashed}$ = -0.11 ± 0.08 ‰, which is not statistically significantly ($p > 0.05$; Figure 4.5a). The heavier Zn isotope composition of the unwashed diatom cells observed by *John et al*. (2007) could be a result of Zn co-precipitation with Fe oxy-

hydroxides or adsorption on cell surfaces (Gelabert et al. 2006; John et al. 2007). *Thalassiosira oceanica* was cultured at high Fe concentration (10^{-5} mol L^{-1} Fe and 10^{-4} mol L^{-1} EDTA), which has been observed to co-precipitate Zn and may constitute a large portion of the total Zn pool associated with cells. However, in this study *E. huxleyi* was cultured at a much lower Fe concentration (5.65 x 10^{-7} mol L^{-1} of Fe and 10^{-4} mol L^{-1} EDTA) where extracellular Zn contributes only a small fraction of the total Zn (John et al. 2007; Tang and Morel 2006). Köbberich and Vance (2017), reported heavier δ^{66}Zn within the cells relative to the culture media for the diatom species *Chaetoceros* at Fe' (inorganically bound unchelated Fe) concentration < 20 pmol L^{-1}. The $\Delta^{66}Zn_{(cell\text{-}media)}$ got heavier with decreasing Fe' concentrations. To explain this observation, one hypothesis put forward by Köberrich and Vance (2017), is scavenging of heavy Zn by extracellular polymeric substances. Alternate hypothesis presented is, slow Zn uptake rate leads to pseudo-equilibrium conditions at the transporter site where more stable surface complexes are formed with heavy Zn isotopes resulting in heavier δ^{66}Zn within the cells. However, for the diatom *T. oceanica* no such effect was observed and the $\Delta^{66}Zn_{(cell\text{-}media)}$ was always negative at Fe' < 700 pmol L^{-1}(Köbberich and Vance 2017). At Fe' concentrations > 700 pmol L^{-1}, the δ^{66}Zn of the cells were heavier than the media for both diatom species due to Fe oxy-hydroxide precipitation(Köbberich and Vance 2017). In this study, *E. huxleyi* was cultured at Fe' concentration of 650 pmol L^{-1}, which is high enough for Fe not to contribute as growth limiting factor but low enough that there is no Fe oxy-hydroxide precipitation.

We did not observe any obvious change in Zn isotope fractionation associated with the "low affinity" uptake system, as reported for the diatom *T. oceanica* (John et al. 2007). The shift in dominance from the "high affinity" pathway to "low affinity" pathway

occurs at pZn < 10.5 for *T. oceanica* (CCMP 1005), whereas for *E. huxleyi* (CS-1016) it appears to occur at a much higher Zn concentration, pZn < 9.5 (Figure 4.5). This observation is similar to that reported by (Sunda and Huntsman 1992) for other strains of *T. oceanica* (clone 13-1) and *E. huxleyi* (BT6). The switch in the predominance of a "high affinity" relative to a "low affinity" uptake pathway was indicated by the change in slope in the sigmoidal relationship of the specific Zn uptake rate to free Zn^{2+} ion concentration of the media (Figure 4.5b) (John et al. 2007). Since we did not measure the δ^{66}Zn of *E. huxleyi* cells at free Zn^{2+} ion concentrations higher than $10^{-8.5}$ mol L^{-1}, it is possible that the extent of Zn fractionation by *E. huxleyi* could be greater at these higher free Zn^{2+} ion concentrations as observed for *T. oceanica* when Zn was taken up predominantly via the "low affinity" pathway. The Δ^{66}Zn values of oxalate-EDTA washed and unwashed *E. huxleyi* cells at pZn 8.5 was -0.66 ± 0.06 ‰ and -0.54 ± 0.06 ‰ respectively and comparable to oxalate-EDTA washed cells of the chlorophyte *Dunaliella tertiolecta* (Δ^{66}Zn = -0.76 ± 0.02 ‰ at pZn~8.5) and the diatom *T. oceanica* (Δ^{66}Zn = -0.80 ± 0.03 ‰ at pZn = 8.5 and Δ^{66}Zn = -0.68 ± 0.02 ‰ at pZn = 9.5) (John and Conway 2014; John et al. 2007).

The Zn isotope composition of the *E. huxleyi* cells at pZn 9.5 was -0.26 ± 0.06 ‰ and the Zn isotopic composition within the cells got lighter with decreasing free Zn^{2+} ion concentration, Δ^{66}Zn = -0.45 ± 0.07 ‰ at pZn 11.9 (Figure 4.5a). This trend of lighter Zn isotopic composition within the cells with decreasing free Zn^{2+}ion concentration statistically significant (r^2 = 0.82, p <0.05). We noted a similar observation for the diatom *T. oceanica*, where the Zn isotope composition within the cells was -0.16 ± 0.10 ‰ at pZn 10.5 and the Δ^{66}Zn was lighter (= -0.29 ± 0.05 ‰) at pZn at 11.5 (Figure 4.6) (John et al. 2007). (John et al. 2007) hypothesised that the lighter Δ^{66}Zn values within

the cells ($\Delta^{66}Zn$= -0.16 ± 0.10 ‰) at pZn 10.5 was due to lighter Zn being available to the diatom since the heavier Zn was bound to EDTA and at equilibrium the $\delta^{66}Zn$ composition of the free Zn^{2+} ion concentration in the media is -0.16 ‰ lighter than Zn bound by EDTA (Ban et al. 2002; John et al. 2007). In this study, the desired free metal ion concentrations were also maintained by using EDTA. As mentioned, EDTA, being a strong ligand, preferentially binds heavier isotopes leaving the biologically available Zn isotopically light. At lower free Zn^{2+} ion concentrations the uptake of Zn by phytoplankton is limited by diffusion of Zn to the cell surface (Figure 4.5b) (Sunda and Huntsman 1992). The diffusion of $^{64}Zn^{2+}$ to the cell surface is faster than $^{66}Zn^{2+}$, which leads to isotopic fractionation with lighter Zn isotope composition within the cells (John et al. 2007; Rodushkin et al. 2004). This could explain the systematic enrichment of lighter Zn within the cells of *E. huxleyi* with decreasing free Zn^{2+} ion concentrations (Figure 4.5a).

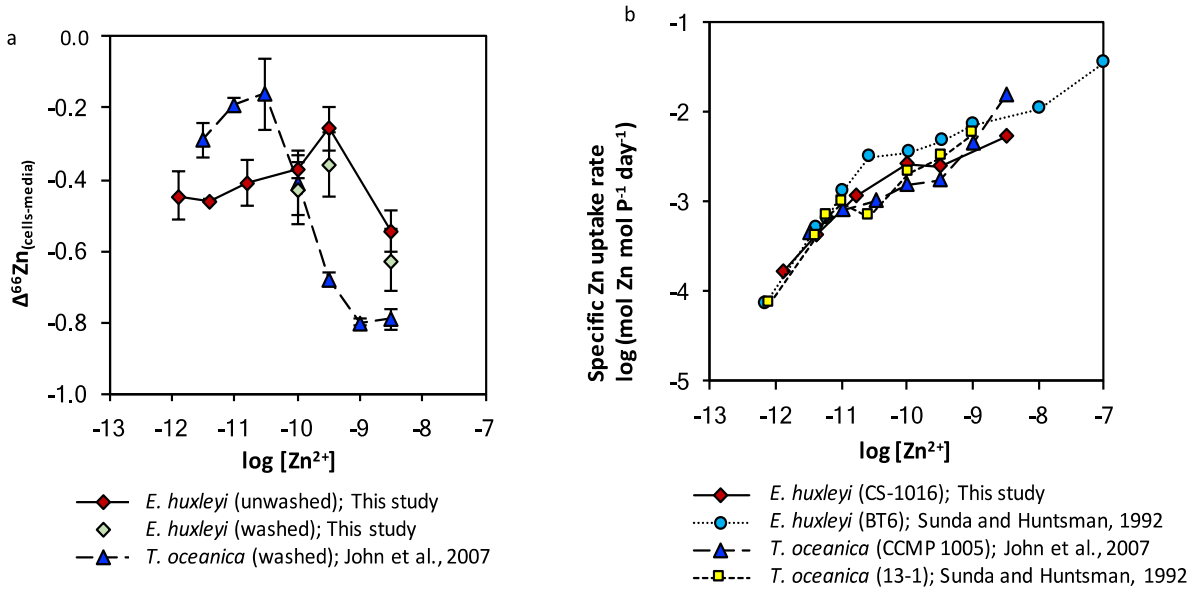

Figure 4.5: (a) Zn isotope fractionation by *E. huxleyi* across a range of free Zn^{2+} ion concentrations (filled diamonds- unwashed/SOW washed cells and hollow diamonds-washed/oxalate-EDTA washed cells to remove extracellular Zn) compared to Zn isotope fractionation by the diatom *T. oceanica* (triangles; John et al., 2007). Error bars represent 2x SD of the triplicate treatments. (b) Specific Zn uptake rates (mol Zn (mol P)-1 day-1) of *E. huxleyi* (clones CS-1016; diamonds (this study) and BT6; circles (Sunda and Huntsman 1992)) and *T. oceanica* (clone CCMP 1005, triangles; (John et al., 2007) and clone 13-1, squares (Sunda and Huntsman 1992)) cultured across a range of free Zn^{2+} ion. The change in slope indicates the switch in the predominance from a "high affinity" uptake pathway to a "low affinity" uptake pathway with increasing free Zn^{2+} ion concentration. The shift in dominance occurs at pZn < 10.5 for *T. oceanica* (clones CCMP 1005 and 13-1), whereas, for *E. huxleyi* it appears to occur at a much higher Zn concentrations, at pZn < 9.5 (clone CS-1016) and pZn < 10 (clone BT6). When Zn uptake is predominantly by the "high affinity" uptake system, the Zn uptake rates decreases proportionately with decreasing free Zn^{2+} ion concentration due to under-saturation of Zn uptake system.

In the surface 100 m of the world ocean, a wide range of δ^{66}Zn values have been reported (between -1.1‰ and +0.9‰) (Andersen et al. 2011; Bermin et al. 2006; Boyle et al. 2012; Conway and John 2014; Conway and John 2015; Conway et al. 2013; Little et al. 2014; Little et al. 2016; Zhao et al. 2014). These variations in δ^{66}Zn values of the surface waters could result from a variety of process, including complexation with organic ligands (Jouvin et al. 2009), biological uptake (Gelabert et al. 2006; John et al. 2007), particle scavenging (John and Conway 2014) and input from rivers and aerosols (Conway and John 2014; Little et al. 2014). Most input sources of Zn in the ocean have a lighter isotopic composition relative to the deep ocean (Little et al. 2014). Adsorption of Zn onto cell surface and scavenging of Zn onto degrading particulate organic matter also results in lighter dissolved Zn isotope composition. Thus, it has been suggested that lighter δ^{66}Zn values observed for the shallow western Atlantic Ocean relative to deeper waters could be explained by the scavenging of heavier Zn on particles (John and Conway 2014). We proposed that the heavier dissolved Zn isotope compositions observed at the depth of the DCM at the south Tasman Sea is due to uptake of lighter Zn by eukaryotic phytoplankton. The lighter dissolved Zn isotope compositions immediately below the DCM associated with an increase in the total dissolved Zn concentration is a consequence of the in situ release of light Zn from degrading organic matter (see Chapter 3).

From this study, we can infer that in the open ocean where Zn speciation is dominated by complexation with strong organic ligands, a bloom of the coccolithophore *E. huxleyi* would result in the lighter ^{64}Zn isotope being taken up at a slightly fast rate by the phytoplankton compared to ^{66}Zn isotope, resulting in the dissolved Zn pool becoming isotopically heavier. This is complementary to our field observations in the south

Tasman Sea, where heavier dissolved Zn isotope values were measured at the chlorophyll maximum (DCM) dominated by coccolithophores (see Chapter 3). The extent of Zn isotope fractionation ($\Delta^{66}Zn_{DCM\text{-}surface} \approx 0.5$ ‰) in the south Tasman Sea, where the free Zn^{2+} ion concentration was less than 10 pmol L^{-1} in the upper 100 m, is comparable to the Zn isotope fractionation by *E. huxleyi* under similar free Zn^{2+} ion concentrations. Growth rates provide an integrated response of the phytoplankton to the environmental condition; since we do not observe any significant reduction in growth rates at the lowest free Zn^{2+} concentration studied, we conclude that this Tasman Sea clone of *E. huxleyi* can adapt to low Zn concentrations observed in the Tasman Sea.

This study also provides further evidence in support of the speculation that the heavier isotopic composition of dissolved Zn in the upper waters observed in disparate parts of the world ocean; viz. the North Atlantic (Boyle et al. 2012; Conway and John 2014) the Atlantic Sector of Southern Ocean (Zhao et al. 2014) and the NE Pacific (Bermin et al. 2006) likely results from biological uptake of lighter Zn.

4.4. Conclusions

In this study, we investigated the physiology (growth and photophysiology) of and the extent of Zn isotope fractionation due to Zn uptake by, the coccolithophore *Emiliania huxleyi* over a range of free Zn^{2+} ion concentration, representing the natural Zn concentration observed in the global oceans.

Across the range of free Zn^{2+} ion concentrations tested in this study, photosynthetic efficiency and electron transport rates of *E. huxleyi* were observed to increase with increasing free Zn^{2+} concentration, which was speculated to be due to increased carbonic anhydrase activity. However, the amount of bioavailable Zn did not have any significant influence on the specific growth rate or cell morphology of *E. huxleyi*, suggesting that this clone was adapted to low free Zn^{2+} ion concentrations.

Over the range of Zn concentration tested, the Zn isotopic composition of *E. huxleyi* cells was lighter relative to the media, with $\Delta^{66}Zn_{cells\text{-}media}$ varying from -0.6 ‰ to -0.2 ‰. These results suggest that even when the free Zn^{2+} ion concentration of the media is in the low picomolar range, the lighter isotope is preferentially taken up by this species, resulting in a heavier $\delta^{66}Zn$ composition of the seawater. This study also indicates that the heavier dissolved Zn isotopic composition observed in the upper waters in other parts of the world ocean could be a result of uptake of lighter Zn by abundant phytoplankton species like *E. huxleyi*.

Acknowledgements

We thank Lucy Wenger for her help with the culturing of *E. huxleyi*. Financial support for this work came from the Australian Research Council (DP130100679). RSES and ANU scholarships to the lead author are also appreciated.

Appendix:

Table 4.3 (alternate): Zn isotope fractionation by *E. huxleyi* across a range of free Zn^{2+} ion concentrations. $\Delta^{66}Zn$ relates Zn isotope composition of cells relative to the media. The Zn isotope composition of the Zn added to the culture media is 0.06 ± 0.01 relative to the standard reference material (SRM) used to calculate $\delta^{66}Zn_{cells}$. Since the isotopic composition of the Zn added is similar to the SRM, no correction was made and the values for $\Delta^{66}Zn_{(cell\text{-}media)}$ reported in the chapter is essentially $\delta^{66}Zn_{cells}$. The corrected $\Delta^{66}Zn_{(cell\text{-}media)}$ are reported here by subtracting 0.06 from $\delta^{66}Zn_{cells}$.

pZn = -log [Zn^{2+}]	8.5	9.5	10.0	10.8	11.4	11.9
$\Delta^{66}Zn$ (‰) SOW washed	-0.60 ± 0.06	-0.32 ± 0.06	-0.43 ± 0.02	-0.47 ± 0.07	-0.52 ± 0.00	-0.51 ± 0.07
$\Delta^{66}Zn$ (‰) oxalate -EDTA washed	-0.69 ± 0.09	-0.42 ± 0.09	-0.49 ± 0.09			

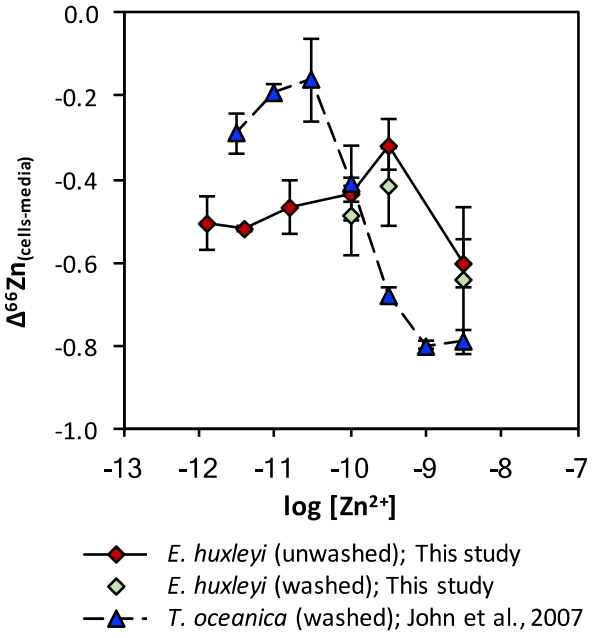

Figure 4.5a (alternate): Zn isotope fractionation by *E. huxleyi* (corrected for relative difference between media and standard) across a range of free Zn^{2+} ion concentrations (filled diamonds- unwashed/SOW washed cells and hollow diamonds- washed/oxalate-EDTA washed cells to remove extracellular Zn) compared to Zn isotope fractionation by the diatom *T. oceanica* (triangles; John et al., 2007). Error bars represent 2x SD of the triplicate treatments

Chapter 5:

Variability in zinc isotope fractionation in *Phaeocystis antarctica* under iron replete and iron limiting conditions

Moneesha Samanta*, Michael J. Ellwood, Robert F. Strzepek, Robin Grün[4]

Abstract

The haptophyte *Phaeocystis antarctica* is a major component of the phytoplankton assemblage in the Southern Ocean. The dissolved iron (Fe) concentration across much of the Southern Ocean is low enough to limit phytoplankton growth. While there is no conclusive evidence of Zn limitation in the Southern Ocean, the effects of Fe limitation on Zn biogeochemistry has not been examined. We thus studied the effect of Fe and zinc (Zn) limitation, alone and in combination, on *P. antarctica*. We measured specific growth rates, Zn accumulation, Zn isotope fractionation and the photophysiological responses of *P. antarctica*. The growth rates for *P. antarctica* were severely reduced under both Fe and Zn limiting conditions. Under Fe limitation, the cells size and the photosynthetic efficiency of photosystem II (F_v/F_m) of *P. antarctica* significantly decreased and the time taken for electron transport from the mobile photosynthetic electron carriers Q_A to Q_B and from Q_A to the plastoquinone (PQ) pool increased. The decrease in cell size could be an adaptive strategy to increase the surface area of Fe diffusion relative to the cell volume, assuming that cell volume reflects the Fe required

[4] Authors' contribution: M.S. analysed the data and drafted the manuscript with contribution from M.J.E and R.F.S.; R.F.S. also assisted with preparation of Aquil media and provided cultures of *P. antarctica*; R.G. measured the Zn isotope composition within *P. antarctica* cultured across a range of Fe' concentrations.

for cellular processes including photosynthetic electron transport. Under Zn limitation, F_v/F_m increased and cell size was not affected significantly. When *P. antarctica* was Fe-limited we observed a significant increase in the cellular quota for Zn (expressed as Zn:P), whereas, under Zn limiting conditions, the cellular Zn quota as well as the Zn uptake rate (given by Zn/P/d) decreased significantly. Lighter isotopes of Zn were taken up by *P. antarctica* under Fe replete conditions irrespective of dissolved Zn^{2+} concentration. However, under Fe-limiting conditions, we observed a heavier Zn isotope composition within the cells. The increased cellular Zn:P ratio under Fe limitation could be a result of an adaptive strategy employed by *P. antarctica* in an attempt to acquire Fe under Fe-limiting condition. Heavier Zn isotope composition within *P. antarctica* observed under Fe limiting condition could thus result from a change from kinetic control of Zn uptake and internalisation to equilibrium control of Zn uptake and internalisation. Alternatively, the heavier isotope composition of *P. antarctica* under Fe limiting condition could result from the potential release of isotopically light Zn from the cells, resulting from cell senescence and death. Our results indicate that in the Southern Ocean, under Fe limiting conditions, a dominance of *P. antarctica* in the phytoplankton community may result in lighter isotope composition of dissolved Zn in surrounding surface seawater. Thus, Fe availability could regulate the dissolved Zn isotope composition of the Southern Ocean, which in turn would be reflected in other parts of the world ocean. This study highlights the importance of carefully analysing the trace metal composition while interpreting Zn isotope composition of the biologically active upper water column of the ocean. Subsequently, more work needs to be done to understand the effect of Fe and other

factors that might influence Zn isotopic fractionation by different phytoplankton species.

5.1. Introduction

The Southern Ocean plays a significant role on the global carbon cycle influencing both ocean circulation and biogeochemistry (Sarmiento et al. 1998). This influence results from its central role in the ocean circulation by connecting the Atlantic Ocean, the Indian Ocean and the Pacific Ocean (Talley 2013). The Southern Ocean also plays a crucial role in controlling many global oceanic processes (e.g. formation of the Antarctic Intermediate Waters and the Subantarctic Mode Waters) which are reflected in other parts of the global ocean (Sarmiento et al. 2004; Sloyan and Rintoul 2001). The upwelling of Circumpolar Deep Water (CDW) in the Antarctic Zone (AAZ) of the Southern Ocean brings nutrient rich waters to the surface which are then transported southwards and northwards. Surface waters that flow southwards tend to sink after encountering the Antarctic ice shelf forming Antarctic Bottom Waters (AABW). The northward flowing water is transported across the Antarctic Polar Front (APF) into the Polar Front Zone (PFZ), where part of the surface water subducts to form Antarctic Intermediate Water (AAIW), another part of the surface water from the PFZ moves across the Subantarctic Front (SAF) into the Subantarctic Zone (SAZ), where Sub Antarctic Mode Water is formed by deep winter convection (Sarmiento et al. 2004). Thus, the processes that influence the biogeochemical composition of surface waters of the Southern Ocean are reflected in other parts of the world ocean via these water masses. To analyse the Zn isotope signature (δ^{66}Zn) of SAMW and AAIW in the Tasman Sea presented in Chapter 3, it is important to understand the factors influencing δ^{66}Zn composition in the formation region of these water masses.

Much of the Southern Ocean has been characterized as 'High-Nitrate Low-Chlorophyll' (HNLC). This nutrient status has been primarily attributed to low Fe bio-availability in

the surface waters of the Southern Ocean, which can reduce phytoplankton growth and can also influence the phytoplankton community composition (Boyd et al. 2000; Coale et al. 2004; Martin 1990; Pollard et al. 2009; Sarmiento et al. 2004). Iron is required by phytoplankton for a variety of cellular processes including electron transport during photosynthesis, respiration and nitrogen (N) assimilation. It acts as a metal centre in several important metalloenzymes, including nitrate and nitrite reductase, chelatase, nitrogenase, catalase, peroxidase, and superoxide dismutase (see (Twining and Baines 2013) and references therein). The Southern Ocean is geographically isolated and consequently has low aeolian dust deposition and riverine or sedimentary source Fe inputs, which combined with its chemical speciation and the dominance of insoluble Fe species, makes bioavailable Fe a limiting factor, thereby impacting primary productivity (Boyd and Ellwood 2010). Increased phytoplankton productivity is observed in some areas of the Southern Ocean where there are elevated Fe concentrations due to resuspension of continental shelf sediments and/or meltwaters from sea ice (Fitzwater et al. 2000). Iron enrichment experiments carried out over the last two decades provide strong evidence of Fe limitation of phytoplankton growth across large parts the Southern Ocean (Boyd et al. 2000; Coale et al. 2004; Cochlan et al. 2002; Scharek et al. 1997).

Zinc is another important trace metal micronutrient which acts as a cofactor in several important enzymes within phytoplankton including carbonic anhydrase, alkaline phosphatase, RNA polymerase, tRNA synthetase, reverse transcriptase, carboxypeptidase and superoxide dismutase ((Twining and Baines 2013) and references therein). The enzyme carbonic anhydrase catalyses the reversible hydration of bicarbonate to carbon dioxide. Hence, it plays an important role in inorganic carbon

acquisition by phytoplankton (Hopkinson et al. 2011; Morel et al. 1994; Sunda and Huntsman 2005); (Christianson and Fierke 1996). Subsequently, Morel et al. (1994) introduced the 'Zn hypothesis' which is analogous to the 'Fe hypothesis' of John Martin, whereby Zn, like Fe, is hypothesised to 'limit oceanic production and influence the global carbon cycle' (Martin 1990; Morel et al. 1994). In the Southern Ocean, there has been no conclusive evidence of Zn limitation (Coale et al. 2003; Cochlan et al. 2002; Frew et al. 2001; Scharek et al. 1997). The dissolved Zn concentration in most parts of the Southern Ocean is in excess of the Zn-binding ligands due to upwelling of Zn and nutrient-rich deep waters (Baars and Croot 2011); consequently, the concentration of bioavailable Zn is not low enough to limit phytoplankton growth.

The haptophyte *Phaeocystis antarctica* is a dominant member of the Southern Ocean phytoplankton community (Annett et al. 2010; Arrigo et al. 1999; Brichta and Nöthig 2003; Petrou et al. 2016; Sedwick et al. 2000) and exerts a strong influence on the biogeochemical cycle of carbon via the drawdown of atmospheric CO_2 and its eventual export into the deep ocean (DiTullio et al. 2000; Timmermans et al. 2001). *Phaeocystis antarctica* is also responsible for the production of climate active gas dimethylsulfide (DMS) consequently favouring the formation of clouds and decreasing the average light penetration (Baumann et al. 1994; Turner et al. 1995; Vance et al. 2013). In a study looking at Zn-Co substitution capability, it was suggested that *P. antarctica* has a preference of Zn over Co since it was observed that growth rates were significantly higher at Zn replete and low Co condition than Co replete and low Zn condition (Saito and Goepfert 2008). The effects of Fe limitation in Southern Ocean phytoplankton, including *P. antarctica,* has been the focus of number of studies (Sedwick et al. 2007; Strzepek et al. 2012; Strzepek et al. 2011; Timmermans et al. 2001); however, to our

knowledge, there has been no research addressing the effect of Fe limitation on Zn quotas and Zn isotope fractionation in the Southern Ocean phytoplankton.

Previous culture experiments have shown that lighter isotope of Zn is preferentially taken up within phytoplankton cells, whereas, heavier isotope adsorb to cell surface (Gelabert et al. 2006; John and Conway 2014; John et al. 2007)(. However, in a recent study looking at the effect of bioavailable Fe in Zn isotope fractionation by diatoms, Köbberich and Vance (2017)reported heavier Zn isotopic composition within the cells of the diatom species *Chaetoceros* at low bioavailable Fe concentration. At this limiting bioavailable Fe concentrations, the diatom grew at less than 60% of its maximum growth rate at ambient Fe concentration (Köbberich and Vance 2017). The possible explanations put forward by Köberrich and Vance (2017), for the observed heavy Zn isotope composition of *Chaetoceros* species at low bioavailable Fe concentrations are: (a) scavenging of heavy Zn by extracellular polymeric substances, and (b) slow Zn uptake rate leading to pseudo-equilibrium conditions at the transporter site where more stable surface complexes are formed with heavy Zn isotopes. However, for the diatom *T. oceanica* no such effect was observed and the diatom preferentially incorporated the lighter isotope of Zn even at very low bioavailable Fe concentration, although its growth was reduced by 50% of its maximum growth rate.

To understand Zn isotope biogeochemistry in the Southern Ocean, measuring Zn isotope fractionation by Southern Ocean phytoplankton under relevant conditions is important. The aim of this chapter is to understand the effect of Fe limitation on Zn isotope fractionation by Southern Ocean haptophyte *P. antarctica*, at ambient concentration of other trace elements and light intensity. We also looked at the Zn isotope fractionation by *P. antarctica* under Fe and Zn co-limiting conditions.

5.2. Methods

5.2.1. Study organism and experimental design

Trace metal manipulation experiment was performed on the Southern Ocean haptophyte *P. antarctica* (Clone SX9). It was isolated from 65°08.72'S and 174°08.94'E in December 2004 and maintained as a stable monoculture since June 2005 (Strzepek et al. 2011). Experimental cultures were grown at 3 ± 1 °C under a continuous irradiance of 60-70 µmol quanta m^{-2} s^{-1}, which was optimal for this species (Strzepek et al. 2012). Irradiance was measured with a calibrated 4π quantum meter (model QSL-2101; Biospherical Instruments). Cultures were subjected to four treatments of Fe and Zn replete (+) and limiting conditions (-), viz. +Fe,+Zn; +Fe,-Zn; -Fe,+Zn and -Fe,-Zn, with three replicates grown for each treatment. Each treatment was maintained at exponential growth phase by dilution of the culture during acclimatisation to the growth media. At least two transfers (14–16 cell divisions) were done before measurements were made. Specific growth rates and photophysiological parameters, including the photochemical efficiency of the photosystem II (PSII) reaction centre (F_v/F_m), effective absorption cross section of PSII (σ_{PSII}), potential storage efficiency of the plastoquinone (PQ) pool, and of the time constants for electron transport from the mobile electron carriers Q_A to Q_B, $\tau 1$, from Q_B to the PQ Pool, $\tau 2$, and from the PQ Pool to photosystem I (PSI) were measured. Cultures of *P. antarctica* were harvested by collection of cells on filters at mid-exponential phase of growth and saved for measurements of Chlorophyll *a* (Chl-*a*), Zn isotope composition ($\delta^{66}Zn$), Zn and phosphorous (P) content of cells. The cell size and cell concentration density were measured on freshly harvested cultures using a Coulter counter.

5.2.2. Medium preparation

Artificial seawater medium (Aquil) was used for trace metal manipulation experiment. Precautions were taken to minimise trace metal and bacterial contaminations. All work for Aquil preparation and culturing was done in class 100 HEPA filtered laminar flow hood which was wiped with 90% (v/v) ethanol before each use. All labwares were rigorously cleaned and microwave sterilised prior to use. Cleaning was done by soaking in detergent (L900, Nalgene) for 2 days before rinsing with Milli-Q water (Millipore, Australia). This was followed by a further soak in 10% (v/v) AR grade hydrochloric acid (HCl) for a week before rinsing with Milli-Q water. To remove trace metal contaminants, Synthetic Ocean Water (SOW), made following the protocol described in (Price et al. 1988), and nutrient stocks were eluted through a column containing Toyopearl AF-chelate-650M ion-exchange resin. Filter sterilized (0.2 µm Gelman Acrodisc PF) nutrients, vitamins and trace metal solutions were then added to the microwave sterilized SOW so that the final concentration of nutrients and vitamins in the Aquil were 10 µmol L^{-1} phosphate, 100 µmol L^{-1} silicate, 300 µmol L^{-1} nitrate, 0.55 µg L^{-1} vitamin B_{12}, 0.5 µg L^{-1} biotin and 100 µg L^{-1} thiamine. The trace metal solution (without Fe and Zn) containing ethylenediaminetetraacetic-acid (EDTA) as the chelating agent was added to the SOW such that final concentration was 50 nmol L^{-1} for cobalt, 19.8 nmol L^{-1} for copper, 228 nmol L^{-1} for manganese, 9.96 nmol L^{-1} for selenium, 100 nmol L^{-1} for molybdenum and 100 µmol L^{-1} for EDTA. The Fe and Zn contamination in the SOW was measured to be 0.5 nmol L^{-1} and 6 nmol L^{-1}, respectively. This was accounted for in calculations when preparing the media for Fe and Zn manipulation experiment.

For the Zn replete media, Zn was added as zinc sulphate solution such that the final Zn concentration was 480 nmol L^{-1}; while for the Zn limited media, no extra Zn was added. The pZn (-log Zn^{+2} concentration) calculated using the chemical equilibrium computer program Visual MINTEQ (version 3.0) for Aquil media at 3°C and pH 8.1 was 10.0 and 11.9 for Zn replete and Zn limited media, respectively.

In the Fe replete media, the final Fe concentration after Fe addition in the form of ferric chloride ($FeCl_3$) solution was 26.2 nmol L^{-1}. For a temperature of 3°C and a mean irradiance of 65 μmol quanta m^{-2} s^{-1} the Fe' (inorganically bound un-chelated Fe) was calculated to be 90 pmol L^{-1} at pH of 8.1 based on methods previously described (Strzepek et al. 2011; Sunda and Huntsman 2003). The overall conditional dissociation constant was calculated by adding the conditional stability constant in the dark (3.52×10^{-7}) and the conditional photo-dissociation constant (2.17×10^{-6}) of the Fe-EDTA complex at 3°C (R. Strzepek, personal communication).

For the Fe limited media, a pre-complexed solution of $FeCl_3$ with the siderophore desferrioxamine B mesylate (DFB) was added to Aquil medium already containing other trace metals buffered/complexed with 100 µmol L^{-1} of EDTA. The siderophore DFB was chosen for Fe limitation because of its ability to complex Fe more strongly than EDTA (Hudson et al 1992; Lis et al 2015). Unlike the Fe-EDTA complex, the FeDFB complex is not photosensitive and hence Fe speciation is not affected by light (Lis et al. 2015; Sunda and Huntsman 2003). For the Fe-limited treatments, 2 nmol L^{-1} $FeCl_3$ premixed with 200 nmol L^{-1} of DFB was added to Aquil medium such that the final Fe:DFB molar ratio was 2.5 : 200 and the Fe' was calculated to be 0.02 pmol L^{-1}. The Fe' for the Fe limiting media was calculated according to the equation $[Fe'] = [FeDFB] / [L'] \times K_{Fe'L}^{cond}$; where $K_{Fe'L}^{cond} = 10^{11.8}$ (Maldonado et al. 2005). *P.* antarctica reportedly grew

at its maximum growth rate at Fe' > 0.17 pmol L^{-1} (at irradiance between 60 and 100 μmol quanta m^{-2} s^{-1}) (Strzepek et al. 2011), thus, for the Fe replete media, Fe' = 90 pmol L^{-1}, and for the Fe limited media, Fe'= 0.02 pmol L^{-1}, was chosen, which also represent conditions comparable to that observed in the Southern Ocean (Nolting et al. 1998).

5.2.3. Growth rate measurement

Growth rates of cultures were determined from *in vivo* chlorophyll *a* fluorescence using a Turner Designs model 10-AU fluorometer. Cultures were dark acclimated for approximately 30 min prior to each fluorescence measurement which was measured once every alternate day. Blanking was done with sterilised SOW before sample analysis. The specific growth rate per day (μ) was then calculated by determining the slope of ln(fluorescence) vs cumulative time during the exponential growth phase.

5.2.4. Photophysiological parameters

The Light Induced Fluorescence Transients (LIFT) technique was used to examine the *in vivo* level of photosynthetic activity of photosystem II (PSII). This technique uses a sequence of Fast Repetition Rate (FRR) short pulses of light (flashlets) to manipulate the level of photosynthetic activity of PSII and record the resulting changes in the fluorescence yield (Kolber and Falkowski 1995). A range of photosynthetic parameters are calculated by the LIFT software by selectively activating different parts of the photosynthetic apparatus by controlling the energy, length and time interval between

the flashlets (Kolber 2002). Measurements of photosynthetic efficiency of different treatments were done during the early-exponential growth phase. Cells were dark acclimatised for 30 mins prior to measurement. The principal of operation of the LIFT-FRR fluorometer (Soliense, Inc., Shoreham, NY; http://soliense.com/LIFT_Marine.php) used in this study is described below.

In darkness, the PSII reaction centre is in an oxidised or "open" state. In the LIFT-FRR protocol, short pulses of light (at wavelength 470 nm) applied to the cells excite the chlorophyll molecules of the antennae of the Light Harvesting Complex of PSII. The excitation energy is transferred to the PSII Reaction Centre (RC) and initiates charge separation leading to the photolysis of water ($2H_2O \rightarrow O_2 + 4H^+ + 4e^-$) (Figure 5.1). Approximately 2% of the light energy absorbed by the chlorophyll antennae is dissipated in the form of radiative decay, which is then detected by the instrument as a fluorescence signal at 685nm. Most of the excitation energy of the initial flashlet, which excites about 2% of the RCII, initiates charge separation with little energy loss as heat or fluorescence. The fluorescence yield of the first flashlet gives the minimum fluorescence yield, F_o (Figure 5.1). The time interval between consecutive flashlets is about 2 µs which is short enough to keep previously hit reaction centre in a reduced or "closed" state. During the fluorescence induction phase, saturation sequence (SS), a train of flashlets induces the maximum level of fluorescence, F_m. Maximum level of fluorescence is observed when most of the RCII is in a reduced state. Maximum quantum yield of the PSII is given by the amplitude of variable fluorescence F_v normalised to maximum fluorescence F_m, (i.e. F_v/F_m, where, $F_v = F_m - F_0$; Figure 5.1), and relates to the number of electrons extracted from water per quanta of light absorbed. F_v/F_m is widely used as an algal health indicator. The functional absorption cross

section of PSII (σ_{PSII}) is calculated from the slope of the initial variable fluorescence and relates to the antennae size and the efficiency of excitation energy transfer from light-harvesting pigments to the RCII (Figure 5.1). Following the saturation sequence, a relaxation sequence (RS) is applied, during which the time interval between flashlets increases exponentially until the fluorescence yield returns to F_0 (Figure 5.1). In the RS, information about the kinetics of electron transport are obtained. The electrons extracted from water are transferred from PSII to PSI via the cytochrome *b_6f* complex and a series of electron carriers, namely Q_A, Q_B, the PQ pool, and plastocyanin (PC) (Figure 5.2). Light absorption at PSI transfers electrons to ferredoxin (FD) where they are redistributed for use in carbon fixation or cyclic electron transport around PSII (Figure 5.2). The electron transport rate from PSII to PSI is dependent on the overall rate of all these processes. Potential storage efficiency of the plastoquinone (PQ) pool is given by the PQ Pool size, which is the number of plastoquinone molecules, and controls the kinetics of electron transport processes. The "SEQ_3" model, which assumes three stages of electron transport from Q_A to Q_B, from Q_B to the PQ Pool, and from the PQ Pool to PSI with time constants τ_1, τ_2 and τ_3 respectively, was fit to experimental data (Figure 5.2). The mean of 200 iterations of the fluorescence induction and relaxation protocol was used by the software to calculate photosynthetic parameters. The quality of the SEQ_3 model fit of the temporal changes in fluorescence signals emitted as a function of the changing flashlet sequence could be judged visually or by assessing the Chi-Square value. The photosynthetic parameters calculated by the instrument is summarised in Table 5.1.

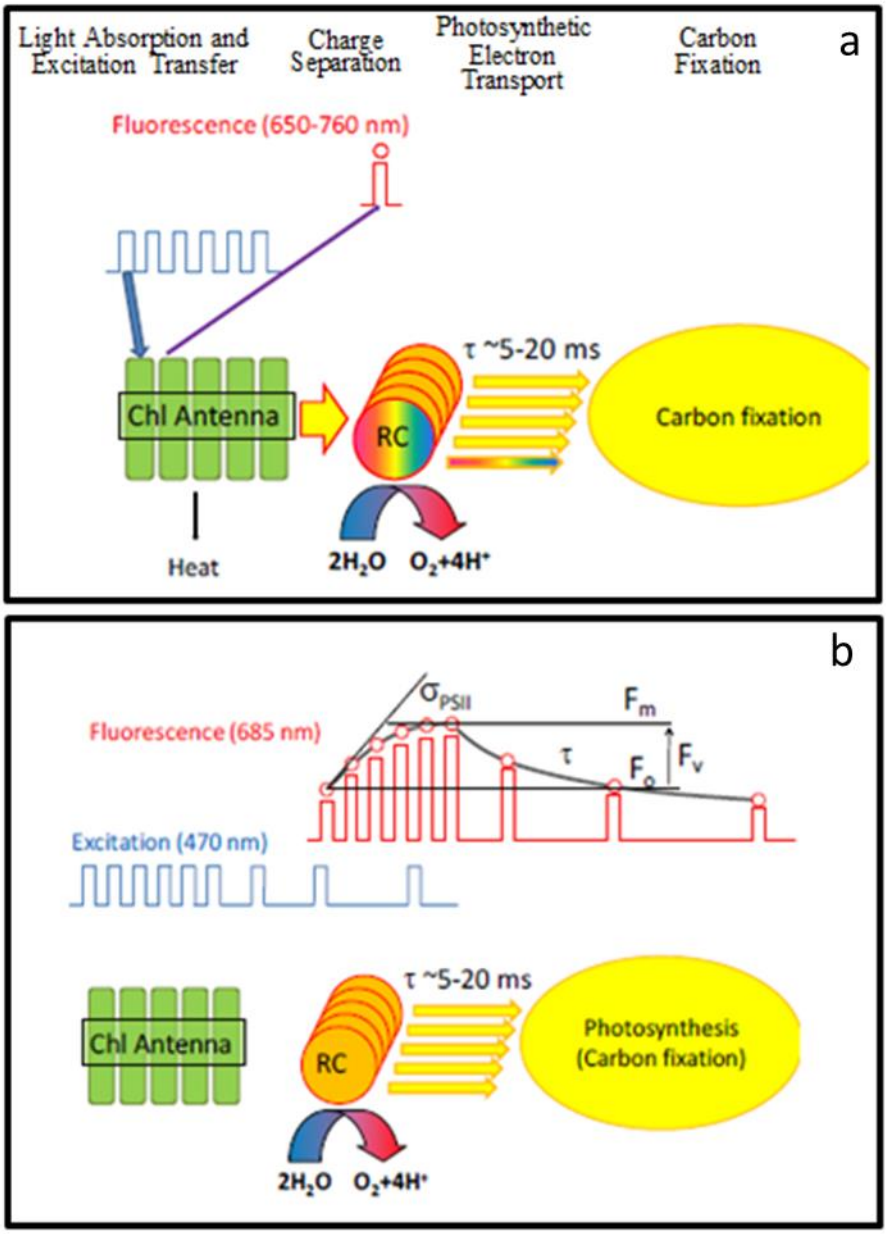

Figure 5.1: a) Excitation of PSII during FRRF and associated photosynthetic pathways b) Calculation of photosynthetic parameters from FRRF (Kolber, http://www.soliense.com/LIFT_Method.php)

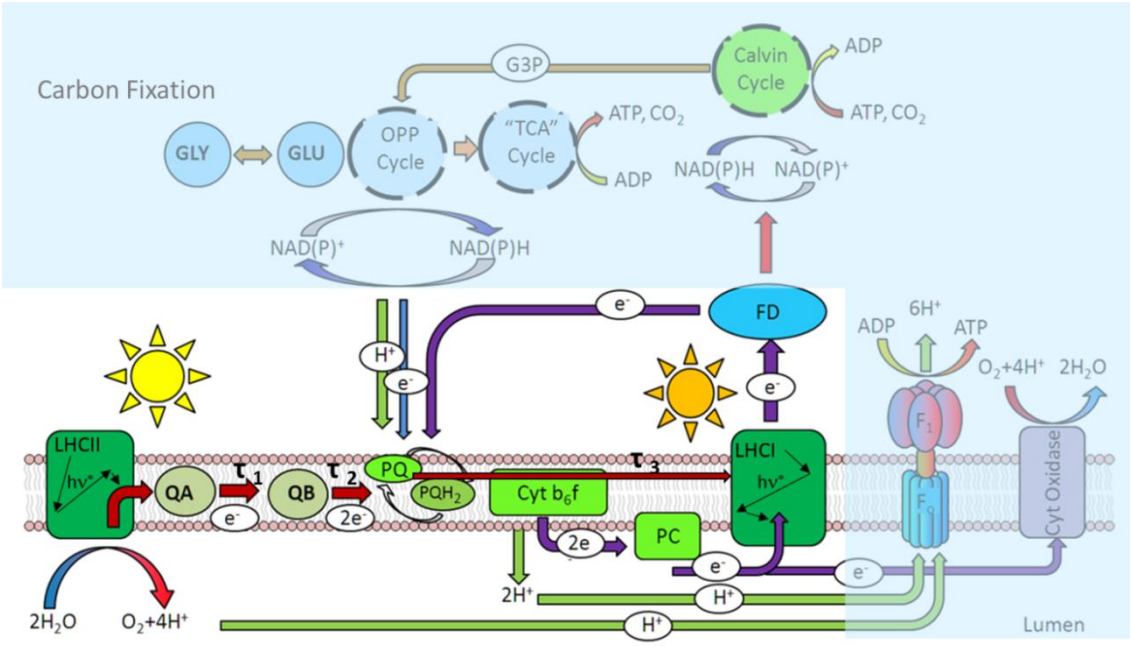

Figure 5.2: Schematic representation of with the electron transport chain from PSII to PSI (in focus/ unshaded) within the photosynthetic apparatus (Kolber; http://www.soliense.com/LIFT_Method.php)

Table 5.1: Photosynthetic parameters calculated by the LIFT-FRRF.

Parameter	Unit	Definition
F_v/F_m	-	Potential photochemical efficiency of PSII reaction centre
σ_{PSII}	$Å^2$ quantum^{-1}	Effective absorption cross section of PSII
τ_1	µs	Duration of electron transport from Q_A to Q_B
τ_2	µs	Duration of electron transport from Q_B to PQ Pool
τ_3	µs	Duration of electron transport from PQ Pool to PSI
PQ Pool size		Potential storage efficiency of the plastoquinone pool

5.2.5. Cell sizing and cell density

A Coulter Counter Multisizer 4 (Beckman) with a 100 µm aperture probe was used to measure cell diameter (µm), cell volume (fL $cell^{-1}$; fL = femtolitre = 10^{-15} L) and cell density (no. of cells per mL) of *P. antarctica*. The coulter counter was set to detect particles within the size range 2 µm and 15 µm and take 3 (technical) replicate measurements, the mean of which was used. A filtered (0.45 µm) 3.5 % sodium chloride (NaCl) solution was used to make blank measurements before every session, flush the instrument between samples, and to dilute cell cultures before measurements. For every experimental culture collected during its mid-exponential growth phase, Coulter Counter measurements were made immediately. Measurements were made without and with glutaraldehyde addition to determine the percentage of *P. antarctica* cells occurring as colonies.

*5.2.6. Cellular chlorophyll-*a *measurement*

Chlorophyll *a* concentration was determined by *in vitro* fluorometry using a Turner Designs model 10-AU fluorometer calibrated with spectrophotometrically measured spinach Chl *a* standards (Sigma-Aldrich) (Parsons et al. 1984). For Chl *a* measurements, 20 mL of culture collected during the mid-exponential growth phase, was passed through 25 mm glass fibre filters (Whatman GF/F) under low vacuum. The filters containing the cells were then stored in 15 mL centrifuge tubes at -20°C until analysis. To the centrifuge tubes, 10 mL of 90 % acetone solution was added and vortexed for 30 s to extract Chl *a* from the cells. The Chl *a* extract was then allowed to sit in dark at 3 ± 1°C for 18-24 hrs, after which it was re-vortexed to homogenise the solution. The

extract was then kept in dark for 30 min at room temperature before measurement. The extract was was measured before and after the addition of 0.5 mL of 10% HCl. Blanking of the fluorometer was done with a 90% acetone solution prior to sample analysis. Chlorophyll *a* concentration was calculated by the following equation:

$$[\text{Chl } a]\ (\mu g\ L^{-1}) = 2.117 \times 1.0188(F_O - F_A) \times (v/V) \quad \ldots (1)$$

Where, F_O is fluorescence before acidification and F_A is fluorescence after acidification; v is the volume of acetone extract (mL), V is the volume of sample filtered (mL) and 2.117 is the acid ratio correction factor.

The cell density (cells mL^{-1}) and cell volume (fL $cell^{-1}$) data obtained from Coulter were used to normalise Chl *a* concentrations per cell volume.

5.2.7. Cellular Zn isotope composition and Zn and P concentrations

For measurement of $\delta^{66}Zn$ and cellular Zn and P content, strict trace-metal clean protocols were followed. All acids used were distilled from AR Grade acid by sub-boiling distillation in a Teflon still (Savillex, USA).

About 450 mL of experimental culture in the mid-exponential growth phase was passed through trace metal clean 2 µm pore size hydrophilic polycarbonate membrane filters (Whatman Nuclepore) under a low vacuum. Cells were then rinsed twice for 5 min with 5 mL of trace metal-free SOW and transferred into a 5mL trace metal clean Teflon beaker. To oxidise the organics, the cells from the filter paper were carefully washed into the Teflon beaker with 0.5 mL of concentrated nitric acid (HNO_3), 0.5 mL of 8 mol L^{-1} HCl and 1 mL of Milli-Q water and the solution was refluxed for several

hours. 0.1 mL of this solution was then taken up in 2 (v/v) % HNO_3 to a final volume of 1 mL for cellular Zn and P concentration measurements. The remaining 1.9 mL of the solution was used for Zn isotope measurements by Multi-Collector Inductively Coupled Plasma Mass Spectrometry (MC-ICPMS; Thermo Scientific Neptune Plus) utilising a ^{67}Zn-^{68}Zn Double Spike (DS). Once the concentration of Zn in the 1.9 mL solution was known, ^{67}Zn-^{68}Zn DS was added such that the DS to sample Zn concentration ratio was 4:1. The sample-DS solution was then dried and taken up in 0.5 mL of distilled 0.5 mol L^{-1} HCl for purification and isolation of Zn by anion exchange chromatography. For this purpose, 0.15 mL of AG1X8 resin was used. The resin was pre-cleaned (using 0.5 mol L^{-1} HNO_3 followed by Milli-Q water rinse) and pre-conditioned (with 0.5 mol L^{-1} HCl) before loading of solution. Once the solution was loaded onto the Teflon columns containing the AG1X8 resin, 3 mL of 0.5 mol L^{-1} HCl was passed to remove potentially interfering elements. Zinc was eluted with 2.5 mL of 0.5 mol L^{-1} HNO_3 into another trace metal clean Teflon beaker. The solution was dried and taken up in an appropriate volume of 2% HNO_3 for measurement of $\delta^{66}Zn$.

5.2.7.1. Cellular Zn and P concentrations

The Neptune Plus at the Research School of Earth Sciences (RSES), The Australian National University (ANU), was used as a single collector for measurement of P and Zn concentration. The instrument was operated in medium resolution mode with a standard Ni sampler cone and a Ni X-skimmer cone. Samples were introduced into the MC-ICPMS via a desolvating system consisting of a quartz flow path (Apex IR, Elemental Scientific Inc.) and a Teflon micro-flow nebuliser (Elemental Scientific Inc.)

operated at an uptake rate of 50 µL per minute. Intensities were measured on the peak centre of the mass scan for ^{66}Zn followed by measurement of intensity on mass 30.958 for ^{31}P to avoid measuring on interferences in the peak from doubly charged ions and polyatomic species. For each sample, a mass scan was monitored between masses 65.84 to 66.02 for ^{66}Zn and 30.93 to 31.01 for ^{31}P to ensure intensities were measured at the correct masses. Measurement on each mass was done as one block of 15 cycles with 2 sec integration time. Interferences observed in medium resolution on ^{31}P was potentially from ^{14}N-^{16}O-^{1}H. Other potential interferences are $^{62}Ni^{++}$and ^{15}N-^{16}O on ^{31}P. Five calibration standards were made from Zn and P concentration standards with Zn to P ratios of 2:20, 5:50, 10:100, 50:500 and 100:1000 (ng mL^{-1}: ng mL^{-1}); and were measured at the beginning of the session. Blank measurement was done on 2% HNO_3. A 'low' standard (containing 2 ng mL^{-1} of Zn and 250 ng mL^{-1} P) and 'high' standard (containing 20 ng mL^{-1} Zn and 1000 ng mL^{-1} P) was measured between every 3 and 6 samples to check instrument drift. Zinc and P concentrations of samples were calculated by comparing the measured intensities of the samples with the intensities of measured standards. Between each sample measurement the probe was cleaned with a 2% HNO_3 wash.

The specific cellular Zn uptake rate was calculated by multiplying the specific growth rate by the cellular Zn:P ratio of the cultures. The number of cells per mL and cell volume data obtained from Coulter counter was used to normalise metal concentrations per cell and per cell volume for each treatment. Elemental incorporation rates were obtained by multiplying the cell volume normalised elemental content and the specific growth rate of the culture.

5.2.7.2. Cellular Zn isotope composition

Zinc isotope measurements were made using the Multicollector-ICPMS (Thermo Scientific Neptune Plus) along with a desolvating sample introduction system (Apex IR, Elemental Scientific Inc.) with an uptake rate of ~ 50 µL per minute. A standard Ni sampler cone and a Ni X-skimmer cone were used to enhance instrument sensitivity. The instrument was operated in low resolution mode and samples were analysed in groups of three, bracketed with a standard-DS mixture. A 2% (v/v) HNO_3 wash was introduced between sample and standards, and blank measurements were made on 2% HNO_3 solution before every sample and standard measurements. All measurements were made as 1 block of 30 cycles with a 4 second integration time. At the start of each measurement session, the instrument was tuned for intensities on mass ^{62}Ni, ^{63}Cu, ^{65}Cu, ^{64}Zn, ^{66}Zn, ^{67}Zn and ^{68}Zn. The procedures, materials and reagents used and instrumental parameters employed in this work have been described in detail in Chapters 2 and 4.

The Zn isotopic composition was expressed in delta notation following the equation:

$$\delta^{66}\mathrm{Zn} = \left(\frac{{}^{66}\mathrm{Zn}/{}^{64}\mathrm{Zn}_{\mathrm{sample}}}{{}^{66}\mathrm{Zn}/{}^{64}\mathrm{Zn}_{\mathrm{standard}}} - 1 \right) \times 1000 \quad \ldots (2)$$

All Zn isotopes in the study were measured relative to the standard reference material IRMM-3702. The isotopic composition of the Zn added to Aquil was 0.06 ± 0.01 (± 2 SD) ‰. Since the standard deviation of the isotopic composition between the replicates of a treatment was more than 0.06 ‰, no correction was made on the $\delta^{66}Zn$ measurement and values reported here are with respect to the Zn standard IRMM-3702. The error bars reported for a treatment represent the standard deviation of three culture (biological) replicates.

5.3. Results and Discussion

The effects of Fe and Zn concentration on *P. antarctica*'s growth rates, cell size, Chl *a* concentration, photophysiological parameters, Zn:P ratio and Zn isotope fractionation are detailed in this section. Results are reported as ± SD of the three biological replicates of each treatment. Significant results are reported at the 95% confidence level ($p < 0.05$) calculated using a two-tailed t-test assuming unequal variances (Microsoft Excel, 2010 version).

5.3.1. Effect of Fe and Zn limitation on growth rates and cell morphology

5.3.1.1. Growth rates

The maximum specific growth rate (μ_{max}) observed under trace metal replete conditions at 3 ± 1 °C under a continuous irradiance of 60-70 µmol quanta m^{-2} s^{-1}, was 0.43 ± 0.02 d^{-1}. Growth rates were significantly reduced ($p < 0.001$) under both Fe and Zn limitation (Figure 5.3, Table 5.2). Under Fe limiting conditions, μ was 0.20 ± 0.03 d^{-1} and the ratio of the Fe-limited and Fe replete growth rates (μ_{-Fe}: μ_{max}) was 0.48 (Figure 5.3, Table 5.2). These results are comparable to those reported in other studies under similar conditions (Strzepek et al. 2012; Strzepek et al. 2011). Similarly, the specific growth rates of Fe replete cultures grown under Zn replete (μ_{max}) and Zn limiting (μ_{-Zn} = 0.26 ± 0.01 d^{-1}) conditions are comparable to those reported under similar conditions for a different strain of *P. antarctica* (strain CCMP 1871) (Saito and Goepfert 2008). Under Fe and Zn co-limiting condition, the growth rate of *P. antarctica* was reduced ($\mu_{-Fe,-Zn}$ = 0.17 ± 0.01 d^{-1}) to ~40% of its maximum growth rate ($\mu_{-Fe,-Zn}$: μ_{max} = 0.39).

These results show that low concentrations of both bio-available Fe and Zn could potentially limit the growth of the Southern Ocean phytoplankton species *P. antarctica*.

Table 5.2: The specific growth rates (μ; d^{-1}) of *P. antarctica* grown under high and low Fe and Zn conditions. μ_{max} is the maximum specific growth rate observed under trace metal replete conditions. Error bars represent 1 SD of the triplicate cultures.

	+Fe +Zn	+Fe -Zn	-Fe +Zn	-Fe -Zn
μ	0.43 ± 0.02	0.26 ± 0.01	0.20 ± 0.03	0.17 ± 0.01
$\mu:\mu_{max}$	1	0.61	0.48	0.39

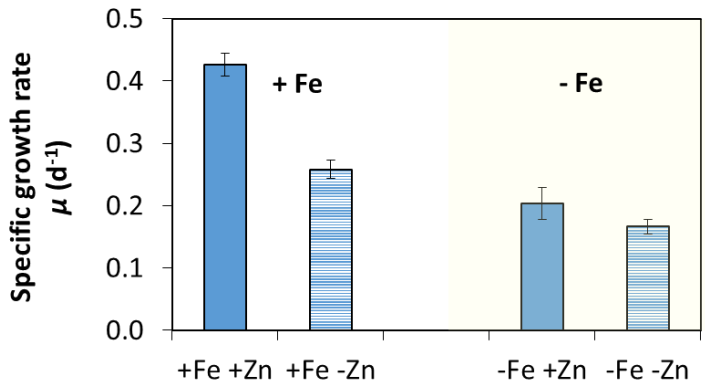

Figure 5.3: Variation in specific growth rates of *P. antarctica* grown under high and low Fe and Zn conditions. Error bars represent 1x SD of triplicates cultures.

5.3.1.2. Cell morphology

Phaeocystis antarctica mostly occurred as solitary cells in all the treatments. This could be due to *P. antarctica* (clone SX9) losing its capability of forming colonies since it has been in culture for more than 10 years. *P. antarctica* (clone AA1) reportedly stopped forming colonies after being in culture for 3 years (Strzepek et al. 2011). In the Fe replete- Zn limiting treatment, 97 % of the cells were solitary whereas for the other treatments the proportion of solitary cells ranged between 90 % and 93 % (Table 5.3).

Under Zn limitation, there was no change in cell size under Fe replete condition and a small increase ($p = 0.058$) under Fe-limiting condition (Figure 5.4 and Table 5.3). Under Fe limitation, the cell diameter decreased and hence the surface area to volume of *P. antarctica* cells increased in both Zn replete and limiting conditions (Figure 5.4 and Table 5.3). These changes in cell size were significant under Zn replete condition ($p< 0.01$) but insignificant under Zn limiting condition ($p=0.1$). The decrease in cell diameter under Fe limitation could be an adaptive strategy employed to increase the cell surface area for Fe supply relative to cell volume, which is proportional to cellular Fe demand (Sunda and Huntsman 1995b). These results are similar to previous reports of a significant decrease in the cell size of *P. antarctica* under Fe limitation (Strzepek et al. 2012; Strzepek et al. 2011).

There was a significant (2.5 to 4 times) decrease in cellular biomass (cell yields were calculated by multiplying cell volume with the number of cells per mL at late exponential phase) under Fe limiting conditions (Figure 5.5), thus highlighting the potential importance of Fe as a "bottom-up" control on atmospheric CO_2 assimilation by Southern Ocean phytoplankton.

Table 5.3: Effect of Fe and Zn limitation on cell morphology of *P. antarctica*

	+Fe +Zn	+Fe -Zn	-Fe +Zn	-Fe -Zn
Cell diameter (µm)	4.14 ± 0.08	4.15 ± 0.13	3.77 ± 0.10	3.96 ± 0.05
Cell volume (fL cell^{-1})	37.16 ± 2.26	37.61 ± 3.68	28.08 ± 2.22	32.56 ± 1.26
Surface area/ volume (µm^{-1})	1.45 ± 0.03	1.45 ± 0.05	1.59 ± 0.04	1.51 ± 0.02
Ratio of Single cells: Colonial cells	0.90 ± 0.05	0.97± 0.02	0.93 ± 0.03	0.90 ± 0.03

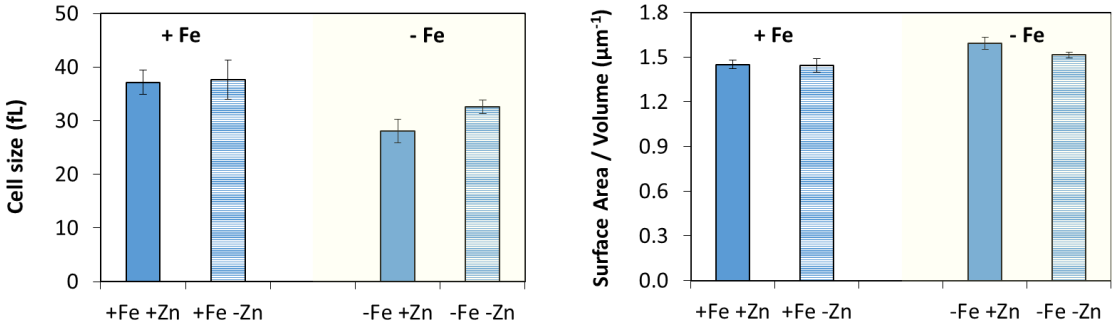

Figure 5.4: Variation in (a) cell size and (b) surface area/volume of *P. antarctica* grown under high and low Fe and Zn conditions. Error bars represent 1x SD of triplicates treatments.

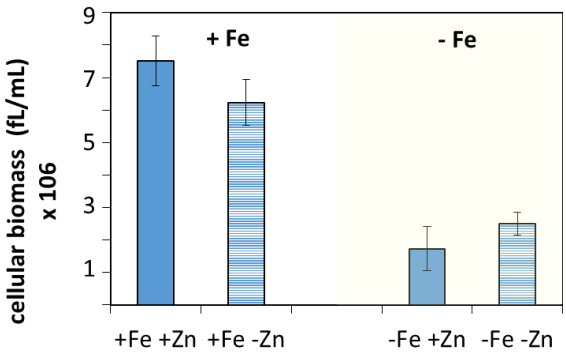

Figure 5.5: Variation in cellular biomass (obtained by multiplying cell volume with no. of cells per mL) of *P. antarctica* grown under high and low Fe and Zn conditions. Error bars represent 1x SD of triplicates treatments.

5.3.2. Effect of Fe and Zn limitation on photophysiological responses and cellular Chl a *concentrations*

Under Fe limitation, there was a significant decrease ($p < 0.05$) in photosynthetic efficiency (F_v/F_m; Table 5.4). F_v/F_m, which is widely used as an algal health indicator, was 0.45 ± 0.04 under trace metal replete conditions whereas under Fe limiting but Zn replete conditions it was 0.34 ± 0.03 (Figure 5.6a). The time taken for transport of electron from Q_A to Q_B, ($\tau1$) and from Q_B to the PQ Pool, ($\tau2$) increased under Fe limitation (Figure 5.6 c and d). However, a complex array of responses was observed in F_v/F_m, $\tau1$ and $\tau2$ under Zn limiting conditions. Under Fe replete conditions, the F_v/F_m increased, $\tau1$ and $\tau2$ increased or remained largely unchanged under Zn limitation. However, under Fe and Zn co-limiting condition, F_v/F_m decreased but $\tau1$ and $\tau2$ increased compared to Zn replete- Fe limiting condition. The functional absorption cross section, σ_{PSII}, decreased under Fe limitation, whereas under Zn limitation, σ_{PSII} increased (Figure 5.6b). The decrease in σ_{PSII} under Fe limitation observed here differs from previous studies on Southern Ocean phytoplankton, including *P. antarctica* (e.g. (Strzepek et al. 2012). The increase in σ_{PSII} relates to an increased potential for photon capture and transfer to RCII and has been interpreted as a stress response. The reason that σ_{PSII} increased under Zn but not Fe limitation is not known. The PQ Pool size remained largely unchanged under both Fe and Zn limitation.

There was only a small decrease in Chl *a* (both per cell and per cell volume) under Fe limitation. However, there was significant decrease ($p> 0.05$) in Chl *a* (both per cell and per cell volume) of Fe replete, Zn-limited *P. antarctica* cells (Figure 5.7, Table 5.4). It is interesting to note that while F_v/F_m increased for *P. antarctica*, it decreased for a

Tasman Sea isolate of the cosmopolitan (found everywhere except in the polar oceans) pico-haptophyte *E. huxleyi,* under Fe replete and Zn limiting conditions (see Chapter 4). However, these changes were small. While the growth rates, which provide an integrated response of phytoplankton to the environmental conditions, decreased significantly under Zn limitation for *P. antarctica,* whereas those of *E. huxleyi* remained largely unchanged under similar conditions.

A decrease in F_v/F_m and cell volume normalised Chl *a*, and a increase in σ_{PSII} under Fe limitation, have been previously reported for *P. antarctica* (Strzepek et al. 2012). Apart from σ_{PSII}, the results reported here largely agree with previous studies. Iron (in Fe-proteins like cytochromes, ferredoxin and other Fe-S proteins) is essential for photosynthetic electron transport (Raven et al. 1999), thus it is not surprising that Fe limitation significantly influences the photophysiological parameters, such as decreasing photosynthetic efficiency. The decreased F_v/F_m observed in our experiment under Fe limitation is consistent with field data where increased photosynthetic competency (F_v/F_m) with artificial Fe enrichment has been reported in the HNLC regions of the Southern Ocean (Boyd et al. 2000; Coale et al. 2004). However, the role of Zn in photophysiology of phytoplankton is unclear and needs further assessment.

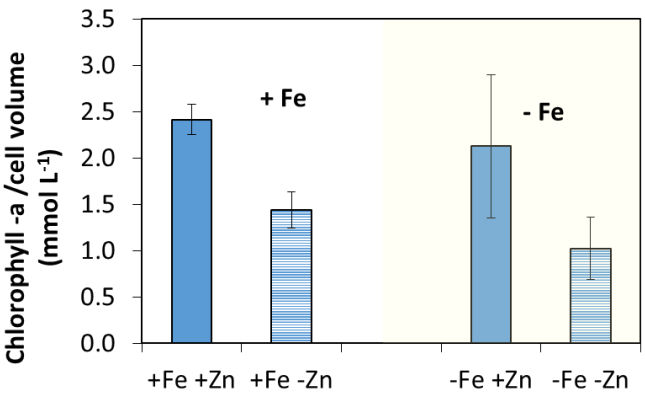

Figure 5.7: Variation in cellular chlorophyll a concentration (normalised to cell volume) of *P. antarctica* grown under high and low Fe and Zn conditions. Error bars represent 1 SD of triplicates treatments.

Table 5.4. Effect of Fe and Zn limitation on cellular chlorophyll *a* concentrations and photophysiological parameters of *P. antarctica.*

	+Fe +Zn	+Fe -Zn	-Fe +Zn	-Fe -Zn
Chl *a*/ cell (fg cell^{-1})	80 ± 10	48 ± 7	54 ± 24	29 ± 9
Chl *a*/ cell vol (mmol L^{-1})	2.41 ± 0.17	1.44 ± 0.19	2.12 ± 0.78	1.02 ± 0.34
F_v/F_m	0.45 ± 0.04	0.49 ± 0.02	0.34 ± 0.03	0.32 ± 0.02
τ1 (µs)	3909 ± 927	4105 ± 1224	7252 ± 1306	6318 ± 1243
τ2 (µs)	7818 ± 1855	8210 ± 2448	14504 ± 2612	12635 ± 2486
σ_{PSII} (Å^2 quantum^{-1})	578 ± 57	612 ± 48	444 ± 94	497 ± 59
PQ Pool size	23 ± 2	20 ± 6	24 ± 1	22 ± 4

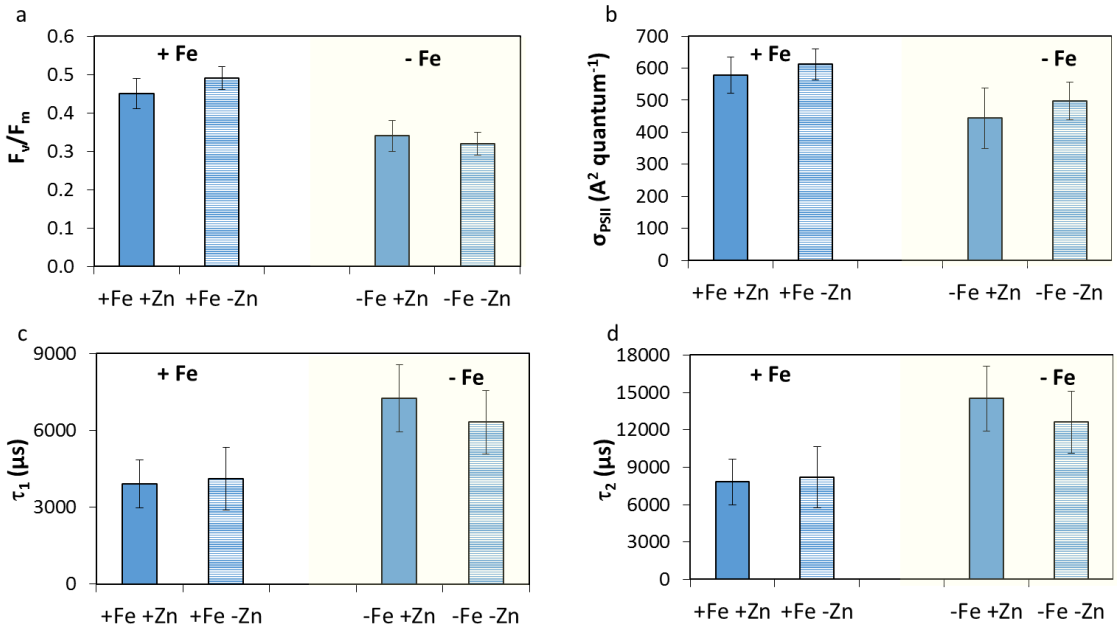

Figure 5.6: Variation in (a) F_v/F_m, (b) σ_{PSII}, (c) τ_1 and (d) τ_2 of *P. antarctica* grown under high and low Fe and Zn conditions. Error bars represent 1 SD of triplicates treatments.

5.3.3. Effect of Fe and Zn limitation on the Zn:P ratio and Zn isotope fractionation

5.3.3.1. Zn:P ratio

The Zn:P ratio increased significantly for *P. antarctica* under Fe limitation (Figure 5.8). This effect of increased Zn:P ratio observed in *P. antarctica* under Fe limitation could be due to "growth rate dilution"; whereby, under Fe limitation there is reduction in growth rate and decrease in P uptake whilst maintaining the rate of Zn uptake (Cullen et al. 2003; Sunda and Huntsman 2000). Indeed, at ambient Zn concentrations, the P incorporation rate (obtained by multiplying the cell normalised P content and the specific growth rate of the culture) decreased significantly (~ 100-fold) under Fe limitation whereas the Zn incorporation rate remained largely the same (Table 5.5). Under Zn limitation, the P incorporation rate doubled under Fe replete condition and remained unchanged under Zn-Fe co-limiting condition relative to trace metal replete conditions (Table 5.5). However, the Zn incorporation rate of *P. antarctica* under Zn-Fe co-limiting condition was significantly greater (> 5 times) than Zn limiting-Fe replete conditions. This resulted in increased specific Zn uptake rate (obtained by multiplying the Zn:P ratio and the specific growth rate of the culture) of *P. antarctica* under Zn-Fe colimiting condition relative to Zn limited-Fe replete condition. At Zn replete conditions, the specific Zn uptake rate remained largely unchanged under Fe limitation (Table 5.5). It is also interesting to note that under comparable free Zn^{2+} ion concentrations, the Zn:P ratio of the Southern Ocean pico-haptophyte *P. antarctica* were similar to that of the Tasman Sea isolate of the coccolithophore *E. huxleyi* (Figure 5.8a; see Chapter 4).

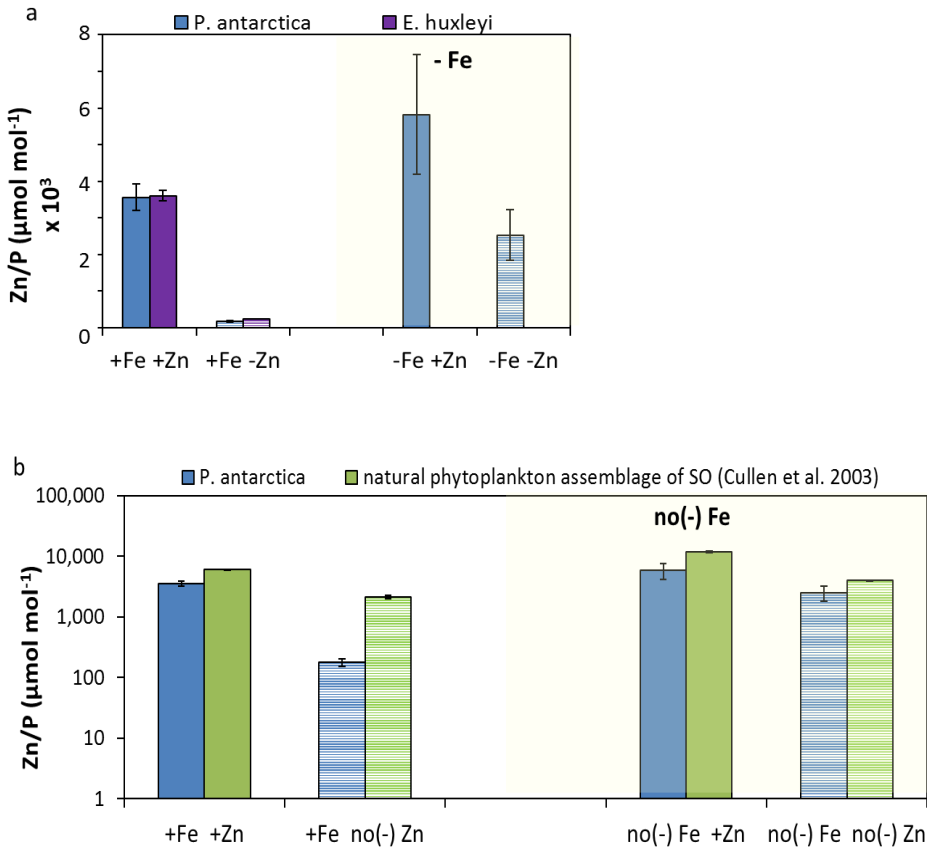

Figure 5.8: Variation in cellular Zn normalised to P content in *P. antarctica* grown under high (+) and low (-), Fe and Zn conditions. Error bars represent 1x SD of triplicates treatments. (a)The Zn:P content of coccolithophore *E. huxleyi* under similar trace metal conditions is shown for comparison. b) Variation in the Zn:P of natural phytoplankton assemblage (no Fe, no Zn) of the Southern Ocean with added (+) Fe and (+) Zn ; (data from (Cullen et al. 2003)

Table 5.5: Effect of Fe and Zn limitation on cellular Zn and P incorporation of *P. antarctica.*

	+Fe +Zn	+Fe –Zn	-Fe +Zn	-Fe -Zn
Zn incorporation rate (µmol cell^{-1} day^{-1}) x 10^{-13}	27.5 ± 2.6	1.6 ± 0.2	24.0 ± 7.9	10.3 ± 2.3
P incorporation rate (µmol cell^{-1} day^{-1}) x 10^{-11}	36.6 ± 5.6	88.4 ± 17.5	0.4 ± 0.2	41.0 ± 8.6
Zn:P (µmol mol^{-1})	3560 ± 364	179 ± 26	5825 ± 1630	2528 ± 695
Zn uptake rate (µmol (mol P)$^{-1}$ day^{-1})	1520 ± 204	46 ± 9	1210 ± 480	421 ± 118

5.3.3.1.i. Comparison with Zn:P ratio of natural phytoplankton assemblages in the Southern Ocean and implications

In a study reporting the effect of Fe additions in incubation experiments with natural phytoplankton assemblages in the Antarctic Zone of Southern Ocean, where large diatoms dominated the biomass with an estimated initial community growth rate of 0.11 d^{-1}, the greatest growth response to Fe addition was for the haptophyte group *Phaeocystis* (0.45 d^{-1}) followed by diatom groups (Cullen et al. 2003). In the same study it was reported that both particulate P and Zn concentrations increased with Fe addition however the Zn:P ratio decreased systematically with increasing Fe concentrations (Cullen et al. 2003). Though this field study cannot be directly compared to our laboratory results due to methodological differences, it is interesting to note the similarities. The maximum growth rate observed in the assemblage after addition of trace metals for *P. antarctica* is comparable to the maximum growth rate observed in this study under trace metal replete condition. The effect of Zn and Fe addition on the Zn:P ratio of the assemblage was also very similar to what was observed in this study for *P. antarctica* (Figure 5.8b). When Zn was added to the natural community without the addition of Fe, the Zn:P ratio of the phytoplankton assemblage was higher relative to control and all other Fe and Zn additions. Upon the addition of Fe, the Zn:P ratio of the phytoplankton assemblage was significantly reduced. However, when Fe and Zn were added together, the Zn:P ratio was significantly higher than when no Zn was added but lower than the control (Cullen et al. 2003). These results suggest that changes in the bioavailability of Fe influences Zn and P removal from the biologically active surface waters. Under Fe limiting conditions, Zn is removed relative to P, whilst under Fe replete conditions, less Zn is removed

relative to P. Thus, these results further validate the hypothesis that in the Fe depleted waters of the Southern Ocean, Zn would be depleted relative to P (Cullen et al. 2003; Ellwood 2008; Sunda and Huntsman 2000; Vance et al. 2017). However, this hypothesis posits that diatoms are primarily responsible for the low Zn:P ratio in the surface waters under Fe limiting conditions. This study shows that the haptophyte *P. antarctica*, among the most abundant species in the Southern Ocean, could also play a significant role in removing Zn from the Fe depleted surface waters.

5.3.3.2. Zn isotope fractionation

The Zn isotope composition ($\Delta^{66}Zn_{cells\text{-}media}$) within the cells of *P. antarctica* was lighter relative to the media, under Fe replete condition [= -0.21 $\pm$ 0.07 ‰(+Zn); -1.64 $\pm$ 0.35 ‰ (-Zn)]. Whereas under Fe limitation, the $\Delta^{66}Zn_{cells\text{-}media}$ was heavier [= 0.49 $\pm$ 0.29 ‰ (+Zn); 0.36 $\pm$ 0.25 ‰ (-Zn)], suggesting that more of the heavier isotope of Zn was taken up under Fe limiting conditions (Figure 5.9). Lighter Zn isotope compositions within phytoplankton cells, $\Delta^{66}Zn_{cells\text{-}media}$, have been reported in previous studies and were attributed to either one or a combination of the following reasons: (i) lighter Zn being more readily bioavailable due to preferential binding of heavier Zn by strong organic ligands present in seawater (or synthetic ligand EDTA in case of culture work); (ii) the preferential retention of the heavier Zn isotopes at the Zn transport binding site(s) within the cell membrane; and (iii) faster diffusion of lighter Zn through cellular ion channels resulting in lighter cellular Zn isotope composition (See chapter 4, (John et al. 2007)).

Köbberich and Vance (2017), reported heavier $\delta^{66}Zn$ within the cells relative to the culture media for the diatom species *Chaetoceros* at Fe' concentration < 20 pmol L^{-1}. The $\Delta^{66}Zn_{cell\text{-}media}$ got heavier with decreasing Fe' concentrations. To explain this observation, one hypothesis put forward by Köbberich and Vance (2017), is scavenging of heavy Zn by extracellular polymeric substances. Heavy $\Delta^{66}Zn_{cells\text{-}media}$ has also been reported during adsorption of Zn on cell surfaces and co-precipitation of Zn with Fe oxy-hydroxides when cultures are grown at very high total Fe concentrations (Fe' > 700 pmol L^{-1}) (Gelabert et al. 2006; John and Conway 2014; John et al. 2007; Köbberich and Vance 2017; Tang and Morel 2006). The free metal ion concentrations of Zn, Cu, Mn, Ni and Co in this study were maintained by complexation with EDTA, except for the Fe limited treatments where Fe was mainly complexed to DFB. Quantum mechanical calculations suggest that heavier isotopes tend to form stronger bonds with ligands than their light isotope counterparts (Criss 1999). It has been reported that EDTA, being a strong ligand, preferentially binds heavier isotope of Zn leaving the biologically available Zn isotopically light (Ban et al. 2002). However, there is limited knowledge of Zn isotope fractionation associated with Zn-DFB complexation. It has been suggested that phytoplankton may be able to take up Zn directly from Zn-DFB complex via formation of a ternary complexes with Zn uptake ligands (Xu et al. 2012). The effect of DFB on Zn isotope fractionation in presence of the strong ligand EDTA was not determined during this study. However, the concentrations of DFB used in this study were at least 500 times less than the concentrations of EDTA used and the estimated stability constant of Zn-DFB complex (9.55 - 10.36) is much lower than that of Zn-EDTA complex (16.5) (Farkas et al. 1997; Hernlem et al. 1996). Thus, we can assume that the isotopic composition of bioavailable Zn in the media would be the

same at fixed concentrations of total Zn and EDTA in the presence of DFB. One possible explanation for the heavier Zn isotope composition within *P. antarctica* observed under Fe limiting condition is internalisation of heavy Zn bound to broad affinity cell surface ligands/transporter. The active uptake of Zn under Fe limiting condition is also suggested by the increased Zn uptake and internalisation rate under Fe-Zn co-limiting condition relative to Fe replete - Zn limiting condition. The increased Zn:P ratio under Fe limitation could thus be a consequence of *P. antarctica* upregulating Fe uptake under Fe-limiting condition. It has been reported that for Fe:DFB complexes, Fe uptake rates in *P. antarctica* exceed the diffusive flux of equilibrium concentrations of Fe' and that Fe uptake by *P. antarctica* apparently involves extracellular reduction of Fe(III) to Fe(II) (Strzepek et al. 2011). Strzepek et al. (2011) showed that the "excess" results from upregulation of both Fe uptake by *P. antarctica* and the reduction of Fe(III) to Fe(II) under Fe limiting conditions. They also found that the Fe uptake mechanism was not ligand specific (Strzepek et al. 2011). The results for *P. antarctica* were comparable to those for the diatom *Thalassiosira oceanica*, which was also cultured under Fe-limiting conditions. It was suggested that Fe-DFB (rather than Fe') was the substrate for the Fe transport system in diatoms and that Fe transport was preceded by cell surface mediated reduction of extracellular Fe (Maldonado and Price 2001; Shaked et al. 2005). Based on the observations for *P. antarctica* and *T. oceanica*, we would argue that under Fe limiting conditions the number of Fe^{2+} transporters on the cell surface is upregulated. These transporters preferentially bind divalent Fe, but might also bind and take up divalent Zn (Lane et al. 2009). If Zn is taken up via a divalent Fe transporter system, then this should lead to a heavy Zn isotope uptake signal as the transport should preferentially bind heavy Zn. This should result in the internalisation of heavier

Zn under Fe limiting conditions as observed for *P. antarctica.* This explanation is similar to that put forward by Köbberich and Vance (2017) where they speculate release of surface bound organics to scavenge Fe at low Fe' concentration is responsible for scavenging of heavy Zn. As the Fe' concentration decreases, more of these organics are released, resulting in heavier $\Delta^{66}Zn_{cell\text{-}media}$ ((Köbberich and Vance 2017). Alternate hypothesis presented by Köbberich and Vance (2017) is, slow Zn uptake rate leads to pseudo-equilibrium conditions at the transporter site where more stable surface complexes are formed with heavy Zn isotopes resulting in heavier $\delta^{66}Zn$ within the cells. However, for *P. antarctica,* the Zn uptake rate remained the same at Fe limiting condition. Thus, this explanation could not be applied in this study.

Another possible explanation for the heavy Zn isotope composition of *P. antarctica* under Fe limiting condition is the release of light Zn from the cells. The cultures in this study were harvested in the mid- to late-exponential phase. At this stage, some organic matter may re-mineralise, especially as cells senesce. Additionally, (John and Conway 2014) demonstrated in a culture experiment employing the diatom *Dunalliela tertiolecta,* that heavier Zn adsorb to the degrading culture. However, for this experiment, *D. tertiolecta* cells at the end of log phase were resuspended in artificial seawater media which was free from EDTA, metal and nutrients and hence cannot be compared to our experiment where EDTA in the media would compete for heavy Zn. In a companion study, it was observed that when *P. antarctica* was harvested very early in exponential phase the Zn:P ratios at comparable Fe' concentrations were 10 times higher than reported here (Robin Grün Honours Thesis 2016; Figure 5.10a). Grün also reported lighter Zn isotope composition within the cells relative to the culture media even at very low Fe' concentration (Figure 5.10b). Comparing the results of this study

and that of (Grün 2016), we suggest that Zn is regenerated at a faster rate than P as cells start degrading during late exponential/stationary phase of growth. This results in a lower Zn:P ratio for the bulk population as Zn is regenerated from these cells (Figure 5.11). However, Zn that is released from the degrading phytoplankton has a lighter isotope composition relative to the total Zn within the phytoplankton cell. This implies that in the open ocean at the initial phase of the bloom there would be high Zn:P ratio with lighter Zn isotope composition within the cells. Whilst, later in the bloom the particulate Zn:P ratio would lower with an increase in δ^{66}Zn value due to decaying of organic matter and release of isotopically lighter Zn. Thus, the Zn:P ratio and δ^{66}Zn composition of both the natural phytoplankton assemblage of the Southern Ocean and the dissolved Zn would be dependent on the sampling period.

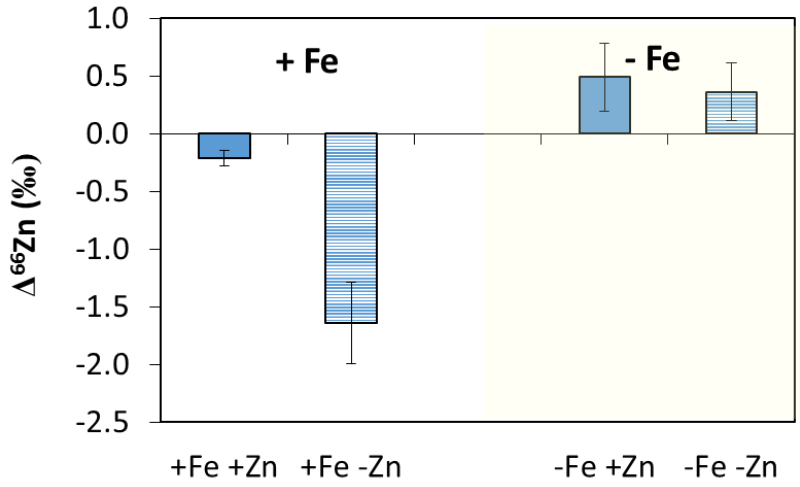

Figure 5.9: Zinc isotope fractionation by *P. antarctica* grown under high and low Fe and Zn conditions. Error bars represent 1 SD of triplicates treatments.

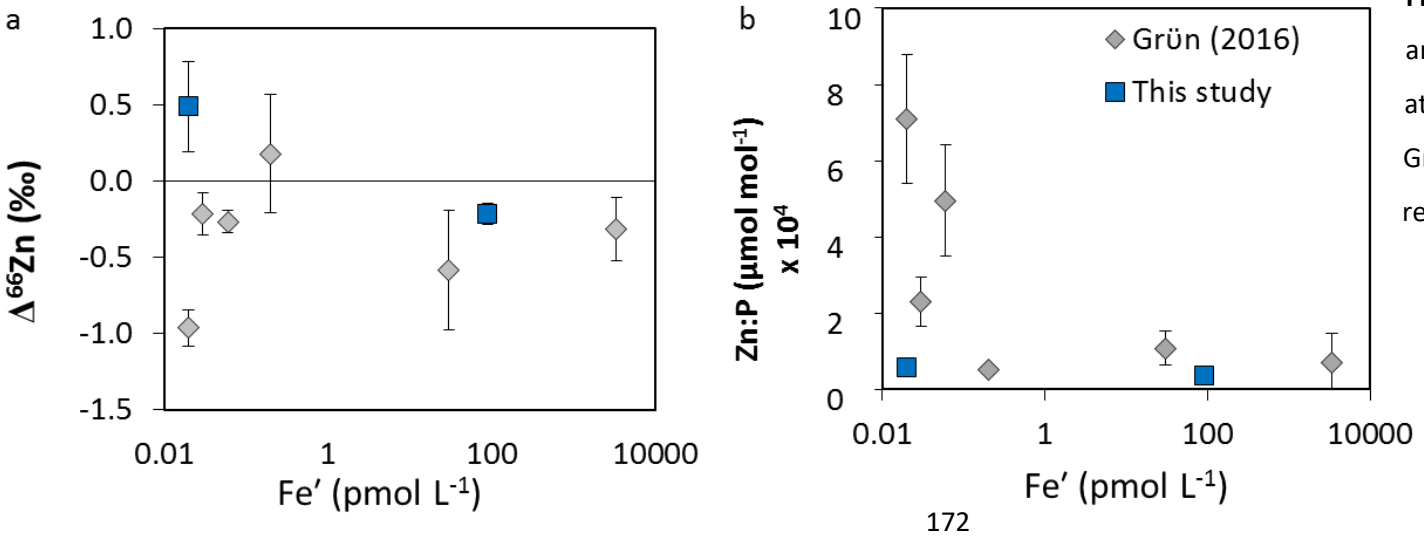

Figure 5.10: (a) Zinc isotope fractionation and (b) Zn:P ratio of *P. antarctica* cultured at a range of Fe' concentrations (data from Grün, 2016). Error bars represent 1SD of replicate treatments.

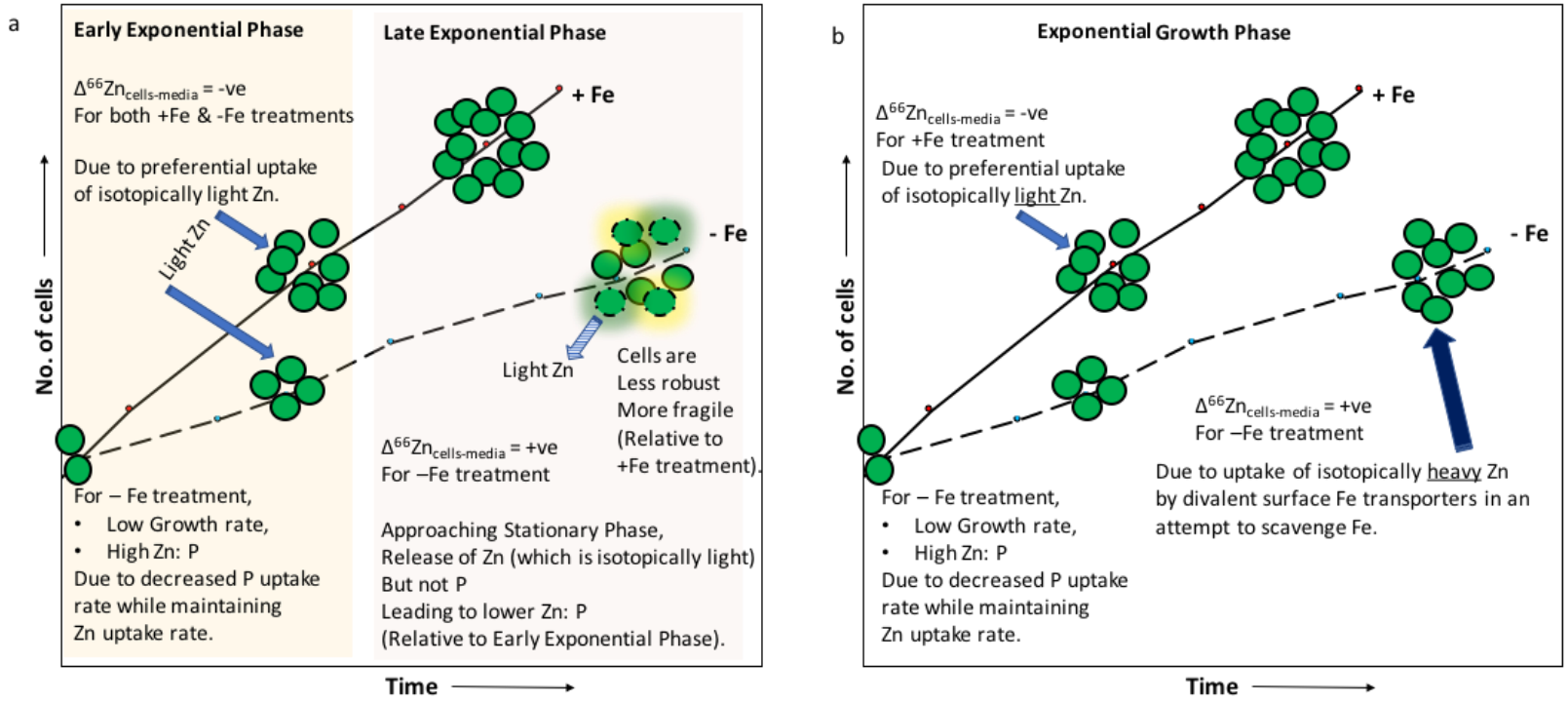

Figure 5.11: Schematic diagrams of alternate hypothesis hypothesis for observed heavy Zn isotopic composition of *P. antarctica* under Fe limiting (-Fe) conditions. (a) Release of isotopically light Zn in the late-exponential phase of growth in the Fe limited treatments due to cells being less robust than Fe replete (+Fe) treatments. This also leads to lower Zn:P ratio in the late-exponential phase relative to the early-exponential phase as Zn is lost but not P. However, the Zn:P ratio is still greater than the Fe replete treatments due to decreased P uptake rate with decreased growth rate under Fe limiting conditions. (b) Uptake of isotopically heavy Zn by divalent surface Fe transporters in an attempt to scavenge Fe under Fe limiting conditions. In both senarios (a and b), lighter isotope of Zn is taken up by the cells in the Fe replete treatments.

Based on our observations and those of Strzepek et al. (2011) and Grün (2016), we can speculate that in the Southern Ocean, where phytoplankton growth is controlled mainly by Fe availability, a dominance of *P. antarctica* in the phytoplankton community may result in lighter isotope composition of dissolved Zn (δ^{66}Zn) under Fe limiting condition. While in the initial phases of the bloom and under Fe replete conditions the dissolved δ^{66}Zn composition of the surface waters would be heavier. The δ^{66}Zn composition in surface waters of the Southern Ocean could therefore potentially be driven by Fe availability.

The processes that influence the biogeochemical composition of surface waters of the Southern Ocean are reflected in other parts of the global ocean via water masses originating in this region. These water masses include SAMW, AAIW and the AABW formed in SAZ, PFZ and near the Antarctic continental ice shelf of the Southern Ocean respectively. Thus, the δ^{66}Zn composition of global water masses influenced by SAMW, AAIW and AABW of Southern Ocean origin might in turn be affected by the δ^{66}Zn composition of surface waters in the formation region of these water masses in the Southern Ocean.

The results from this study could potentially explain the variability observed in δ^{66}Zn composition of SAMW and AAIW in the Tasman Sea (Figure 5.12; see Chapter 3). The δ^{66}Zn composition of SAMW was lighter relative to the deep ocean δ^{66}Zn value of 0.50 ± 0.14 ‰. This was especially true for the south Tasman Sea station (P3) which had the greatest influence of water masses with Southern Ocean origin. The δ^{66}Zn value of SAMW at station P3 was consistently low ranging between 0.18 ± 0.09 ‰ and 0.27 ± 0.10 ‰ between 200m and 500m of water depth. At a depth of 1000 m of the south

Tasman Sea station was the core of AAIW with δ^{66}Zn value of 0.59 ± 0.03 ‰. At the north Tasman Sea station (P1), SAMW and AAIW were significantly modified by mixing with water masses of the subtropical gyres. At station P1, the δ^{66}Zn values were heavier for SAMW and lighter for AAIW relative to the δ^{66}Zn values at station P3. The mid Tasman Sea station (P2) had δ^{66}Zn values intermediate of that observed for stations P3 and P1 for SAMW and AAIW (Figure 5.12). From these observations, we could speculate that the surface waters of the Southern Ocean which forms SAMW have lighter δ^{66}Zn values and the surface water forming AAIW have heavier δ^{66}Zn composition. This is consistent with the reported δ^{66}Zn values of the surface water (2-5 m) in the Southern Ocean (Zhao et al. 2014)(. The surface water in the Antarctic Zone, which is transported across the Antarctic Polar Front, and part of which eventually subducts in the Polar Frontal Zone to form the AAIW, has heavier isotope composition (+ 0.46‰ to + 0.60‰). The only surface water sample in the PFZ analysed by Zhao et al. (2014) has a significantly lighter δ^{66}Zn value of + 0.10‰ (relative to the upwelled deep water in the AAZ). Part of the surface water from the PFZ moves across the Subantarctic Front and eventually forms the SAMW in the Subantarctic Zone. The lighter δ^{66}Zn values of dissolved Zn in the surface water in the PFZ could probably be a result of heavier Zn uptake (or release of lighter Zn) by organisms like *P. antarctica* under Fe limiting condition, or adsorption of heavy Zn to particulate organic matter(John and Conway 2014). Whereas, the heavier δ^{66}Zn values of AAIW could be a result of lighter Zn uptake. Thus, the Zn isotopic signature of the water masses having a Southern Ocean origin could potentially be influenced by Fe bioavailability.

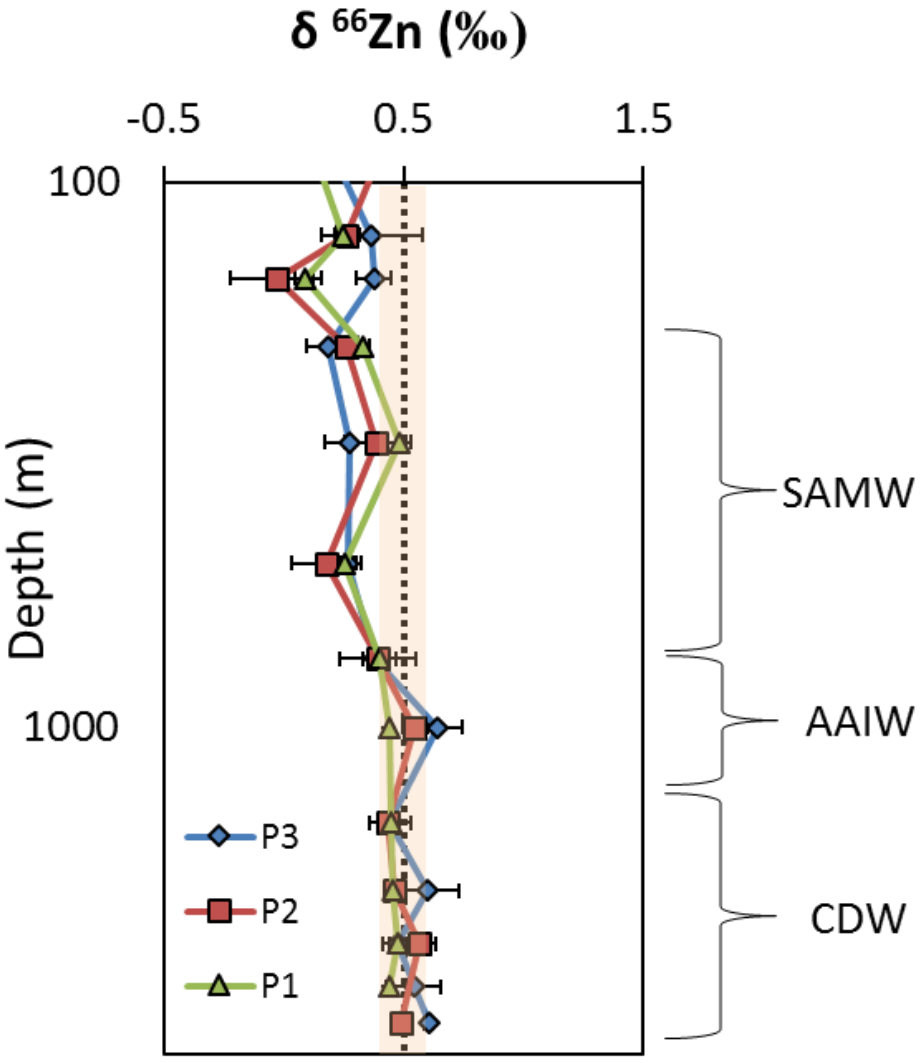

Figure 5.12: Profile of dissolved Zn isotope composition (δ^{66}Zn) versus depth along with corresponding water masses, for process stations P1, P2 and P3. SAMW = Sub Antarctic Mode Water; AAIW = Antarctic Intermediate Water; CDW = Circumpolar Deep Water. The dotted line along with the shaded region represents the global deep ocean δ^{66}Zn average value (0.50 ± 0.14 ‰). Error bars represents 2 SD of replicate extractions.

5.4: Conclusions

In this chapter, we studied the effect of Fe and Zn limitation on specific growth rates and photophysiology of the haptophyte *Phaeocystis antarctica*. The growth rates were severely reduced under both Fe and Zn limitations suggesting that low concentrations of both bio-available Fe and Zn could potentially limit the growth of Southern Ocean phytoplankton. Under Fe limitation, the photosynthetic efficiency was significantly reduced for both species. Iron is essential for photosynthetic electron transport, and our results clearly demonstrate impaired photosynthetic function due to Fe limitation: F_v/F_m was significantly reduced and the time taken for electron transport from Q_A to Q_B, ($\tau 1$), and from Q_A to Q_B, ($\tau 2$), increased significantly.

In this study, we show that Fe bio-availability plays an important role in controlling both the cellular Zn quota (expressed as Zn:P ratio) and Zn isotope fractionation by by *P. antarctica* and potentially other phytoplankton species. Under Fe limitation the cellular Zn:P ratio increased significantly for *P. antarctica*.

Previously, (John et al. 2007) reported that Zn isotope fractionation by the oceanic diatom *T. oceanica* was dependent on the free Zn concentration [Zn^{2+}], which is believed to be the bio-available form of Zn (John et al 2007). This study shows that Zn isotope fractionation by phytoplankton is not just dependent on the Zn bio-availability but also on other factors such as Fe bio-availability. We observed a lighter Zn isotope composition in *P. antarctica* under Fe replete conditions, whereas a heavier Zn isotope composition within the cells was observed under Fe limiting conditions.

Currently, the primary productivity in the Southern Ocean is thought to be limited seasonally by Fe (Watson et al. 2000). This would suggest that in the natural phytoplankton assemblage a dominance of *P. antarctica,* under Fe limiting conditions and at the end of the blooming phase would make the $\delta^{66}Zn$ composition of seawater lighter irrespective of Zn concentration. It would be interesting to see what effect Fe limitation has on Zn isotope fractionation by other phytoplankton species. It is also important to characterise other factors that might influence Zn isotope fractionation by phytoplankton. This study shows the need to carefully analyse the trace metal composition while interpreting zinc isotope composition of the biologically active upper water column of the ocean. Future research should focus on understanding the mechanisms controlling Zn uptake by phytoplankton by culturing different phytoplankton species at their environmentally relevant conditions under well-defined trace metal concentrations.

Acknowledgements

We thank Leslie Kinsley for his technical advice on ICPMS. Financial support for this work came from the Australian Research Council (DP130100679). RSES and ANU scholarships to the lead author are also appreciated.

Chapter 6:

Thesis Conclusion

6.1. Summary

The four chapters which form the core of this thesis are connected by the common objective of trying to understand Zn cycling and bioavailability in marine realm using the Zn isotope composition of dissolved samples collected from the Tasman Sea, SW Pacific Ocean. To complement the interpretation of these samples, I cultured phytoplankton under well-defined environmental conditions and then determined the Zn isotope composition of phytoplankton. The purpose is to understand the factors that influence Zn isotope fractionation within phytoplankton and how they imprint this on seawater.

6.1.1. Chapter 2

In chapter 2, I present a method developed in this PhD to determine the dissolved Zn isotope composition (δ^{66}Zn) of seawater. The method makes use of the double spike (DS) technique in conjunction with the pre-concentration of Zn from seawater utilising Toyopearl AF Chelate 650M resin. This method has a high extraction efficiency for Zn (~99%) and a low processing blank. The reproducibility of the procedure is excellent for deep-water [6.55 ± 0.34 nmol L-1 and 0.59 ± 0.02 ‰ (n = 9) w.r.t JMC-Lyon] and shallow-water samples [0.05 ± 0.01 nmol L-1 and 0.08 ± 0.02 ‰ (n = 3). w.r.t JMC-

Lyon] analysed over a period of one year. This method is well suited to analyse surface water samples with low dissolved Zn concentrations. The isotopic values obtained through analysis of inter-calibration samples using this procedure are in good agreement with published values. The suitability of this method for analysis of seawater samples was demonstrated by analysing a water column profile for dissolved Zn concentration and δ^{66}Zn versus depth. The results from development of this procedure were published in the journal *Microchemical Journal* (Samanta et al. 2016).

6.1.2. Chapter 3

In chapter 3, I reported δ^{66}Zn values of samples collected from the three stations in the Tasman Sea. Dissolved Zn isotopes revealed significant δ^{66}Zn fractionation within the upper ocean (0 – 200 m), while at depth (≥ 1000 m) the dissolved δ^{66}Zn composition is relative homogenous and within the range observed for the deep ocean (δ^{66}Zn = 0.50 ± 0.14‰). At the mesotrophic mid Tasman Sea station (P2) and the highly productive south Tasman Sea station (P3), eukaryotic phytoplankton dominated whereas at the north Tasman Sea station cyanobacteria and diazotrophs dominated. A coccolithophore bloom is seen during sampling of station P3. A significant correlation is obtained between the dissolved δ^{66}Zn composition and the relative fluorescence in the upper 200 m for stations P2 and P3, while no coupling is observed at the oligotrophic north Tasman Sea station (P1). A seasonal change in δ^{66}Zn signal is also observed for station P1 with heavier δ^{66}Zn values appearing to be coupled to an increase in biological production during the austral autumn. Combining the δ^{66}Zn values and corresponding ligand data and biological data (from companion studies) for

the three stations, it appears that the species composition of the resident phytoplankton community controls Zn isotope fractionation and Zn speciation in the upper water column for the Tasman Sea. These results suggest that eukaryotic phytoplankton, such as *Emiliania huxleyi*, fractionate Zn isotopes with the preferential uptake of lighter isotopes thereby making the remaining dissolved Zn isotopically heavier. The extent of Zn isotope fractionation ($\Delta^{66}Zn_{DCM\text{-}surface}$) observed in the surface ocean at stations P3 and P2 are 0.5 ‰ and 0.3 ‰, respectively. Immediately below the chlorophyll maxima, the $\delta^{66}Zn$ composition of dissolved Zn is light relative to the overlying waters due to preferential regeneration of isotopically lighter Zn from sinking particulate organic material. At station P3, which has the greatest influence of water masses originating in the Southern Ocean, SAMW (between 200 m- 750 m) has a distinctively lighter $\delta^{66}Zn$ composition relative to the deep ocean, while the core of AAIW at 1000 m is isotopically heavier. These isotopic signatures are diluted moving from south to north where these water masses are heavily influenced by subtropical water mases. It is speculated that the $\delta^{66}Zn$ signatures of SAMW and AAIW at the south Tasman Sea could have its origin in the Southern Ocean. However, the lighter $\delta^{66}Zn$ values observed for most of the upper 500 m relative to the deep ocean could be due scavenging of heavier Zn onto sinking particles, which is regenerated at depth ((John and Conway 2014). At station P3, a strong (negative) correlation is observed between $\delta^{66}Zn$ values (depth ≥ 200 m) and Si isotopes (at corresponding depths from a nearby station in the SAZ region). It is further speculated that this biogeochemical processing of Zn and Si in the Southern Ocean is the key to their coupling. The findings from this chapter has been accepted for publication in the journal *Marine Chemistry* and is available in the online version of the journal (Samanta et al. 2017).

6.1.3. Chapter 4

In Chapter 4, I report the effect of Zn on physiology (growth and photophysiology) and Zn isotope fractionation by a Tasman Sea isolate of the coccolithophore *E. huxleyi* cultured across a range of free Zn^{2+} ion concentration, representing the natural free Zn^{2+} concentrations observed in the global ocean. Here I have shown that lighter Zn isotope is preferentially taken by *E. huxleyi* over a wide range of free Zn^{2+} ion concentrations. The observed extent of Zn isotope fractionation due to Zn uptake by *E. huxleyi* ($\Delta^{66}Zn_{cells\text{-}media}$ varying from -0.6 ‰ to -0.2 ‰) is complementary to the conclusions detailed in chapter 3 that heavier $\delta^{66}Zn$ value of dissolved Zn measured at the chlorophyll maximum is due to uptake of lighter Zn by eukaryotic phytoplankton, especially at stations P2 and P3. The results in this chapter also supports the conclusion that the $\delta^{66}Zn$ composition of the upper water column of the Tasman Sea is controlled by the resident phytoplankton community and that phytoplankton in the south Tasman Sea can adapt to the low Zn concentrations. The specific growth rates remained largely unchanged over the range of free Zn^{2+} ion concentrations examined, suggesting that this strain of *E. huxleyi* is well adapted to low Zn^{2+} ion concentrations. An increase in photosynthetic efficiency is observed with increasing free Zn^{2+} concentrations, which I speculate to be due to increased carbonic anhydrase activity.

6.1.4. Chapter 5

In Chapter 5, I report the effect of Fe and Zn limitation on physiology, Zn quota and Zn isotope fractionation by the Southern Ocean haptophyte *Phaeocystis antarctica*. Under Fe limiting conditions, the growth rates, photosynthetic efficiency and cell size significantly decreased. However, in contrast to *E. huxleyi,* the growth rates of *P. antarctica* are greatly reduced whereas photosynthetic efficiency either increased or remained unaffected under Zn-limiting conditions. Zinc had no significant effect on cell size for *P. antarctica*. The results further show that both Fe and Zn are essential for growth of *P. antarctica.* Iron is involved in the electron transport process during photosynthesis, thus it is not surprising that under Fe limitation F_v/F_m is significantly reduced and that the time taken for electron transport from QA to QB, (τ1), and from QA to QB, (τ2), are increased significantly. However, it is unclear of the exact role Zn plays in the electron transport chain and hence the photophysiology of *P. antarctica*. Under Fe limitation, the cellular Zn:P ratio is found to increase significantly for *P. antarctica* and a heavier Zn isotope composition within cells is observed. One possible explanation for this heavier Zn isotope composition is that more Zn is taken up when cells are Fe stressed. In an attempt to acquire Fe under Fe-limiting conditions *P. antarctica* upregulates cell surface Fe^{2+} transporters, which preferentially binds divalent Fe (Strzepek et al. 2011) and might potentially bind divalent Zn (Lane et al. 2009). The increased Zn:P ratio under Fe limitation could thus be a result of an adaptive strategy employed by *P. antarctica* in an attempt to acquire Fe under Fe-limiting conditions. The internalisation of heavy Zn bound to cell surface ligands/transporter may be via this Fe^{2+} transporter.

Another possible explanation could be the release of isotopically light Zn from the cell under Fe-limiting conditions. In a companion study to this one, it is observed that when *P. antarctica* is harvested very early on in the exponential phase of growth the Zn:P ratios at comparable Fe' concentrations are 10 times higher and Zn isotope composition within the cells are lighter relative to the culture media. Combining the results from this study and the companion study, it could be suggested that isotopically light Zn is preferentially released later in the exponential phase of growth, making the cells isotopically heavier relative to the culture media. In this study, I showed that Fe bio-availability plays an important role in controlling both the cellular Zn quota (expressed as Zn:P ratio) and Zn isotope fractionation by phytoplankton. My results also suggest that the Zn:P ratio and the Zn isotope composition of both dissolved phase and within phytoplankton in the Southern Ocean would be dependent on the sampling period. It is also speculated that the lighter dissolved Zn isotopic signature observed for SAMW (between 200 and 750 m) of the south Tasman Sea station could potentially be caused by the uptake of heavy Zn by organisms like *P. antarctica* in the Fe limited waters of the Southern Ocean where these water masses originate. However, the lighter isotope composition of SAMW could be due to regeneration of light Zn from sinking particulate organic matter and/or scavenging of heavy Zn onto sinking organic matter. The heavier AAIW could be due to release of scavenged heavy Zn back into the dissolved phase (John and Conway 2014).

6.2. General conclusions

The identification of zinc isotope variability in the upper ocean provides a useful tool to understanding the biogeochemical cycling of zinc in the ocean and thus highlights the value of this work.

In this study, I have shown that

(i) the composition of the phytoplankton community plays an important role in determining the dissolved Zn isotope composition;

(ii) the Zn isotope fractionation by phytoplankton is not just dependent on the Zn bio-availability but also on other factors such as Fe bio-availability.

My research shows the need to carefully analyse the phytoplankton community structure and the trace metal composition while interpreting Zn isotope composition of the biologically active upper water column of the ocean.

6.3. Future research directions

Analysis of multiple variables is essential to fully comprehend the biogeochemical cycling of Zn in the ocean. Analysis of the particulate phase along with the dissolved phase at various stages during a phytoplankton bloom formation would give a more concrete evidence of how phytoplankton fractionate Zn isotopes in the open ocean. The lighter isotope composition of margin sediments is believed to be due to export of organic matter with lighter Zn isotope composition that did not undergo remineralisation (Little et al. 2016). The lighter isotope composition of dissolved phase observed immediately below the depth the chlorophyll maximum could be due to release of lighter Zn from sinking organic matter (as proposed in this thesis) or scavenging of heavier Zn onto the sinking particulate matter (John and Conway 2014), or combination of both. These hypotheses could be tested by looking at remineralisation intensity of sinking particles and the Zn isotope composition of both particulate matter and seawater as algal detrital matter degraded. If the light Zn isotope compositions below the DCM is due to the *in-situ* release of light Zn, a correlation between 'remineralisation intensity' and dissolved Zn isotope compositions would be expected. In regions where particle remineralisation is particularly intense and/or restricted to a narrow depth horizon, lighter dissolved Zn isotope composition with increased Zn concentration is expected. Whereas, in regions where more organic matter is exported and there is less overall remineralisation, such as the margin sediments, such a signal would be 'smoothed out'. The uptake of lighter Zn by eukaryotic phytoplankton at the DCM would result in lower concentration of dissolved Zn with heavier isotope composition and increased Zn concentration in the particulate

phase which would be isotopically light. The release of light Zn from organic matter would result in decreased Zn concentration in the particulate phase and increased dissolved Zn concentration, which is isotopically lighter. Whereas, scavenging would result in lower dissolved Zn concentrations with a lighter isotope composition and a heavier particulate Zn isotope composition. When this scavenged Zn is released back into solution, the Zn concentration of the particulate phase would decrease and the Zn concentration of the dissolved phase would increase, and at the same time become isotopically heavier. These measurements would also give a clearer idea if the dissolved Zn isotope composition of SAMW and AAIW in the south Tasman Sea has its origin in the Southern Ocean, or if it is due to *in-situ* biogeochemical processes.

To understand the mechanism behind the correlation between Zn and Si in the global ocean, measurements of dissolved and particulate Zn and Si isotopes are necessary. It is speculated that biogeochemical processing of Zn and Si in the Southern Ocean is the key to their coupling. The anti-correlation observed between Zn and Si isotopes (below 200 m) in the SAZ region could be due to either *in situ* biogeochemical processes or represent the isotopic signature of water masses having its origin in the Southern Ocean. This could be tested by analysing the dissolved Zn and Si isotope composition at stations in the Southern Ocean and at stations where there is less influence of Southern Ocean water masses and mixing of two geochemically disparate end members. Measurement of Zn and Si isotope composition both dissolved and particulate phases would give better appreciation of the mechanism behind Zn and Si coupling.

To understand the relationship between Zn and phytoplankton and how Zn is fractionated by different phytoplankton species under different trace metal conditions and what other factors influence Zn uptake and fractionation; future work should focus on culturing different phytoplankton species under environmentally relevant conditions. It is unclear how Zn influences the photophysiological response of phytoplankton, such as the decreased photosynthetic efficiency is observed for the cosmopolitan haptophyte *E. huxleyi* under Zn limitation, whereas for the Southern Ocean haptophyte *P. antarctica* photosynthetic efficiency increased under Zn limiting condition. Thus, the role Zn plays in different cellular processes in different phytoplankton needs to be researched. In this thesis, I have shown that Fe plays an important role in controlling Zn isotope fractionation by a Southern Ocean haptophyte. It would be interesting to see what effect Fe limitation has on Zn isotope fraction by other phytoplankton species. Also, it is important to characterise other factors (concentration of macro and other micro nutrients, light, temperature, pH) that might influence Zn isotope fractionation by phytoplankton. Since Southern Ocean significantly influences both ocean circulation and biogeochemistry, interest needs to be paid to understanding Zn isotope fractionation by Southern Ocean phytoplankton.

Finally, I would like to focus once again on the importance of analysing multiple variables to better understand Zn biogeochemical cycling in the ocean. A comprehensive study with analysis of Zn concentration and isotope composition of both particulate and dissolved phase, Zn speciation, biological data including the phytoplankton community structure, concentration of macro and micronutrients as well as the usual parameters- temperature, pressure, salinity, oxygen and fluorescence

is important in field studies. In laboratory, culturing different phytoplankton species under relevant environmental conditions is essential to discern the mechanism/s of Zn uptake by different phytoplankton species and improve our understanding of the relationship between Zn and phytoplankton.

List of References

Andersen, M. B., D. Vance, C. Archer, R. F. Anderson, M. J. Ellwood, and C. S. Allen. 2011. The Zn abundance and isotopic composition of diatom frustules, a proxy for Zn availability in ocean surface seawater. Earth and Planetary Science Letters **301:** 137-145.

Anderson, M., F. Morel, and R. Guillard. 1978. Growth limitation of a coastal diatom by low zinc ion activity.

Annett, A. L., D. S. Carson, X. Crosta, A. Clarke, and R. S. Ganeshram. 2010. Seasonal progression of diatom assemblages in surface waters of Ryder Bay, Antarctica. Polar biology **33:** 13-29.

Arar, E. J., and G. B. Collins. 1997. Method 445.0: In vitro determination of chlorophyll a and pheophytin a in marine and freshwater algae by fluorescence. United States Environmental Protection Agency, Office of Research and Development, National Exposure Research Laboratory Cincinnati.

Archer, C. and others 2017. Inter-calibration of a proposed new primary reference standard AA-ETH Zn for zinc isotopic analysis. Journal of Analytical Atomic Spectrometry.

Archer, C., and D. Vance. 2004. Mass discrimination correction in multiple-collector plasma source mass spectrometry: an example using Cu and Zn isotopes. Journal of Analytical Atomic Spectrometry **19:** 656-665.

Arnold, T. and others 2010. Measurement of zinc stable isotope ratios in biogeochemical matrices by double-spike MC-ICPMS and determination of the isotope ratio pool available for plants from soil. Analytical and Bioanalytical Chemistry **398:** 3115-3125.

Arrigo, K. R. and others 1999. Phytoplankton community structure and the drawdown of nutrients and CO2 in the Southern Ocean. Science **283:** 365-367.

Baars, O., and P. L. Croot. 2011. The speciation of dissolved zinc in the Atlantic sector of the Southern Ocean. Deep Sea Research Part II: Topical Studies in Oceanography **58:** 2720-2732.

Badger, M. R., and G. D. Price. 1994. The role of carbonic anhydrase in photosynthesis. Annual review of plant biology **45:** 369-392.

Ban, Y., M. Aida, M. Nomura, and Y. Fujii. 2002. Zinc Isotope Separation by Ligand Exchange Chromatography Using Cation Exchange Resin. J. Ion Exchange **13:** 46-52.

Baumann, M. E., F. P. Brandini, and R. Staubes. 1994. The influence of light and temperature on carbon-specific DMS release by cultures of Phaeocystis antarctica and three antarctic diatoms. Marine Chemistry **45:** 129-136.

Bermin, J. 2006. Determination of the isotopic composition of Cu and Zn in seawater. University of London**:** 224.

Bermin, J., D. Vance, C. Archer, and P. Statham. 2006. The determination of the isotopic composition of Cu and Zn in seawater. Chemical geology **226:** 280-297.

Bostock, H. C., P. J. Sutton, M. J. M. Williams, and B. N. Opdyke. 2013. Reviewing the circulation and mixing of Antarctic Intermediate Water in the South Pacific using evidence from geochemical tracers and Argo float trajectories. Deep-Sea Research Part I: Oceanographic Research Papers **73:** 84-98.

Boyd, P., and M. Ellwood. 2010. The biogeochemical cycle of iron in the ocean. Nature Geoscience **3:** 675-682.

Boyd, P. W. and others 2000. A mesoscale phytoplankton bloom in the polar Southern Ocean stimulated by iron fertilization. Nature **407:** 695-702.

Boyle, E. A. and others 2012. GEOTRACES IC1 (BATS) contamination-prone trace element isotopes Cd, Fe, Pb, Zn, Cu, and Mo intercalibration. Limnology and Oceanography: methods **10:** 653-665.

Brand, L. E., W. G. Sunda, and R. R. L. Guillard. 1983. Limitation of marine phytoplankton reproductive rates by zinc, manganese, and iron. Limnology and Oceanography**:** 1182-1198.

Brichta, M., and E.-M. Nöthig. 2003. Proboscia inermis: A key diatom species in Antarctic autumn.

Bruland, K. W. 1980. Oceanographic distributions of cadmium, zinc, nickel, and copper in the North Pacific. Earth and Planetary Science Letters **47:** 176-198.

---. 1989. Complexation of zinc by natural organic ligands in the central North Pacific. Limnology and Oceanography**:** 269-285.

Bruland, K. W., R. P. Franks, G. A. Knauer, and J. H. Martin. 1979. Sampling and analytical methods for the determination of copper, cadmium, zinc and nickel at the nanogram per liter level in sea water. Analytica Chimica Acta **105:** 233-245.

Bruland, K. W., G. A. Knauer, and J. H. Martin. 1978. Zinc in north-east Pacific water. Nature **271:** 741-743.

Bruland, K. W., K. J. Orians, and J. P. Cowen. 1994. REACTIVE TRACE-METALS IN THE STRATIFIED CENTRAL NORTH PACIFIC. Geochimica Et Cosmochimica Acta **58:** 3171-3182.

Buitenhuis, E. T., K. R. Timmermans, and H. J. W. de Baar. 2003. Zinc-bicarbonate colimitation of Emiliania huxleyi. Limnology and Oceanography**:** 1575-1582.

Cardinal, D., L. Y. Alleman, F. Dehairs, N. Savoye, T. W. Trull, and L. Andre. 2005. Relevance of silicon isotopes to Si-nutrient utilization and Si-source assessment in Antarctic waters. Global Biogeochemical Cycles **19:** doi:10.1029/2004GB002364.

Christianson, D. W., and C. A. Fierke. 1996. Carbonic anhydrase: evolution of the zinc binding site by nature and by design. Accounts of Chemical Research **29:** 331-339.

Cloquet, C., J. Carignan, M. F. Lehmann, and F. Vanhaecke. 2008. Variation in the isotopic composition of zinc in the natural environment and the use of zinc isotopes in biogeosciences: a review. Analytical and Bioanalytical Chemistry **390:** 451-463.

Coale, K. H. and others 2004. Southern Ocean iron enrichment experiment: carbon cycling in high- and low-Si waters. Science **304:** 408-414.

Coale, K. H., X. Wang, S. J. Tanner, and K. S. Johnson. 2003. Phytoplankton growth and biological response to iron and zinc addition in the Ross Sea and Antarctic Circumpolar Current along 170 W. Deep Sea Research Part II: Topical Studies in Oceanography **50:** 635-653.

Cochlan, W. P., D. A. Bronk, and K. H. Coale. 2002. Trace metals and nitrogenous nutrition of Antarctic phytoplankton: experimental observations in the Ross Sea. Deep Sea Research Part II: Topical Studies in Oceanography **49:** 3365-3390.

Conway, T. M., and S. G. John. 2014. The biogeochemical cycling of zinc and zinc isotopes in the North Atlantic Ocean. Global Biogeochemical Cycles.

---. 2015. The cycling of iron, zinc and cadmium in the North East Pacific Ocean–Insights from stable isotopes. Geochimica et Cosmochimica Acta **164:** 262-283.

Conway, T. M., A. D. Rosenberg, J. F. Adkins, and S. G. John. 2013. A new method for precise determination of iron, zinc and cadmium stable isotope ratios in seawater by double-spike mass spectrometry. Analytica chimica acta **793:** 44-52.

Criss, R. E. 1999. Principles of stable isotope distribution. Oxford University Press, USA.

Croot, P. L., O. Baars, and P. Streu. 2011. The distribution of dissolved zinc in the Atlantic sector of the Southern Ocean. Deep Sea Research Part II: Topical Studies in Oceanography **58:** 2707-2719.

Cullen, J. T., Z. Chase, K. H. Coale, S. E. Fitzwater, and R. M. Sherrell. 2003. Effect of iron limitation on the cadmium to phosphorus ratio of natural phytoplankton assemblages from the Southern Ocean. Limnology and Oceanography **48:** 1079-1087.

Cutter, G. and others 2014. Sampling and Sample-handling Protocols for GEOTRACES Cruises.

Danielsson, L., B. Magnusson, and K. Zhang. 1982. Trace metal determinations in estuarine waters by electrothermal atomic adsorption spectroscopy after extraction of dithiocarbamate complexes into freon. Analytica Chimica Acta **144:** 183-188.

Danilovtseva, E., V. Aseyev, M. Karesoja, and V. Annenkov. 2009. Sorption of silicic acid from non-saturated aqueous solution by a complex of zinc ions with poly(vinylamine). European Polymer Journal **45:** 1391-1396.

De Souza, G., B. Reynolds, G. Johnson, J. Bullister, and B. Bourdon. 2012. Silicon stable isotope distribution traces Southern Ocean export of Si to the eastern South Pacific thermocline. Biogeosciences **9:** 4199-4213.

DiTullio, G. and others 2000. Rapid and early export of Phaeocystis antarctica blooms in the Ross Sea, Antarctica. Nature **404:** 595-598.

Ellwood, M. J. 2004. Zinc and cadmium speciation in subantarctic waters east of New Zealand. Marine chemistry **87:** 37-58.

Ellwood, M. J. 2008. Wintertime trace metal (Zn, Cu, Ni, Cd, Pb and Co) and nutrient distributions in the Subantarctic Zone between 40–52 S; 155–160 E. Marine Chemistry **112:** 107-117.

Ellwood, M. J., and K. A. Hunter. 2000. The incorporation of zinc and iron into the frustule of the marine diatom Thalassiosira pseudonana. Limnology and Oceanography**:** 1517-1524.

Ellwood, M. J. and others 2013. Relationships between nutrient stocks and inventories and phytoplankton physiological status along an oligotrophic meridional transect in the Tasman Sea. Deep Sea Research Part I: Oceanographic Research Papers **72:** 102-120.

Ellwood, M. J., and C. M. G. Van den Berg. 2000. Zinc speciation in the northeastern Atlantic Ocean. Marine chemistry **68:** 295-306.

Falkowski, P. G. 1994. The role of phytoplankton photosynthesis in global biogeochemical cycles. Photosynthesis Research **39:** 235-258.

Farkas, E., H. Csóka, G. Micera, and A. Dessi. 1997. Copper(II), nickel(II), zinc(II), and molybdenum(VI) complexes of desferrioxamine B in aqueous solution. Journal of Inorganic Biochemistry **65:** 281-286.

Field, C. B., M. J. Behrenfeld, J. T. Randerson, and P. Falkowski. 1998. Primary production of the biosphere: integrating terrestrial and oceanic components. Science **281:** 237.

Fitzwater, S., K. Johnson, R. Gordon, K. Coale, and W. Smith. 2000. Trace metal concentrations in the Ross Sea and their relationship with nutrients and phytoplankton growth. Deep Sea Research Part II: Topical Studies in Oceanography **47:** 3159-3179.

Frew, R., A. Bowie, P. Croot, and S. Pickmere. 2001. Macronutrient and trace-metal geochemistry of an in situ iron-induced Southern Ocean bloom. Deep-Sea Research Part Ii-Topical Studies in Oceanography **48:** 2467-2481.

Fujii, T., F. Moynier, J. Blichert-Toft, and F. Albarède. 2014. Density functional theory estimation of isotope fractionation of Fe, Ni, Cu, and Zn among species relevant to geochemical and biological environments. Geochimica et Cosmochimica Acta **140:** 553-576.

Gelabert, A., O. Pokrovsky, J. Viers, J. Schott, A. Boudou, and A. Feurtet-Mazel. 2006. Interaction between zinc and freshwater and marine diatom species: surface complexation and Zn isotope fractionation. Geochimica Et Cosmochimica Acta **70:** 839-857.

Grachev, M., T. Sherbakova, Y. Masyukova, and Y. Likhoshway. 2005. A potential zinc-binding motif in silicic acid transport proteins of diatoms. Diatom Research **20:** 409-411.

Grün, R. 2016. The Relationship between Iron Limitation and the Incorporation of Zinc into Southern Ocean Phytoplankton with Implications for the Global Oceanic Zinc Budget. Honours Thesis, The Australian National University.

Hassler, C. and others 2014. Primary productivity induced by iron and nitrogen in the Tasman Sea: an overview of the PINTS expedition. Marine and Freshwater Research **65:** 517-537.

Hassler, C. S., M. Sinoir, L. A. Clementson, and E. C. V. Butler. 2012. Exploring the link between micronutrients and phytoplankton in the Southern Ocean during the 2007 austral summer. Frontiers in Microbiology **3**.

Hendry, K. R., and M. B. Andersen. 2013. The zinc isotopic composition of siliceous marine sponges: Investigating nature's sediment traps. Chemical Geology **354:** 33-41.

Hernlem, B. J., L. M. Vane, and G. D. Sayles. 1996. Stability constants for complexes of the siderophore desferrioxamine B with selected heavy metal cations. Inorganica Chimica Acta **244:** 179-184.

Hoefs, J. 2009. Stable isotope geochemistry. Springer Verlag.

Hopkinson, B. M., C. L. Dupont, A. E. Allen, and F. M. M. Morel. 2011. Efficiency of the CO2-concentrating mechanism of diatoms. Proceedings of the National Academy of Sciences **108:** 3830-3837.

Hunter, K. A., and P. Boyd. 1999. Biogeochemistry of trace metals in the ocean. Marine and Freshwater Research **50:** 739-753.

Jakuba, R. W., M. A. Saito, J. W. Moffett, and Y. Xu. 2012. Dissolved zinc in the subarctic North Pacific and Bering Sea: Its distribution, speciation, and importance to primary producers. Global Biogeochemical Cycles **26**.

Jeffrey, S., and M. Vesk. 1997. Introduction to marine phytoplankton and their pigment signatures. na.

Jeffrey, S., and S. Wright. 2006. Photosynthetic pigments in marine microalgae: insights from cultures and the sea. Algal cultures, analogues of blooms and applications. Science Publishers**:** 33-90.

John, S. G., and T. M. Conway. 2014. A role for scavenging in the marine biogeochemical cycling of zinc and zinc isotopes. Earth and Planetary Science Letters **394:** 159-167.

John, S. G., R. W. Geis, M. A. Saito, and E. A. Boyle. 2007. Zinc isotope fractionation during high-affinity and low-affinity zinc transport by the marine diatom Thalassiosira oceanica. Limnology and Oceanography **52:** 2710-2714.

John, S. G., J. Helgoe, and E. Townsend. 2017a. Biogeochemical cycling of Zn and Cd and their stable isotopes in the Eastern Tropical South Pacific. Marine Chemistry.

John, S. G., M. Kunzmann, E. J. Townsend, and A. D. Rosenberg. 2017b. Zinc and cadmium stable isotopes in the geological record: A case study from the post-snowball Earth Nuccaleena cap dolostone. Palaeogeography, Palaeoclimatology, Palaeoecology **466:** 202-208.

John, S. G., O. J. Rouxel, P. R. Craddock, A. M. Engwall, and E. A. Boyle. 2008. Zinc stable isotopes in seafloor hydrothermal vent fluids and chimneys. Earth and Planetary Science Letters **269:** 17-28.

Johnson, C. M., B. L. Beard, F. Albarède, A. G. U. Meeting, and C. G. Union. 2004. Geochemistry of non-traditional stable isotopes. Mineralogical Society of America Washington, DC.

Jouvin, D., P. Louvat, F. Juillot, C. N. Maréchal, and M. F. Benedetti. 2009. Zinc isotopic fractionation: why organic matters. Environmental science & technology **43:** 5747-5754.

Kalaji, H. M. and others 2014. Frequently asked questions about in vivo chlorophyll fluorescence: practical issues. Photosynthesis research **122:** 121-158.

Kana, T. M., R. J. Geider, and C. Critchley. 1997. Regulation of photosynthetic pigments in micro-algae by multiple environmental factors: a dynamic balance hypothesis. New Phytologist **137:** 629-638.

Klaas, C., and D. E. Archer. 2002. Association of sinking organic matter with various types of mineral ballast in the deep sea: Implications for the rain ratio. Global Biogeochemical Cycles **16**.

Köbberich, M., and D. Vance. 2017. Kinetic control on Zn isotope signatures recorded in marine diatoms. Geochimica et Cosmochimica Acta **210:** 97-113.

Kolber, Z. 2002. Laser Induced Fluorescence Transient (LIFT) Method for Measuring Photosynthetic Performance and Primary Productivity in Terrestrial Ecosystems. Earth Science Technology Conference, Paper B1P2, Pasadena, California. Citeseer.

Kolber, Z., and P. Falkowski. 1995. Fast repetition rate (FRR) fluorometer and method for measuring fluorescence and photosynthetic parameters. Google Patents.

Kolber, Z. S., O. Prášil, and P. G. Falkowski. 1998. Measurements of variable chlorophyll fluorescence using fast repetition rate techniques: defining methodology and experimental protocols. Biochimica et Biophysica Acta (BBA)-Bioenergetics **1367:** 88-106.

Kuenzler, E. J., and J. P. Perras. 1965. Phosphatases of marine algae. Biological Bulletin **128:** 271-284.

Kunzmann, M., G. P. Halverson, P. A. Sossi, T. D. Raub, J. L. Payne, and J. Kirby. 2013. Zn isotope evidence for immediate resumption of primary productivity after snowball Earth. Geology **41:** 27-30.

Lane, E. S., D. M. Semeniuk, R. F. Strzepek, J. T. Cullen, and M. T. Maldonado. 2009. Effects of iron limitation on intracellular cadmium of cultured phytoplankton: Implications for surface dissolved cadmium to phosphate ratios. Marine Chemistry **115:** 155-162.

Law, C. S. and others 2012. No stimulation of nitrogen fixation by non-filamentous diazotrophs under elevated CO 2 in the South Pacific. Global Change Biology **18:** 3004-3014.

Law, C. S., E. M. S. Woodward, M. J. Ellwood, A. Marriner, S. J. Bury, and K. A. Safi. 2011. Response of surface nutrient inventories and nitrogen fixation to a tropical cyclone in the southwest Pacific. Limnology and Oceanography **56:** 1372-1385

Lis, H., Y. Shaked, C. Kranzler, N. Keren, and F. M. Morel. 2015. Iron bioavailability to phytoplankton: An empirical approach. The ISME journal **9:** 1003-1013.

Little, S., D. Vance, C. Walker-Brown, and W. Landing. 2014. The oceanic mass balance of copper and zinc isotopes, investigated by analysis of their inputs, and outputs to ferromanganese oxide sediments. Geochimica et Cosmochimica Acta **125:** 673-693.

Little, S. H., D. Vance, J. McManus, and S. Severmann. 2016. Key role of continental margin sediments in the oceanic mass balance of Zn and Zn isotopes. Geology **44:** 207-210.

Maldonado, M. T., and N. M. Price. 2001. Reduction and transport of organically bound iron by Thalassiosira oceanica (Bacillariophyceae). Journal of Phycology **37:** 298-310.

Maldonado, M. T., R. F. Strzepek, S. Sander, and P. W. Boyd. 2005. Acquisition of iron bound to strong organic complexes, with different Fe binding groups and photochemical reactivities, by plankton communities in Fe-limited subantarctic waters. Global Biogeochem. Cycles **19:** GB4S23.

Maréchal, C., and F. Albarède. 2002. Ion-exchange fractionation of copper and zinc isotopes. Geochimica Et Cosmochimica Acta **66:** 1499-1509.

Maréchal, C. N., E. Nicolas, C. Douchet, and F. Albarède. 2000. Abundance of zinc isotopes as a marine biogeochemical tracer. Geochemistry, Geophysics, Geosystems **1**.

Maréchal, C. N., P. Telouk, and F. Albarede. 1999. Precise analysis of copper and zinc isotopic compositions by plasma-source mass spectrometry. Chemical geology **156:** 251-273.

Martin, J. H. 1990. Glacial-interglacial CO2 change: The iron hypothesis. Paleoceanography **5:** 1-13.

Mason, T. F. D. and others 2004. High-precision Cu and Zn isotope analysis by plasma source mass spectrometry Part 2. Correcting for mass discrimination effects. Journal of Analytical Atomic Spectrometry **19:** 218-226.

Milligan, A. J., and F. M. M. Morel. 2002. A proton buffering role for silica in diatoms. Science **297:** 1848-1850.

Milne, A., W. Landing, M. Bizimis, and P. Morton. 2010. Determination of Mn, Fe, Co, Ni, Cu, Zn, Cd and Pb in seawater using high resolution magnetic sector inductively coupled mass spectrometry (HR-ICP-MS). Analytica Chimica Acta **665:** 200-207.

Moeller, K., R. Schoenberg, R. B. Pedersen, D. Weiss, and S. Dong. 2011. Calibration of the New Certified Reference Materials ERM-AE633 and ERM-AE647 for Copper and IRMM-3702 for Zinc Isotope Amount Ratio Determinations. Geostandards and Geoanalytical Research.

Morel, F., and N. Price. 2003. The biogeochemical cycles of trace metals in the oceans. Science **300:** 944.

Morel, F., J. Reinfelder, S. Roberts, C. Chamberlain, J. Lee, and D. Yee. 1994. Zinc and carbon co-limitation of marine phytoplankton. Nature **369:** 740-742.

Moynier, F., D. Vance, T. Fujii, and P. Savage. 2017. The isotope geochemistry of zinc and copper. Reviews in Mineralogy and Geochemistry **82:** 543-600.

Nanninga, H., and T. Tyrrell. 1996. Importance of light for the formation of algal blooms by Emiliania huxleyi. Marine Ecology Progress Series **136:** 195-203.

Nolting, R., L. Gerringa, M. Swagerman, K. Timmermans, and H. De Baar. 1998. Fe (III) speciation in the high nutrient, low chlorophyll Pacific region of the Southern Ocean. Marine Chemistry **62:** 335-352.

O'Sullivan, J. E., R. J. Watson, and E. C. V. Butler. 2013. An ICP-MS procedure to determine Cd, Co, Cu, Ni, Pb and Zn in oceanic waters using in-line flow-injection with solid-phase extraction for preconcentration. Talanta **115:** 999-1010.

Parsons, T. R., Y. Maita, and C. M. Lalli. 1984. A manual of biological and chemical methods for seawater analysis. Publ. Pergamon Press, Oxford.

Peel, K., D. Weiss, and L. Sigg. 2009. Zinc isotope composition of settling particles as a proxy for biogeochemical processes in lakes: Insights from the eutrophic Lake Greifen, Switzerland. Limnology and Oceanography **54:** 1699.

Petrou, K. and others 2016. Southern Ocean phytoplankton physiology in a changing climate. J Plant Physiol **203:** 135-150.

Pichat, S., C. Douchet, and F. Albarède. 2003. Zinc isotope variations in deep-sea carbonates from the eastern equatorial Pacific over the last 175 ka. Earth and Planetary Science Letters **210:** 167-178.

Pollard, R. T. and others 2009. Southern Ocean deep-water carbon export enhanced by natural iron fertilization. Nature **457:** 577-580.

Price, N. M. and others 1988. Preparation and chemistry of the artificial algal culture medium Aquil. Biol. Oceanogr **6:** 443-461.

Raven, J. A., M. C. Evans, and R. E. Korb. 1999. The role of trace metals in photosynthetic electron transport in O2-evolving organisms. Photosynthesis Research **60:** 111-150.

Reynolds, B. C. and others 2007. An inter-laboratory comparison of Si isotope reference materials. Journal of Analytical Atomic Spectrometry **22:** 561-568.

Ridgway, K. R., and J. R. Dunn. 2003. Mesoscale structure of the mean East Australian Current System and its relationship with topography. Progress In Oceanography **56:** 189-222.

Rodushkin, I., A. Stenberg, H. Andrén, D. Malinovsky, and D. C. Baxter. 2004. Isotopic fractionation during diffusion of transition metal ions in solution. Analytical chemistry **76:** 2148-2151.

Rosman, K. 1972. A survey of the isotopic and elemental abundance of zinc. Geochimica Et Cosmochimica Acta **36:** 801-819.

Rost, B., and U. Riebesell. 2004. Coccolithophores and the biological pump: responses to environmental changes, p. 99-125. *In* H. R. Thierstein and J. R. Young [eds.],

Coccolithophores: From Molecular Processes to Global Impact. Springer Berlin Heidelberg.
Rudge, J. F., B. C. Reynolds, and B. Bourdon. 2009. The double spike toolbox. Chemical geology **265:** 420-431.
Rueter, J. G., and F. M. M. Morel. 1981. THE INTERACTION BETWEEN ZINC-DEFICIENCY AND COPPER TOXICITY AS IT AFFECTS THE SILICIC-ACID UPTAKE MECHANISMS IN THALASSIOSIRA-PSEUDONANA. Limnology and Oceanography **26:** 67-73.
Saito, M. A., and T. J. Goepfert. 2008. Zinc-cobalt colimitation of Phaeocystis antarctica. Limnology and Oceanography **53:** 266.
Saito, M. A., J. Moppett, S. W. Chisholm, and J. B. Waterbury. 2002. Cobalt limitation and uptake in Prochlorococcus. Limnology and Oceanography **47:** 1629-1636.
Samanta, M., M. J. Ellwood, and G. E. Mortimer. 2016. A method for determining the isotopic composition of dissolved zinc in seawater by MC-ICP-MS with a 67Zn–68Zn double spike. Microchemical Journal **126:** 530-537.
Samanta, M., M. J. Ellwood, M. Sinoir, and C. S. Hassler. 2017. Dissolved zinc isotope cycling in the Tasman Sea, SW Pacific Ocean. Marine Chemistry.
Sarmiento, J. L., N. Gruber, M. A. Brzezinski, and J. P. Dunne. 2004. High-latitude controls of thermocline nutrients and low latitude biological productivity. Nature **427:** 56-60.
Sarmiento, J. L., T. M. Hughes, R. J. Stouffer, and S. Manabe. 1998. Simulated response of the ocean carbon cycle to anthropogenic climate warming. Nature **393:** 245-249.
Scharek, R., M. A. Van Leeuwe, and H. J. De Baar. 1997. Responses of Southern Ocean phytoplankton to the addition of trace metals. Deep Sea Research Part II: Topical Studies in Oceanography **44:** 209-227.
Schlitzer, R. 2006. Ocean Data View. http://odv.awi-bremerhaven.
Schulz, K., I. Zondervan, L. Gerringa, K. Timmermans, M. Veldhuis, and U. Riebesell. 2004. Effect of trace metal availability on coccolithophorid calcification. Nature **430:** 673-676.
Sedwick, P., N. Garcia, S. Riseman, C. Marsay, and G. DiTullio. 2007. Evidence for high iron requirements of colonial Phaeocystis antarctica at low irradiance. Biogeochemistry **83:** 83-97.
Sedwick, P. N., G. R. DiTullio, and D. J. Mackey. 2000. Iron and manganese in the Ross Sea, Antarctica: Seasonal iron limitation in Antarctic shelf waters. Journal of Geophysical Research: Oceans **105:** 11321-11336.
Shaked, Y., A. B. Kustka, and F. M. M. Morel. 2005. A general kinetic model for iron acquisition by eukaryotic phytoplankton. Limnology and Oceanography **50:** 872-882.
Sherbakova, T. A. and others 2005. Conserved motif CMLD in silicic acid transport proteins of diatoms. Molecular Biology **39:** 269-280.
Shiel, A. E., J. Barling, K. J. Orians, and D. Weis. 2009. Matrix effects on the multi-collector inductively coupled plasma mass spectrometric analysis of high-precision cadmium and zinc isotope ratios. Analytica Chimica Acta **633:** 29-37.
Siebert, C., T. F. Nägler, and J. D. Kramers. 2001. Determination of molybdenum isotope fractionation by double-spike multicollector inductively coupled plasma mass spectrometry. Geochem. Geophys. Geosyst **2:** 1032.
Sinoir, M., A. R. Bowie, M. Mongin, E. C. Butler, and C. S. Hassler. 2016a. Zinc requirement for two phytoplankton strains of the Tasman Sea. Marine and Freshwater Research.
Sinoir, M., M. J. Ellwood, E. C. Butler, A. R. Bowie, M. Mongin, and C. S. Hassler. 2016b. Zinc cycling in the Tasman Sea: Distribution, speciation and relation to phytoplankton community. Marine Chemistry.
Sloyan, B. M., and S. R. Rintoul. 2001. Circulation, renewal, and modification of Antarctic mode and intermediate water*. Journal of Physical Oceanography **31:** 1005-1030.

Sokolov, S., and S. Rintoul. 2000. Circulation and water masses of the southwest Pacific: WOCE section P11, Papua New Guinea to Tasmania. Journal of Marine Research **58:** 223-268.

Soto, A. R., H. Zheng, D. Shoemaker, J. Rodriguez, B. A. Read, and T. M. Wahlund. 2006. Identification and preliminary characterization of two cDNAs encoding unique carbonic anhydrases from the marine alga Emiliania huxleyi. Applied and environmental microbiology **72:** 5500-5511.

Stewart, M. K. 1975. Stable isotope fractionation due to evaporation and isotopic exchange of falling waterdrops: Applications to atmospheric processes and evaporation of lakes. Journal of Geophysical Research **80:** 1133-1146.

Strzepek, R. F., K. A. Hunter, R. D. Frew, P. J. Harrison, and P. W. Boyd. 2012. Iron-light interactions differ in Southern Ocean phytoplankton. Limnology and Oceanography **57:** 1182-1200.

Strzepek, R. F., M. T. Maldonado, K. A. Hunter, R. D. Frew, and P. W. Boyd. 2011. Adaptive strategies by Southern Ocean phytoplankton to lessen iron limitation: Uptake of organically complexed iron and reduced cellular iron requirements. Limnology and Oceanography **56:** 1983-2002.

Sunda, W. 2012. Feedback interactions between trace metal nutrients and phytoplankton in the ocean. Frontiers in microbiology **3:** 204.

Sunda, W., and S. Huntsman. 2003. Effect of pH, light, and temperature on Fe–EDTA chelation and Fe hydrolysis in seawater. Marine Chemistry **84:** 35-47.

Sunda, W. G., and S. A. Huntsman. 1992. Feedback interactions between zinc and phytoplankton in seawater. Limnology and Oceanography**:** 25-40.

---. 1995a. Cobalt and zinc interreplacement in marine phytoplankton: Biological and geochemical implications. Limnology and Oceanography**:** 1404-1417.

Sunda, W. G., and S. A. Huntsman. 1995b. Iron uptake and growth limitation in oceanic and coastal phytoplankton. Marine Chemistry **50:** 189-206.

---. 2000. Effect of Zn, Mn, and Fe on Cd accumulation in phytoplankton: Implications for oceanic Cd cycling. Limnology and Oceanography **45:** 1501-1516.

Sunda, W. G., and S. A. Huntsman. 2004. Relationships among photoperiod, carbon fixation, growth, chlorophyll a, and cellular iron and zinc in a coastal diatom. Limnology and Oceanography **49:** 1742-1753.

---. 2005. Effect of CO2 supply and demand on zinc uptake and growth limitation in a coastal diatom. Limnology and Oceanography **50:** 1181-1192.

Takano, S. and others 2017. A simple and rapid method for isotopic analysis of nickel, copper, and zinc in seawater using chelating extraction and anion exchange. Analytica Chimica Acta **967:** 1-11.

Talley, L. D. 2013. Closure of the global overturning circulation through the Indian, Pacific, and Southern Oceans: Schematics and transports. Oceanography **26:** 80-97.

Tang, D., and F. M. Morel. 2006. Distinguishing between cellular and Fe-oxide-associated trace elements in phytoplankton. Marine Chemistry **98:** 18-30.

Thamatrakoln, K., and M. Hildebrand. 2008. Silicon uptake in diatoms revisited: A model for saturable and nonsaturable uptake kinetics and the role of silicon transporters. Plant physiology **146:** 1397-1407.

Thompson, C. M., and M. J. Ellwood. 2014. Dissolved copper isotope biogeochemistry in the Tasman Sea, SW Pacific Ocean. Marine Chemistry **165:** 1-9.

Timmermans, K. R. and others 2001. Growth rates of large and small Southern Ocean diatoms in relation to availability of iron in natural seawater. Limnology and Oceanography **46:** 260-266.

Tovar-Sanchez, A., S. A. Sañudo-Wilhelmy, M. Garcia-Vargas, R. S. Weaver, L. C. Popels, and D. A. Hutchins. 2003. A trace metal clean reagent to remove surface-bound iron from marine phytoplankton. Marine Chemistry **82:** 91-99.

Turner, S., P. Nightingale, W. Broadgate, and P. Liss. 1995. The distribution of dimethyl sulphide and dimethylsulphoniopropionate in Antarctic waters and sea ice. Deep Sea Research Part II: Topical Studies in Oceanography **42:** 1059-1080.

Twining, B. S., and S. B. Baines. 2013. The trace metal composition of marine phytoplankton. Annual review of marine science **5:** 191-215.

Van Heukelem, L., and C. S. Thomas. 2001. Computer-assisted high-performance liquid chromatography method development with applications to the isolation and analysis of phytoplankton pigments. Journal of Chromatography A **910:** 31-49.

Vance, D. and others 2016. The oceanic budgets of nickel and zinc isotopes: the importance of sulfidic environments as illustrated by the Black Sea. Phil. Trans. R. Soc. A **374:** 20150294.

Vance, D., S. H. Little, G. F. de Souza, S. Khatiwala, M. C. Lohan, and R. Middag. 2017. Silicon and zinc biogeochemical cycles coupled through the Southern Ocean. Nature Geoscience **10:** 202-206.

Vance, T. R. and others 2013. Rapid DMSP production by an Antarctic phytoplankton community exposed to natural surface irradiances in late spring. Aquatic Microbial Ecology **71:** 117.

Veguería, S. F. J., J. M. Godoy, R. C. de Campos, and R. A. Gonçalves. 2013. Trace element determination in seawater by ICP-MS using online, offline and bath procedures of preconcentration and matrix elimination. Microchemical Journal **106:** 121-128.

Walczyk, T. 2004. TIMS versus multicollector-ICP-MS: coexistence or struggle for survival? Analytical and Bioanalytical Chemistry **378:** 229-231.

Warnken, K. W., D. Tang, G. A. Gill, and P. H. Santschi. 2000. Performance optimization of a commercially available iminodiacetate resin for the determination of Mn, Ni, Cu, Cd and Pb by on-line preconcentration inductively coupled plasma-mass spectrometry. Analytica Chimica Acta **423:** 265-276.

Watson, A., D. Bakker, A. Ridgwell, P. Boyd, and C. Law. 2000. Effect of iron supply on Southern Ocean CO2 uptake and implications for glacial atmospheric CO2. Nature **407:** 730-733.

Willie, S., Y. Iida, and J. McLaren. 1998a. Determination of Cu, Ni, Zn, Mn, Co, Pb, Cd, and V in seawater using flow injection ICP-MS. ATOMIC SPECTROSCOPY-NORWALK CONNECTICUT- **19:** 67-72.

Willie, S. N., Y. Iida, and J. W. McLaren. 1998b. Determination of Cu, Ni, Zn, Mn, Co, Pb, Cd, and V in seawater using flow injection ICP-MS. Atomic Spectroscopy **19:** 67-72.

Wyatt, N. and others 2014. Biogeochemical cycling of dissolved zinc along the GEOTRACES South Atlantic transect GA10 at 40 S. Global Biogeochemical Cycles **28:** 44-56.

Xu, Y., D. Shi, L. Aristilde, and F. M. M. Morel. 2012. The effect of pH on the uptake of zinc and cadmium in marine phytoplankton: Possible role of weak complexes. Limnology and Oceanography **57:** 293.

Xu, Y., D. Tang, Y. Shaked, and F. M. M. Morel. 2007. Zinc, cadmium, and cobalt interreplacement and relative use efficiencies in the coccolithophore Emiliania huxleyi. Limnology and Oceanography**:** 2294-2305.

Zhao, Y., D. Vance, W. Abouchami, and H. De Baar. 2014. Biogeochemical cycling of zinc and its isotopes in the Southern Ocean. Geochimica et Cosmochimica Acta **125:** 653-672.

Zondervan, I. 2007. The effects of light, macronutrients, trace metals and CO 2 on the production of calcium carbonate and organic carbon in coccolithophores—a review. Deep Sea Research Part II: Topical Studies in Oceanography **54:** 521-537.

Appendices

1. The published version of Chapter 2 is attached as appendix 1

Full reference:

Samanta, M., M. J. Ellwood, and G. E. Mortimer. 2016. A method for determining the isotopic composition of dissolved zinc in seawater by MC-ICP-MS with a 67Zn–68Zn double spike. Microchemical Journal 126: 530-537.

2. The online published version of Chapter 3 is attached as appendix 2

Reference:

Samanta, M., M. J. Ellwood, M. Sinoir, and C. S. Hassler.2017. Dissolved Zinc Isotope Cycling in the Tasman Sea, Sw Pacific Ocean. Marine Chemistry.

3. The online published version of Chapter 4 is attached as appendix 3

Reference:

Samanta, M., M. J. Ellwood, and R. F. Strzepek. Zinc isotope fractionation by Emiliania huxleyi cultured across a range of free zinc ion concentrations. Limnology and Oceanography**:** n/a-n/a.

4. Collaborative study

The method developed in Chapter 2 for Zn isotope measurement was used in a major inter-collaborative study for inter-calibration of a new primary Zn isotope reference standard.

Reference:

Archer, C., M.B. Andersen, C. Cloquet, T.M. Conway, S. Dong, M. Ellwood, R. Moore, J. Nelson, M. Rehkämper, O. Rouxel, M. Samanta, K. C. Shin, Y. Sohrin, S. Takano and L. Wasylenki. 2017. Inter-calibration of a proposed new primary reference standard AA-ETH Zn for zinc isotopic analysis. Journal of Analytical Atomic Spectrometry.